

17698

NATIONAL LIBRARY
OTTAWA



BIBLIOTHÈQUE NATIONALE
OTTAWA

NAME OF AUTHOR..... GORDON STEAD.....

TITLE OF THESIS..... A FINITE ELEMENT.....
 APPROACH TO SOUND.....
 TRANSMISSION BETWEEN ROOMS.....

UNIVERSITY OF ALBERTA.....

DEGREE FOR WHICH THESIS WAS PRESENTED..... M. Sc.....

YEAR THIS DEGREE GRANTED..... 1973.....

Permission is hereby granted to THE NATIONAL LIBRARY
 OF CANADA to microfilm this thesis and to lend or sell copies
 of the film.

The author reserves other publication rights, and
 neither the thesis nor extensive extracts from it may be
 printed or otherwise reproduced without the author's
 written permission.

(Signed)..... Gordon Stead

PERMANENT ADDRESS:

102-10549 80 AVE
 EDMONTON, ALTA

DATED..... Oct 1..... 19 73

THE UNIVERSITY OF ALBERTA

A FINITE ELEMENT APPROACH TO SOUND TRANSMISSION
BETWEEN ROOMS

BY

C

GORDON STEAD

A THESIS

SUBMITTED TO THE FACULTY OF GRADUATE STUDIES AND RESEARCH
IN PARTIAL FULFILMENT OF THE REQUIREMENTS FOR THE DEGREE
OF MASTER OF SCIENCE

DEPARTMENT OF MECHANICAL ENGINEERING

EDMONTON, ALBERTA

FALL, 1973

THE UNIVERSITY OF ALBERTA
FACULTY OF GRADUATE STUDIES AND RESEARCH

The undersigned certify that they have read, and recommend to the Faculty of Graduate Studies and Research, for acceptance, a thesis entitled "A FINITE ELEMENT APPROACH TO SOUND TRANSMISSION BETWEEN ROOMS" submitted by GORDON STEAD in partial fulfilment of the requirements for the degree of Master of Science.

A. Cragg
Supervisor

Gary Faulkner

D. W. Murray

Date . *Sept. 6. 1. 73.*

ABSTRACT

A set of two dimensional finite elements were developed to approximate three dimensional coupled plate-acoustic systems. Though quite generally applicable, these elements were restricted to problems in small enclosure acoustics and sound transmission between rooms.

An experimental apparatus was constructed to substantiate the theoretical results. Agreement was found to be good in all except the most adverse cases.

ACKNOWLEDGMENTS

The author wishes to thank

- Dr. A. Craggs for his guidance and supervision of this thesis
- Dr. J. S. Kennedy, Dr. G. Faulkner and Dr. R. Tait for their helpful suggestions
- The members of the Mechanical Engineering Technical Staff for their assistance in construction and instrumentation of the experimental equipment
- My wife for her patience in typing
- The National Research Council of Canada (Scholarship) and The University of Alberta for their financial support and the National Research Council Research Fund No. A 7431 for computing funds

TABLE OF CONTENTS

		Page
CHAPTER I	INTRODUCTION	1
	1.1 Review of Related Work	2
	1.2 Aim of Thesis	4
CHAPTER II	UNCOUPLED ELEMENTS	6
	2.1 Element Formulation	7
	2.2 Rectangular Acoustic Element	10
	2.3 Triangular Acoustic Element	14
	2.4 Beam Plate Element	20
	2.5 Application of Acoustic Elements	30
	2.5.1 Odd Shaped Room	30
CHAPTER III	COUPLED ELEMENTS	40
	3.1 The Coupling Matrix	40
	3.2 Sound Transmission Between Panel Coupled Rooms	50
	3.2.1 Theoretical Considerations	54
	3.3 Sound Transmission Between Orifice Coupled Rooms	76
CHAPTER IV	DISCUSSION AND RESULTS	78
	4.1 Discussion	78
	4.2 Future Research	79
	4.3 Results	80

BIBLIOGRAPHY

APPENDIX A

APPENDIX B

APPENDIX C

Page

86

107

LIST OF TABLES

Table		Page
2.1	Convergence of Four Lowest Eigenvalues for Sloped Ceiling Reverberation Chamber	33
3.1	Results of Test Model	49

LIST OF FIGURES

Fig.		Page.
1	Element Label and Notation	9
2	Convergence of Rectangular Acoustic Element	13
2.3	Convergence of Triangular Acoustic Element	19
2.4	Convergence of Line Plate Element (n=0)	28
2.5	Convergence of Line Plate Element (n=1)	29
2.6	Sloped Ceiling Reverberation Chamber	32
2.7	First Mode - Rooms With Sloped Ceiling	37
2.8	Second Mode - Rooms With Sloped Ceiling	38
2.9	Third Mode - Rooms With Sloped Ceiling	39
3.1	Test Acoustic Model	49
3.2	Experimental Apparatus	51
3.3	Pictorial Layout of Components	52
3.4	First Mode - Sound Transmission Between Symmetric Rooms	56
3.5	Second Mode - Sound Transmission Between Symmetric Rooms	57
3.6	Third Mode - Sound Transmission Between Symmetric Rooms	58
3.7	Fourth Mode - Sound Transmission Between Symmetric Rooms	59
3.8	Fifth Mode - Sound Transmission Between Symmetric Rooms	60
3.9	First Mode - Normalized Longitudinal Pressure Variation and Plate Displacement	61

Figure		Page
3.10	Second Mode - Normalized Longitudinal Pressure Variation and Plate Displacement	62
3.11	Third Mode - Normalized Longitudinal Pressure Variation and Plate Displacement	63
3.12	Fourth Mode - Normalized Longitudinal Pressure Variation and Plate Displacement	64
3.13	Full Coupling Panel - Resonant Frequencies for Sound Transmission	65
3.14	73.7 Per Cent Coupling Panel - Resonant Frequencies for Sound Transmission	66
3.15	42.5 Per Cent Coupling Panel - Resonant Frequencies for Sound Transmission	67
3.16	42.5 Per Cent Orifice Coupling - Resonant Fre- quencies for Sound Transmission	73
3.17	4.2 Per Cent Orifice Coupling - Resonant Fre- quencies for Sound Transmission	74
3.18	Example of Orifice Coupling Mode Shapes	75
A1	Infinitesimal Acoustic Element	85
A2	P-V Curve	90
B1	Element Shape for Triangular Integral	100

NOTATION

$[A], [A]^{-1}$	matrices relating the arbitrary constants and the nodal pressure coordinates for a triangular acoustic finite element
a_{lm}	member of the arbitrary constants for a triangular acoustic finite element
B_a	pressure-displacement work at a panel-acoustic interface
c	velocity of sound
D	the plate modulus = $Eh_p^3/12 (1-\nu^2)$
E	Young's modulus
$f_i(x^*)$	the i th Hermitian Interpolation Polynomial of a variable x^* , $0 < x^* < 1$
$g(x,y)$	vector containing the ten variable elements of a cubic polynomial
h_p	thickness of plate element
$J, \delta J$	Hamiltonian or action integral and its first variation
$[K]$	stiffness matrix for plate finite element
l, m, n	number of acoustical half-cosine waves between the boundaries in a rectangular room
$[M]$	mass matrix for plate finite element
M_{xx}, M_{yy}	bending moments about the x and y axis, respectively

M_{xy}	twisting moment
n_e	number of elements used in convergence test
\vec{n}	unit normal vector to a surface
$[P], [P_e]$	overall and elemental acoustic pressure matrices
$\{p_n\}, \{p_n\}_e$	overall and elemental pressure co-ordinates
p_e	elemental pressure
$p, \delta p$	pressure and its first variation
p, p_0	initial and final pressure
p_i	excess acoustic pressure = $p - p_0$
$p_i, \frac{\delta p_i}{\delta x}, \frac{\delta p_i}{\delta y}$	nodal pressure and its directional derivatives at the i th node
Q	plate shear
$[S], [S_e]$	overall and elemental acoustic stiffness
s	condensation
$T, \delta T$	kinetic energy and its first variation
t_1, t_2	end values of a time interval
u	displacement within the acoustic fluid
$U, \delta U$	potential energy and its first variation
v_0, v	initial and final specific volumes
$\{w_n\}$	plate transverse deflection co-ordinates
w, w_p	transverse deflection of plate
$w_{p,x}, w_{p,z}$	slope of the plate in the x and z directions, respectively
$w_{p,xx}, w_{p,zz}$	plate curvature about the x and z axis, respectively

$w_{p,xz}$	plate twist
x,y,z	co-ordinate directions
γ	ratio of the specific heats of a gas
Δ	dilatation
O	acoustic panel coupling matrix
$[\theta]_a, [\theta]_p$	acoustic and plate rotational matrices
λ	eigenvalue of the eigenvalue problem
ν	Poisson's ratio
ρ, ρ_0	initial and final acoustic densities
ρ, ρ_a	acoustic density
ρ_p	plate density
$\{\phi_n\}, \{\phi_n\}_e$	overall and elemental velocity potential co-ordinates
$\{\eta\}_i, \{\psi\}$	normalized eigenvectors or principal mode shapes

CHAPTER I
INTRODUCTION

The study of sound, similar to most other forms of science, found its origin in a practical "trial and error" sense long before the mathematical theories were developed. Experimentation on motion by Galileo Galilei [1]* and extensive research on musical instruments and listening rooms by Mersenne [2] were grouped under the field of "new sciences" until the name acoustics was introduced by Sauveur [3]. These early treatises, although mostly non-mathematical, defined the field and even made an approach at dividing it into sub-fields - geometrical, statistical and wave acoustics.

Geometrical and statistical are more generally grouped under architectural acoustics as they were the first techniques to find engineering application. The former allows the sound waves only to have ray characteristics thereby allowing the path of the sound to be traced much as a light ray with its intensity diminishing with distance and reflection. Statistical acoustics derives its name from the requirement of a "statistically diffuse sound field." Diffuse in the sense that the pressure level within the volume can be considered uniform. This can usually be approximated in very large enclosures, i.e. auditoriums, large halls, etc. where the longest sound wavelength present is less than one-tenth the minimum dimension and the multiplicity of sound frequencies is sufficient to eliminate pressure nodes and appreciable pressure maxima. This also allows the wave characteristics of sound

*Entries in [] square brackets refer to the bibliography.

to be totally neglected. Instead, sound radiation becomes independent of spatial location and the time dependency of a sound is only a function of the statistical average of damping surfaces within the enclosure. Much of the early work done in architectural acoustics [4, 5, 6] took this form of analysis.

Wave acoustics does not neglect the obtrusive wave characteristics of sound, increasing many-fold the difficulty of mathematical calculations. It is necessary to include reflection, absorption, diffraction and phase shift at every incidence of the sound waves with a boundary, not to mention cancellation and reinforcement of sound waves coincident within the enclosure. This approach can be used for any size of enclosure but is usually limited to smaller volumes, i.e. small rooms, ducting, etc. where the sound wavelengths present are of the same order as the enclosure's dimensions. The sheer futility of analyzing a geometrically complicated structure can be appreciated. Major early theoretical contributions in wave acoustics were made by Rayleigh [7] and Lamb [8]. Their contributions by no means embody the entire field of acoustics, but it has been said, "... it behooves all of us. . . to read Rayleigh's Science of Sound regularly." [9]

It might be well mentioned here that between these two approaches to acoustics lies a zone that must be approached with an extensive "salting" of experience.

1.1 Review of Related Work

In 1944, Morse and Bolt published a "state-of-the-art" article [10] on room acoustics. A discussion of geometric and wave

acoustics was given with special reference to different types of absorbing materials. These panels were characterized by an acoustic impedance which is the complex ratio of the acoustic pressure and the air velocity just outside the surface. The real part of this ratio is the dissipative term whereas the imaginary part is the reactive term. The exact analysis of a regular acoustically hard rectangular room with one rigid but absorbing wall was presented but the intricacies in the calculations caused the authors to go to more approximate solutions for general application. The introduction of more rigid, absorbing walls only complicated the analysis. A simplified model that could handle different geometries and absorption at the walls would be desirable.

Principal mode analysis supplies an effective method of studying mechanical vibration. The inclusion of damping (hysteretic and viscous) cause problems but these are not insurmountable. Bishop and Gladwell [11] discuss this method quite fully concluding that ". . . when damping of the most general type is present, the system can vibrate in a principal mode at a natural frequency without there being any phase difference between the displacement at various points." This would tend to indicate that a study of undamped systems would supply an insight into lightly damped systems. The orthogonality of the principal mode allows the deformed shape of the structure to be represented by a linear combination of the principal mode shapes. Though principal mode analysis was discussed in terms of structural systems, it could be applied equally as well to acoustics with the corresponding "stiffness" and "mass" effects (more correctly kinetic and potential effects, respectively).

Later, authors became more interested in cases where the flexural natural frequencies of the panel were in the same range as the acoustical natural frequencies. The previous model of a complex acoustic impedance for an absorbing panel was no longer sufficient. Sound transmission between rooms [12] and noise effects on flexible structural enclosures [13, 14, 15, 16, 17, 18] can only be handled by a coupled plate-acoustic system. The idea of such a coupled system, with slight alteration, is also used in the study of liquid sloshing in containers [19].

1.2 Aim of Thesis

Previous finite element work by Craggs [15, 16] produced large three dimensional acoustic and plate elements. They were used to study transient responses of a plate-acoustic system. Each element required relatively large computer core area, therefore even small problems required a long execution time which is approximately proportional to the square of the storage space required. By assuming two of the boundaries to be parallel and hard, the exact solution can be used for the direction perpendicular to these boundaries, i.e. the z-direction. A similar approach (sometimes credited to Kantorovich) was used by Cheung and Zienkiewicz [20] in the study of plates and shafts. A reduction of element storage area by a factor of 3.0 and a consequent reduction in computation time by 7.0 is realized using this assumption. Though the elements are now effectively two dimensional, total freedom is retained in the remaining coordinate directions as to method of solution. It was proposed to develop second order plate and acoustic elements, i.e. approximating displacements and pressures and their first derivatives.

Also, instead of a transient study of a coupled plate-acoustic system, a principal mode analysis was undertaken. The natural frequencies and principal mode shapes of a system can be obtained by studying the free vibration problem. This entails assuming that all time dependent variables obey the same harmonic function, thus removing the time dependency of the system. The problem then reduces to the solution of an eigenvalue problem.

$$([A] - \lambda[B])\{x\} = 0$$

The numerical results presented are the natural frequencies and principal mode shapes for:

- i) a rigid room with a sloping wall
- ii) two rigid rooms coupled by a flexible panel
of various widths
- iii) two rigid rooms coupled by an air slit of
various widths

CHAPTER II

UNCOUPLED ELEMENTS

The finite element method is basically the approximation of the desired solution over a well defined geometric space, i.e. cuboid, tetrahedron, etc. Interpolation functions modified by arbitrary parameters make up the general form of the solution. This general form is then forced to satisfy the equations throughout the well defined geometric space (from now on called an element). Though it is not necessary, the interpolation functions are usually picked in such a way that the arbitrary parameters take on physical significance at certain points in the element (called nodes). What remains is to join several elements into a desired configuration that has some degree of continuity between elements and to satisfy the natural boundary conditions.

Convergence (and rate of convergence) to the correct solution is of interest. It is extremely difficult, if not impossible, to prove convergence to the correct solution for all configurations which can be produced by finite elements. The generally accepted approach [19, 20] is to obtain an approximate solution to a problem that is mathematically solvable. Successively finer "grids" of elements are used to better approximate this solution. Percentage error (between the exact and approximate solution) is plotted against the number of elements on logarithmic graph paper. The slope of the resulting curve is an indication of the rate of convergence. Beyond this, "the proof is in the tasting". Results for other desired geometric configurations obtained from this method must be accepted (with due caution,

of course) and if possible checked out by experimentation.

2.1 Element Formulation

It has been found more convenient to work with functionals than with the actual equations of motion and the boundary conditions because certain symmetries arise in the functionals that can be taken advantage of. If a functional can be found whose stationary condition satisfies the equation of motion and the natural boundary conditions, then the functional can be used just as effectively in the solution of the problem [21]. In fact, the functionals required for the uncoupled panel and acoustic subsystems are the Hamiltonians or action integrals J of the subsystems

$$J = \int_{t_1}^{t_2} [T-U] dt$$

where T is the kinetic energy and U is the potential energy. The governing equation and boundary conditions are obtained by setting the first variation to zero

$$\delta J = 0$$

The first variation is obtained by replacing the required parameters by themselves plus a small arbitrary increment (i.e. p is replaced by $p + \delta p$) then the resulting equation $J + \delta J$ and the original equation J are subtracted to give the first variation.

Appendix A offers a relatively detailed formulation of the acoustic finite element. From the basic acoustic and energy equations (Appendices A1 and A2, respectively) through to the finite element or matrix formulation of the acoustic functional (Appendix A4), there was no assumption made as to the form of time dependency. This would

allow the study of transient acoustic systems; however, since the steady-state response of an undamped system is desired, the time function was written as

$$\sin(\omega t + \theta)$$

where ω is the cyclic frequency and θ is a phase angle defined by initial conditions. Since all variables in the system obey this time function (A16)* of Appendix A4 can be written

$$\{[S_e] - \omega_e^2 [P_e]\} \{p_n\}_e = 0$$

which is a standard form of the eigenvalue problem with $\{p_n\}_e$ corresponding to the elemental nodal pressure coordinates. For a system composed of several elements, the 'e' subscript can be dropped.

The overall [S] matrix can be derived by noting that the energy of the total system is a linear summation of its component energies [8, 22]

$$\begin{aligned} T &= \sum T_e = \frac{1}{2} \{p_n\}^T [S] \{p_n\} \\ &= \frac{1}{2} \sum \{p_n\}_e^T [S_e] \{p_n\}_e \end{aligned}$$

with a similar formula for [P]. Leading to

$$\{[S] - \omega^2 [P]\} \{p_n\} = 0 \quad (2.1)$$

where $\{p_n\}$ is the overall pressure coordinate.

*Entries in () refer to equations.

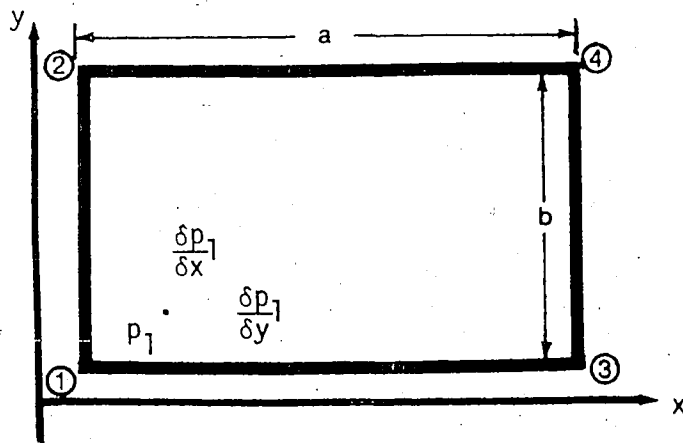


Figure 2.1 (a) RECTANGULAR ACOUSTIC ELEMENT

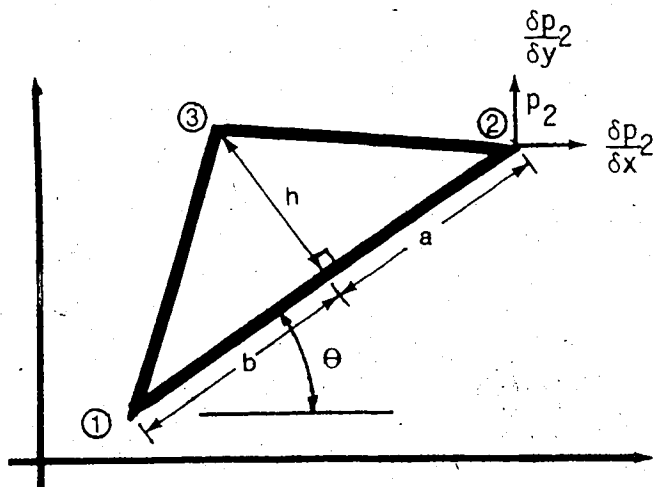


Figure 2.1 (b) TRIANGULAR ACOUSTIC ELEMENT

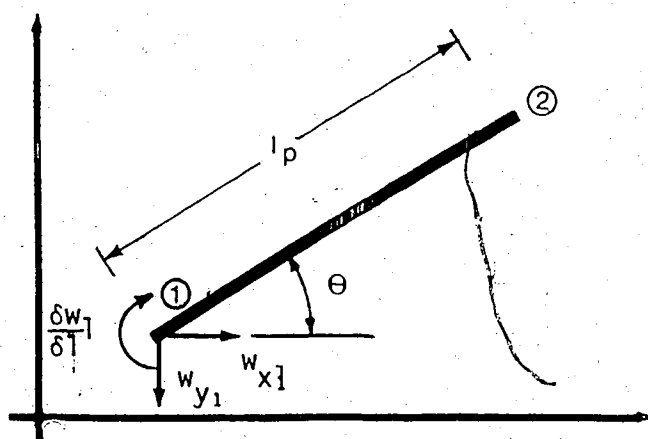


Figure 2.1 (c) LINE PLATE ELEMENT

Figure 2.1 ELEMENT SHAPES AND NOTATION

2.2. Rectangular Acoustic Element

Figure 2.1(a) gives the element shape and dimension in the x-y plane. The encircled numbers are the nodal numbers and the nodal values of p , $\frac{\delta p}{\delta x}$, $\frac{\delta p}{\delta y}$ are p_i , $\frac{\delta p_i}{\delta x}$, $\frac{\delta p_i}{\delta y}$, $i = 1, 2, 3, 4$ which are functions of time. Since this is a "pseudo" three dimensional approach, there should be an identical x-y plane at a distance d behind the plane shown. These planes were previously defined as rigid and parallel, allowing the exact solution for the z-direction to be found. This solution, a single Fourier cosine series, can easily be used to approximate many mode shapes in the z-direction (as is shown in Appendix B1), although only the n th term of the series will be used in the following calculations to simplify the notation. In the x-y plane, pressure and pressure variation can be approximated by the product of two sets of Hermitian interpolation polynomials $f(x^*)$, $f(y^*)$, where $x^* = x/a$ and $y^* = y/b$. These polynomials, their characteristics and their integrals are given in Appendix B2. The desirable characteristics of these interpolation polynomials allow p_e , the pressure distribution throughout the element for the n th node in the z-direction, to be expressed as

$$\begin{aligned}
 p_e = & \{ p_1 f_1(x^*) f_1(y^*) + \frac{\delta p_1}{\delta x} a f_2(x^*) f_1(y^*) + \frac{\delta p_1}{\delta y} b f_1(x^*) f_2(y^*) \\
 & + p_2 f_1(x^*) f_3(y^*) + \frac{\delta p_2}{\delta x} a f_2(x^*) f_3(y^*) + \frac{\delta p_2}{\delta y} b f_1(x^*) f_4(y^*) \\
 & + p_3 f_3(x^*) f_1(y^*) + \frac{\delta p_3}{\delta x} a f_4(x^*) f_1(y^*) + \frac{\delta p_3}{\delta y} b f_3(x^*) f_2(y^*) \\
 & + p_4 f_3(x^*) f_3(y^*) + \frac{\delta p_4}{\delta x} a f_4(x^*) f_3(y^*) + \frac{\delta p_4}{\delta y} b f_3(x^*) \\
 & f_4(y^*) \} \cos \frac{n\pi z}{d}
 \end{aligned} \tag{2.2}$$

where the dimensions a, b are a result of the chain-rule.

$$\frac{\delta p}{\delta x} = \frac{\delta p}{\delta x^*} \frac{\delta x^*}{\delta x} \text{ or } \frac{\delta p}{\delta x^*} = a \frac{\delta p}{\delta x}$$

introduced here

$$p_e = \{f(x^*) \ f(y^*)\}^T \{p_n\}_e \cos \frac{n\pi z}{d}$$

where the superscript "T" indicates the transpose of the vector and

$$\{f(x^*) \ f(y^*)\} = \begin{bmatrix} f_1(x^*) \ f_1(y^*) \\ af_3(x^*) \ f_1(y^*) \\ \cdot \\ \cdot \\ bf_3(x^*) \ f_4(y^*) \end{bmatrix} \text{ and } \{p_n\}_e = \begin{bmatrix} p_1 \\ \frac{\delta p_1}{\delta x} \\ \cdot \\ \cdot \\ \frac{\delta p_4}{\delta y} \end{bmatrix}$$

It would be best to note here that

$$\begin{aligned} \frac{\delta p}{\delta x} e &= \frac{1}{a} \{f'(x^*) \ f(y^*)\}^T \{p_n\}_e \cos \frac{n\pi z}{d} \\ \frac{\delta p}{\delta y} e &= \frac{1}{b} \{f(x^*) \ f'(y^*)\}^T \{p_n\}_e \cos \frac{n\pi z}{d} \\ \frac{\delta p}{\delta z} e &= \frac{-n\pi}{d} \{f(x^*) \ f(y^*)\}^T \{p_n\}_e \sin \frac{n\pi z}{d} \end{aligned}$$

The prime "'" denotes differentiation with respect to the variables in round brackets.

Substituting these formulas in the energy equation as done in Appendix A4, the acoustic stiffness $[S_e]_R$ and pressure $[P_e]_R$ matrices can be written

$$\begin{aligned}
[S_e]_R &= \frac{ab}{\rho} \int_0^1 \int_0^1 \left[\frac{1}{a^2} \{f'(x^*) f(y^*)\} \{f'(x^*) f(y^*)\}^T \right. \\
&\quad \left. + \frac{1}{b^2} \{f(x^*) f'(y^*)\} \{f(x^*) f'(y^*)\}^T \right] dx^* dy^* \cdot \int_0^d \cos^2 \frac{n\pi z}{d} dz \\
&\quad + \frac{ab}{\rho} \left(\frac{n\pi}{d} \right)^2 \int_0^1 \int_0^1 \{f(x^*) f(y^*)\} \{f(x^*) f(y^*)\}^T dx^* dy^* \cdot \int_0^d \sin^2 \frac{n\pi z}{d} dz
\end{aligned}
\tag{2.3}$$

$$[P_e]_R = \frac{ab}{\rho c^2} \int_0^1 \int_0^1 \{f(x^*) f(y^*)\} \{f(x^*) f(y^*)\}^T dx^* dy^* \cdot \int_0^d \cos^2 \frac{n\pi z}{d} dz
\tag{2.4}$$

The integrals with respect to z are defined in Appendix B1, and the integrals with respect to x^* and y^* are defined in Appendix B2.

The rectangular acoustic element was programmed for the IBM 360/67 computer and with the aid of the IBM Scientific Subroutine Package, the eigenvalue problem, as shown by (2.1) was performed. A cubical room of unit side and rigid boundaries was approximated as a check for convergence. This system has an exact set of principal mode solutions

$$p = p^* \cos \ell\pi x \cdot \cos m\pi y \cdot \cos n\pi z$$

$$\omega^2 = c^2 (\ell^2 + m^2 + n^2)$$

where the pressure p^* is a periodic function of time and ℓ, m, n are the number of half-cosine waves between the boundaries in the x, y, z directions, respectively. Grid refinement was done only in the x -direction. Percentage error in the eigenvalue (the square of the natural frequency) versus the number of elements is plotted for various $(\ell, m, 0)$ mode shapes in Fig. 2.2.

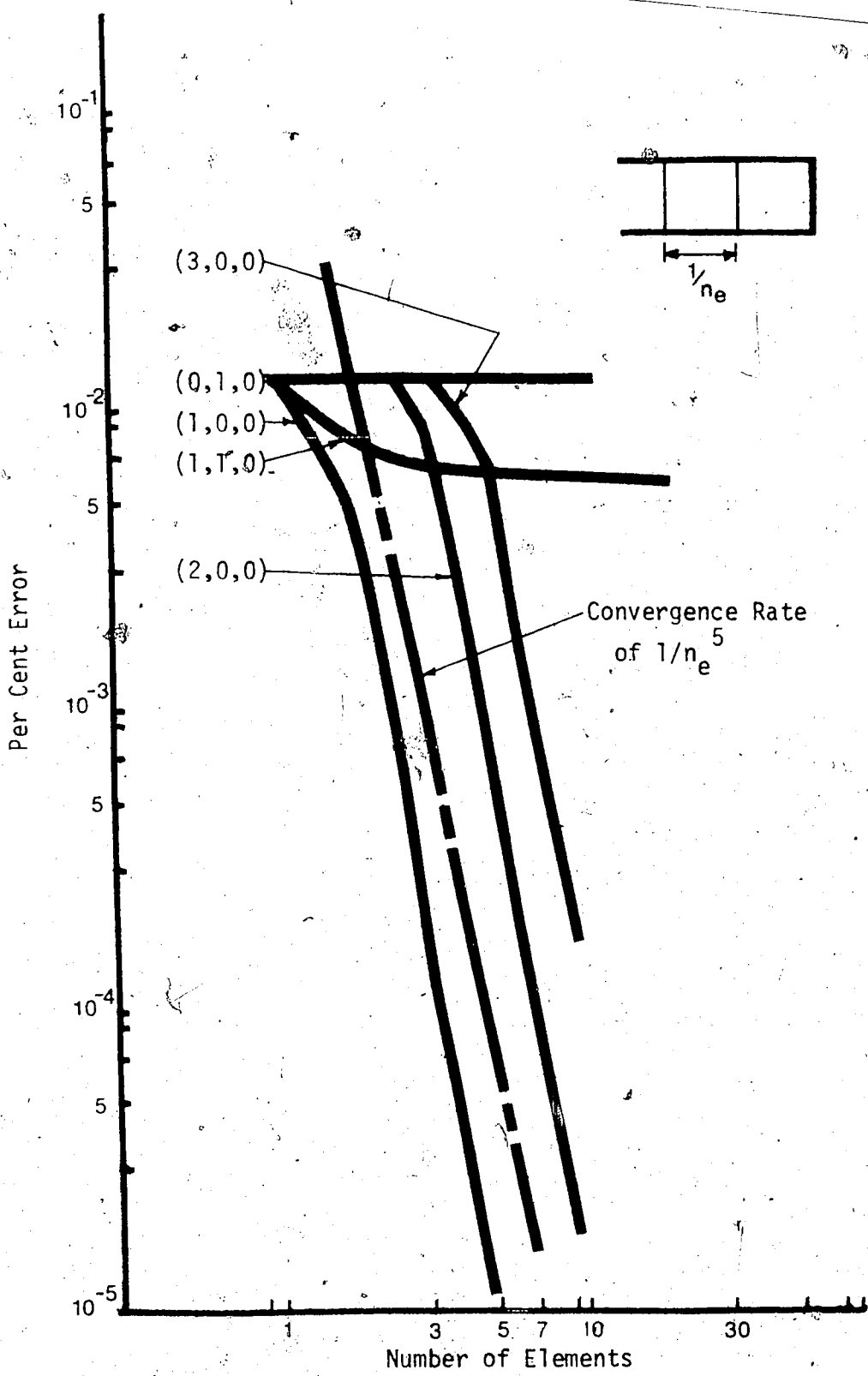


Figure 2.2 CONVERGENCE OF RECTANGULAR ACOUSTIC ELEMENT

The convergence of the results is at the rate of $1/n_e^5$, (n_e being the number of elements) for $(l, 0, 0)$ modes because of the x-direction grid refinement. The two $(l, 1, 0)$ modes plotted, which had no y-direction grid refinement, show no improvement with increase in element number. Note that even one element made a good initial approximation. Although not plotted, (l, m, n) modes would give exactly the same type of curves as $(l, m, 0)$ curves because the exact solution between rigid boundaries is used in the formulation of the elements for the z-direction.

2.3 Triangular Acoustic Element

Because of the change in geometry, the method of approximating the pressure p_e within the element was done by a cubic polynomial in x and y, and the exact solution in the z-direction.

$$p_e = \left(\sum_{m=0}^3 \sum_{l=0}^{3-m} a_{lm} x^l y^m \right) \cos \frac{n\pi z}{d}$$

where the a_{lm} were a set of arbitrary constants.

A complete cubic polynomial has ten arbitrary parameters, but to approximate the pressure and the pressure variation in x and y-directions for three nodes required only nine parameters. There are several methods to remove the extra parameter; two were tried but the one presented in Appendix C1 was rejected, in this case because the added computational time required did not improve (and in some cases worsened) the element's accuracy. The method chosen was to simply equate the a_{21} and a_{12} coefficients, so the elemental pressure p_e was written as

$$\begin{aligned}
 p_e = & \{a_{00} + a_{10}x + a_{01}y + a_{11}xy \\
 & a_{20}x^2 + a_{02}y^2 + a_{12}(x^2y + xy^2) \\
 & + a_{30}x^3 + a_{03}y^3\} \cos \frac{n\pi z}{d}
 \end{aligned}
 \tag{2.5}$$

The problems with this formulation will be discussed later. A third possibility would have been to define an internal node where pressure was the only parameter, but this would cause problems with the storage and manipulation of the resulting matrices.

Using a notation similar to Section 2.1,

$$p_e = \{g(x,y)\}^T \{a\} \cos \frac{n\pi z}{d}$$

where

$$\{g(x,y)\} = \begin{bmatrix} 1 \\ x \\ y \\ \vdots \\ y^3 \end{bmatrix} \quad \text{and} \quad \{a\} = \begin{bmatrix} a_{00} \\ a_{10} \\ a_{01} \\ \vdots \\ a_{03} \end{bmatrix}$$

Considering the element and notation of Fig. 2.1(b), it is now necessary to relate the arbitrary constant $\{a\}$ to the nodal characteristics p_i , $\frac{\delta p_i}{\delta x}$, $\frac{\delta p_i}{\delta y}$, $i = 1, 2, 3$. This is simply done by writing down the nine simultaneous equations for $z = 0$

$$\{p_n\}_e = [A] \{a\}$$

where

$$\{p_n\}_e = \begin{bmatrix} p_1 \\ \frac{\delta p_1}{\delta x} \\ \cdot \\ \cdot \\ \frac{\delta p_3}{\delta y} \end{bmatrix}$$

and $[A]$ is a matrix of the nodal values of $\{g(x,y)\}$ and its directional derivatives $\left\{\frac{\delta g}{\delta x}\right\}$ and $\left\{\frac{\delta g}{\delta y}\right\}$, respectively. Then it can be written

$$\{a\} = [A]^{-1} \{p_n\}$$

If the formulation was carried to completion from this point, the resulting integrals over the triangle would be arduous and could only be handled numerically. It is more convenient to set up a localized $x' - y'$ coordinate system, for the triangle, where $x' = \frac{\xi + b}{a + b}$ and $y' = \eta/h$ perform the required integration (shown in Appendix B3) then "rotate" the results into the $x - y$ coordinate system (shown in Appendix B4). The formulation for the $x' - y'$ coordinate system is identical to what has been presented for the $x - y$ coordinate system, but gives some simplifications in $[A]$ and $[A]^{-1}$, as shown in Appendix B5. The formulation can be carried on in terms of x' and y' .

The elemental pressure can be written as

$$p_e = \{g(x',y')\}^T [A]^{-1} \{p_n\}_e$$

Note that the variables in round brackets are omitted in future to simplify the formulation. The acoustical stiffness $[S_e']_T$ and pressure $[P_e']_T$ matrices are derived by substituting into the energy equations (A14).

$$\begin{aligned}
 [S_e'] = & \frac{1}{\rho} \cdot [A^T]^{-1} \int \int_{x' y'} \left\{ \left\{ \frac{\delta g}{\delta x'} \right\} \left\{ \frac{\delta g}{\delta x'} \right\}^T \right. \\
 & + \left. \left\{ \frac{\delta g}{\delta y'} \right\} \left\{ \frac{\delta g}{\delta y'} \right\}^T \right\} dx' dy' \cdot \int_0^d \cos^2 \frac{n\pi z}{d} dz \cdot [A]^{-1} \\
 & + \frac{1}{\rho} \cdot [A^T]^{-1} \int \int_{x' y'} \{g\} \{g\}^T dx' dy' \cdot \int_0^d \sin^2 \frac{n\pi z}{d} dz \\
 & \cdot [A]^{-1} \left(\frac{n\pi}{d} \right)^2
 \end{aligned} \tag{2.6}$$

where $[A^T]^{-1}$ is the transpose of $[A]^{-1}$

$$[P_e'] = \frac{1}{\rho c^2} \cdot [A^T]^{-1} \int \int_{x' y'} \{g\} \{g\}^T dx' dy' \cdot \int_0^d \cos^2 \frac{n\pi z}{d} dz \cdot [A]^{-1} \tag{2.7}$$

The integrals with respect to x' and y' are given in Appendix B3. The integrals with respect to z are given in Appendix B1. The rotation of the nodal velocity potential $\{\phi_n'\}_e$ from the $x' - y'$ coordinate system, is shown in Appendix B4. Since energy is independent of coordinate transformation, it can be written

$$\begin{aligned}
T_e &= \frac{1}{2} \{\phi'_n\}_e^T [S'_e] \{\phi'_n\}_e \quad \text{in } x' - y' \text{ system} \\
&= \frac{1}{2} \{\phi_n\}_e^T [\theta]_a^T [S'_e] [\theta]_a \{\phi_n\}_e \\
&= \frac{1}{2} \{\phi_n\}_e [S_e] \{\phi_n\}_e \quad \text{in } x - y \text{ system}
\end{aligned}$$

or

$$[S_e] = [\theta]_a^T [S'_e] [\theta]_a$$

where $[\theta]_a$ is the acoustic rotational matrix defined in Appendix B4.

The triangular element acoustic stiffness and pressure matrices derived above were programmed and the convergence tests were run on the cubical room used in Section 2.2. The orientation of the elements and the percentage error versus number of elements plot, are shown in Fig. 2.3. The rate of convergence was slightly less than $1/n_e^5$ in the direction of grid refinement with a poorer initial approximation than the rectangular elements, but overall still gave good results. It was interesting to note that by changing the pattern of subdividing the cuboid, even for a one-directional grid refinement, the results (and the resulting percentage errors) were changed, but this could be a study in itself, so will not be gone into here.

By studying the formulation of the exact solution and by comparing the finite element equations (2.3) and (2.5) it is possible to arrive at a natural frequency equation for the (m, n, q) mode in

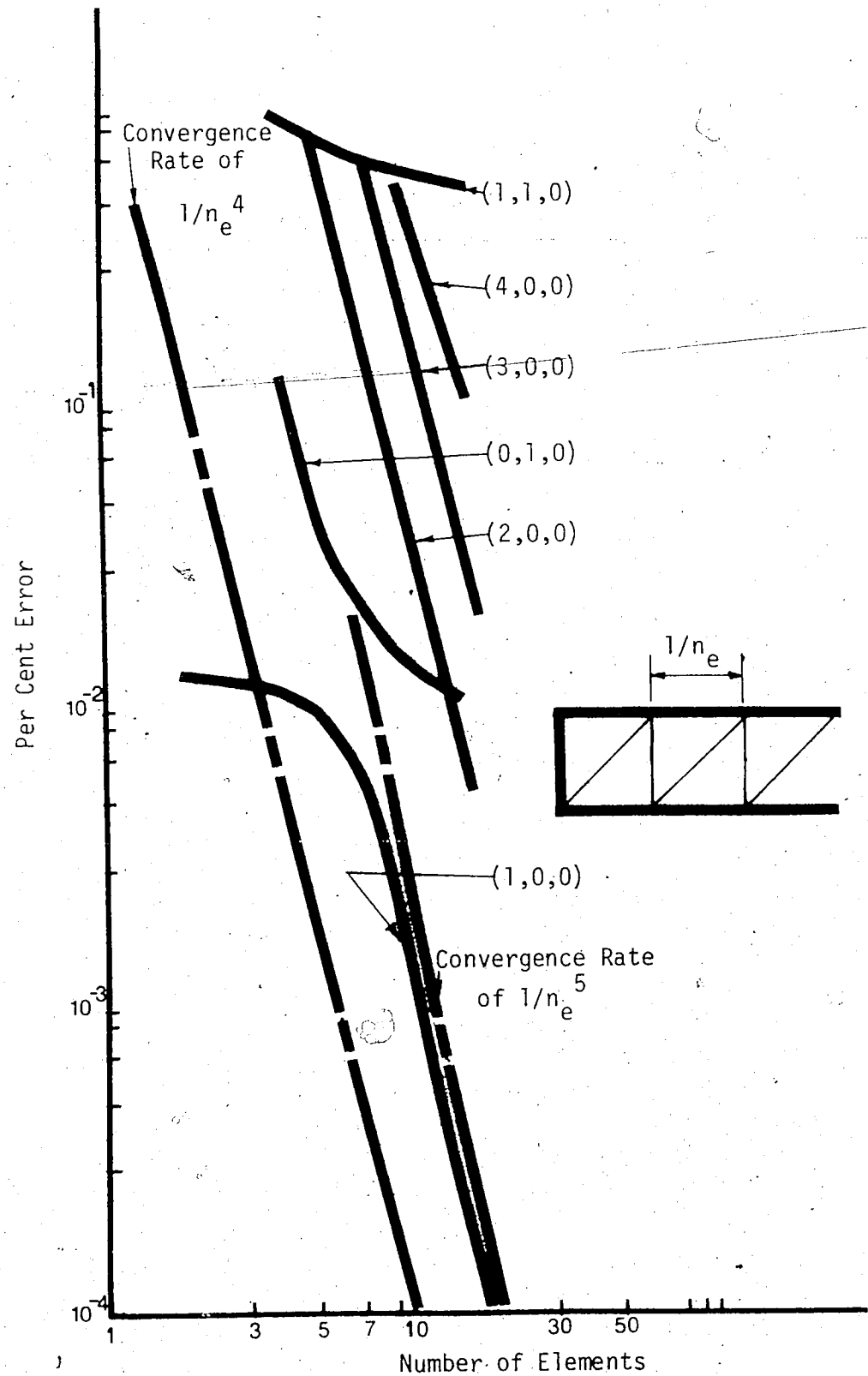


Figure 2.3 CONVERGENCE OF TRIANGULAR ACOUSTIC ELEMENT

terms of the (m, n, 0) mode.

$$\omega_{mnq}^2 = \omega_{mn0}^2 + \left\{ \frac{q\pi c}{d} \right\}^2 \quad (2.8)$$

where ω_{mnq} is the natural frequency for the (m, n, q) mode.

c is the velocity of sound

d is the depth of the room

2.4 Beam Plate Element

A similar detailed formulation to the one given in Appendix A could be undertaken for flat plates, but would serve no useful purpose, so will be forgone in favour of writing only the energy equations according to S. Timoshenko [23] for cartesian coordinates. It is, however, initially necessary to discuss the orientation of the plate. To use Kantorovich's approach the plate must be placed between the two rigid planes perpendicular to the z-direction, but the other direction must be general. It will be seen that the rotational concept used in the triangular acoustic element can be used here. Therefore, the plate will initially take an x-z plane orientation for the formulation and later be rotated to the x' - z' plane by a rotational matrix $[\theta]_p$.

$$T = \frac{1}{2} \rho_p h_p \iint_A \dot{w}_p^2 dx dz \quad (2.9)$$

where \dot{w}_p is the time derivative of the transverse deflection of the plate and $dxdz$ is an infinitesimal surface area on the plate in the x - z plane.

It is also convenient to introduce the differentiation convention $w_{,x} = \frac{\delta w}{\delta x}$, $w_{,xx} = \frac{\delta^2 w}{\delta x^2}$, etc. So,

$$U = \frac{D}{2} \iint_A \{ w_{p,xx}^2 + w_{p,zz}^2 + 2\nu w_{p,xx} w_{p,zz} + 2(1-\nu) (w_{p,xz})^2 \} dx dz \quad (2.10)$$

where

$D = Eh_p^3 / 12 (1-\nu^2)$ is the Plate Modulus

E is Young's Modulus

ν is Poisson's Ratio

Again, it is necessary to show that the equation of motion and the natural boundary conditions can be derived from the action integral by variational calculus.

The first variation is

$$\delta J = \int_{t_1}^{t_2} (\delta T - \delta U) dt = 0$$

$$\begin{aligned}
\delta J = & \int_{t_1}^{t_2} \left[\rho_p h_p \int_z \int_x \dot{w}_p \delta \dot{w}_p \, dx dz - D \int_z \int_x \{ w_p',_{xx} \delta w_p',_{xx} \right. \\
& + w_p',_{zz} \delta w_p',_{zz} + \nu (w_p',_{xx} \delta w_p',_{zz} + w_p',_{zz} \delta w_p',_{xx}) \\
& \left. + 2(1 - \nu) w_p',_{xz} \delta w_p',_{xz} \right] dx dz \, dt = 0 \quad (2.11)
\end{aligned}$$

The first term can be integrated by parts with respect to time to give

$$\rho_p h_p \int_A \int [w_p \delta w_p \Big|_{t_1}^{t_2} - \int_{t_1}^{t_2} \dot{w}_p \delta w_p \, dt] dx dz$$

The rest of the terms in (2.11) can be integrated by parts twice, with due care in the evaluation of the integral. The third term in (2.11) can be written as

$$\begin{aligned}
-D \int_{t_1}^{t_2} \left[\int_x w_p',_{zz} \delta w_p',_z \Big|_0^d dx - \int_x w_p',_{zzz} \delta w_p \Big|_0^d dx \right. \\
\left. + \int_A w_p',_{zzzz} \delta w_p \, dx dz \right] dt
\end{aligned}$$

where the first and second terms are evaluated at the front and rear boundary ($z=0$ and $z=d$, respectively) before they are integrated with respect to x . The last term in (2.11) is divided into two halves and integrated twice by parts; one half is integrated first with respect to x , then with respect to z ; the other half is integrated in the

reverse order. Noting again that δw_p and $\delta w_{p,x}$ are arbitrary and small and $\delta w_p = 0$ at t_1 and t_2 , the following equations result.

For $x = 0$ or l_p

$$\frac{\delta}{\delta x} [\delta w_p (w_{p,xx} + \nu w_{p,zz} + (1 - \nu) w_{p,xz})] = 0$$

$$\delta w_p [w_{p,xxx} + w_{p,xzz} - \frac{\delta}{\delta x} (w_{p,xx} + \nu w_{p,zz} + (1 - \nu) w_{p,xz})] = 0$$
(2.12)

where l_p is the length of the plate in the x-direction.

For $z = 0$ or d

$$\frac{\delta}{\delta z} [\delta w_p (w_{p,zz} + \nu w_{p,xx} + (1 - \nu) w_{p,zx})] = 0$$

$$\delta w_p [w_{p,zzz} + w_{p,zxx} - \frac{\delta}{\delta z} (w_{p,zz} + \nu w_{p,xx} + (1 - \nu) w_{p,zx})] = 0$$
(2.13)

and within the plate boundaries

$$D(w_{p,xxxx} + w_{p,zzzz} + 2w_{p,xxzz}) + \rho_p h_p \ddot{w}_p = 0 \quad (2.14)$$

These sets of equations show the power of the functional approach. Besides (2.14) being the equation of motion for a free vibrating plate, (2.12) and (2.13) embody all the natural boundary

conditions on a rectangular plate. According to Timoshenko [24]

$$M_{xx} = -D (w_p'_{,xx} + \nu w_p'_{,zz})$$

$$M_{zx} = -D (1 - \nu) w_p'_{,xz}$$

$$Q_x = -D (w_p'_{,xxx} + w_p'_{,xzz})$$

where M_{xx} is the bending moment (in the x-direction on the plate edge perpendicular to the x-direction), M_{zx} is the twisting moment and Q_x is the shear on edges perpendicular to the x-direction.

Using these relations in (2.12)

$$\frac{\delta}{\delta x} [\delta w_p (M_{xx} + M_{zx})] = 0$$

$$\delta w_p [Q_x - \frac{\delta}{\delta x} (M_{xx} + M_{zx})] = 0 \quad (2.15)$$

$$\text{for } x = 0, l_p$$

For example, a pinned edge on $x = 0$ is defined by $\delta w_p = 0$ and $M_{xx} = 0$. This allows for non-zero Q_x and M_{zx} . All other boundary conditions [24] can be derived from these equations.

Although (2.14) has no assumption as to the time function, it will be considered as harmonic (the time function) and real, i.e. $\sin(\omega t + \theta)$.

For simplicity the exact solution in the z-direction will be taken as a single Fourier sine series, i.e. pinned boundary conditions at $z = 0$ and $z = d$. Only one term (the kth) of the exact solution is to be used to simplify notation, although again a multi-term approximation of a mode shape could be handled.

If the notation used in Fig. 2.1 (c) is adopted (noting that $\theta = 0$ for initial consideration), we can write the deflection of plate w_p , in terms of a product of a set of Hermitian interpolation polynomials $\{f(x^*)\}$ and the exact solution where $x^* = \epsilon/l_p$ and $0 \leq \epsilon \leq l_p$.

$$w_p = \{w_1 f_1(x^*) + l_p \frac{\delta w_1}{\delta x} f_2(x^*) + w_2 f_3(x^*) + l_p \frac{\delta w_2}{\delta x} f_4(x^*)\} \sin \frac{k\pi z}{d} \quad (2.16)$$

where $w_i, \frac{\delta w_i}{\delta x}, i = 1, 2$ - are the nodal characteristics which may vary with time

$f_i(x^*), i = 1, 4$ - are the Hermitian polynomials

definition Appendix B2.

This can be written in short hand notation as in Sec. 2.2

$$w_p = \{f(x^*)\}^T \{w_n\} \sin \frac{k\pi z}{d}$$

where

$$\{f(x^*)\} = \begin{bmatrix} f_1(x^*) \\ \cdot \\ \cdot \\ l_p f_4(x^*) \end{bmatrix} \quad \text{and} \quad \{w_n\} = \begin{bmatrix} w_1 \\ \cdot \\ \cdot \\ \frac{\delta w_2}{\delta x} \end{bmatrix}$$

The elemental mass $[M_e]$ and stiffness $[K_e]$ can be defined by the equations

$$T_e = \frac{1}{2} \{\dot{w}_n\}^T [M_e] \{\dot{w}_n\}$$

$$U_e = \frac{1}{2} \{w_n\}^T [K_e] \{w_n\}$$

By substituting into the respective energy equations (2.9) and (2.10),

$$\begin{aligned}
 [K_e] = D l_p \int_0^1 & \left[\{f''(x^*)\} \{f''(x^*)\}^T / l_p^4 + \{f(x^*)\} \{f(x^*)\}^T \left\{ \frac{k\pi}{d} \right\}^4 \right. \\
 & \left. - \frac{\nu}{l_p^2} \left\{ \frac{k\pi}{d} \right\}^2 (\{f'(x^*)\} \{f(x^*)\}^T + \{f(x^*)\} \{f'(x^*)\}^T) \right] dx^* \\
 & \cdot \int_0^d \sin^2 \frac{k\pi z}{d} dz \\
 & + 2(1-\nu) \frac{D}{l_p} \int_0^1 \{f'(x^*)\} \{f'(x^*)\}^T dx^* \int_0^d \cos^2 \frac{k\pi z}{d} dz \left\{ \frac{k\pi}{d} \right\}^2 \quad (2.17)
 \end{aligned}$$

where the third term has been arranged to retain the symmetry of the stiffness matrix.

$$[M_e] = \rho_p h_p l_p \int_0^1 \{f(x^*)\} \{f(x^*)\}^T dx^* \cdot \int_0^d \sin^2 \frac{k\pi z}{d} dz \quad (2.18)$$

The integrals with respect to x^* can be found in Appendix B2. The integrals with respect to z can be found in Appendix B1.

This element can now be rotated to any position, letting l^* denote the dimension along the sloped plate as shown in Fig. 2.1(c).

By direct comparison with Appendix B4,

$$\begin{bmatrix} \delta w_i \\ \delta x^* \end{bmatrix} = \begin{bmatrix} \sin \theta & \cos \theta & 0 \\ 0 & 0 & 1 \end{bmatrix} \begin{bmatrix} w_{xi} \\ w_{yi} \\ \delta l^* \end{bmatrix}$$

The plate rotational matrix $[\theta]$ can be written

$$[\theta]_p = \begin{bmatrix} \sin \theta & \cos \theta & 0 & 0 & 0 \\ 0 & 0 & 1 & 0 & 0 \\ 0 & 0 & 0 & \sin \theta & \cos \theta & 0 \\ 0 & 0 & 0 & 0 & 0 & 1 \end{bmatrix}$$

These plate element stiffness and mass matrices were programmed for the IBM 360/67 and convergence tests run on harmonically vibrating plates of unit side with pinned boundary conditions on all edges. This plate has an exact principal mode solution

$$w_p = w_p^* \sin r\pi x \sin k\pi z$$

$$\omega^2 = \frac{4D}{\rho_p h_p} (r^2 + k^2)^2$$

where r and k are the number of half-sine waves in the x and z -direction, respectively.

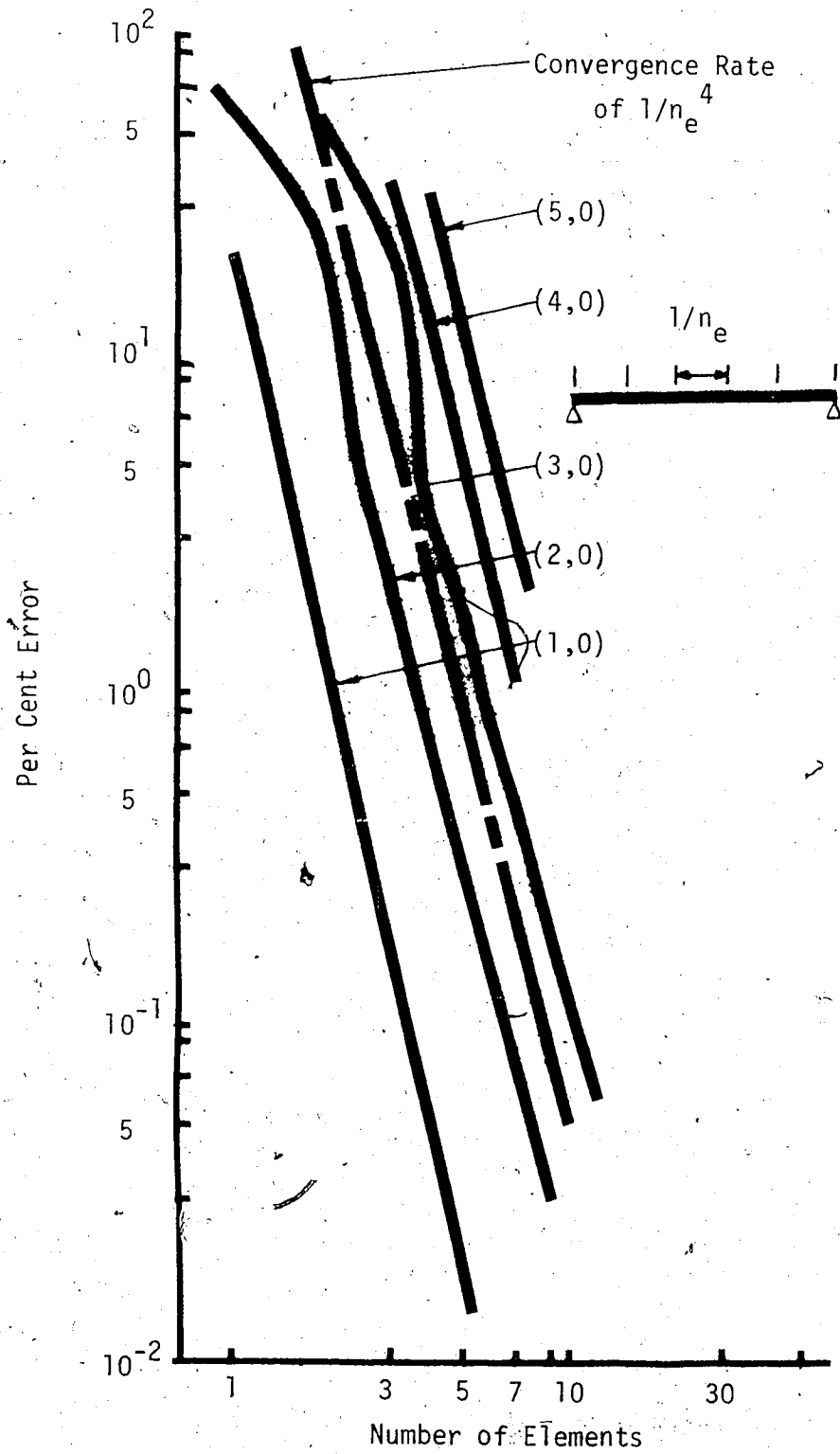


Figure 2.4 CONVERGENCE OF LINE PLATE ELEMENT ($n=0$)

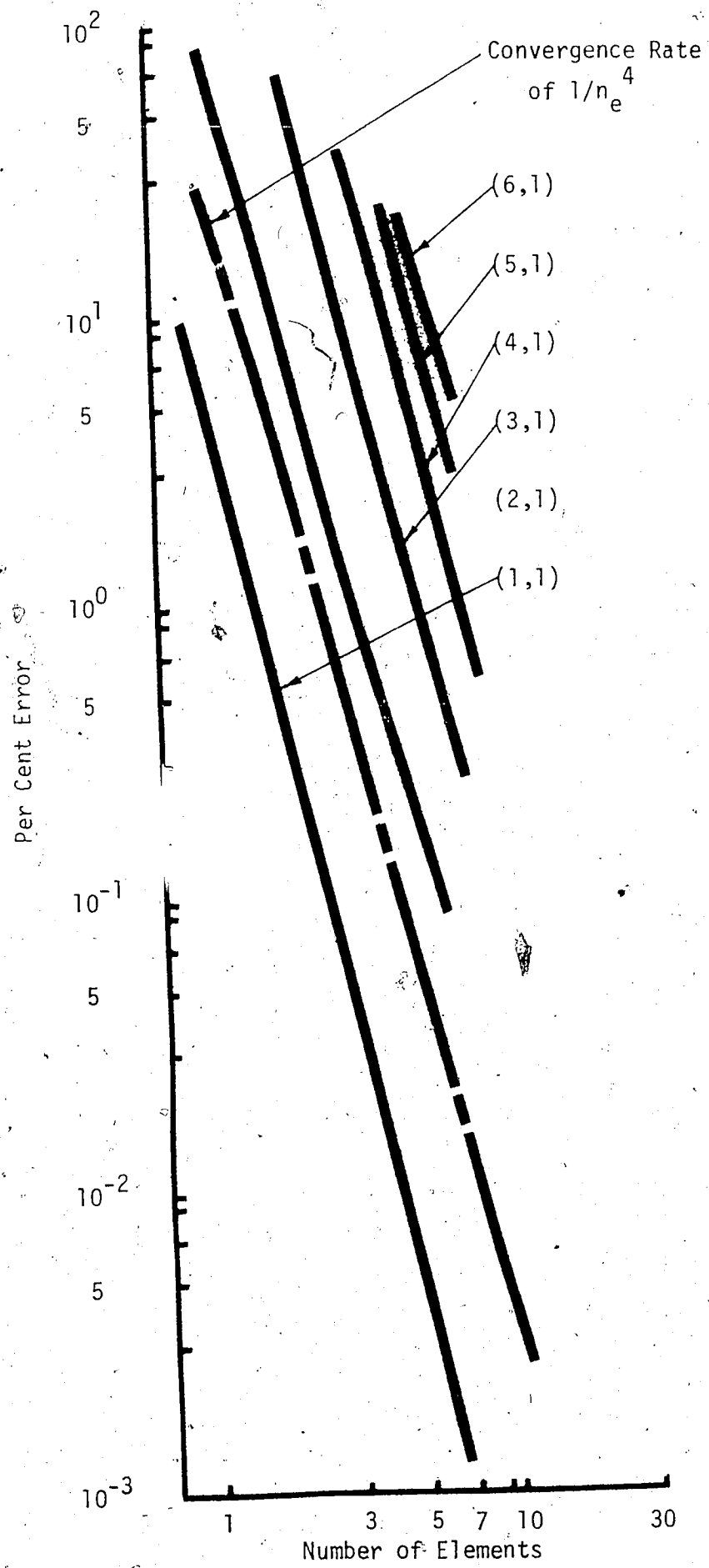


Figure 2.5 CONVERGENCE OF LINE PLATE ELEMENT (n=1)

ρ_p , h_p and D were picked so the coefficient in front of the natural frequency equation was unity, i.e. $\omega^2 = (r^2 + k^2)^2$.

There is no similar formula to (2.8) that can be easily derived for a plate system so the plots of percentage error versus number of elements are given for both $k = 0$ and $k = 1$ (Fig. 2.4 and Fig. 2.5, respectively). The initial approximation in some modes are about 60 per cent in error in the square of natural frequency (8 per cent in the natural frequency). This is not good, but fortunately a slightly higher number of elements gives accuracy of 2 per cent in the lower natural modes. These lower modes will be used in the study of sound transmission. It may also be noted that the results of the theory are integers close to unity for which the error associated with truncation could be significant. Later results tend to bear this up.

The plate element, as developed, was effectively a beam. Independently they can be used to study the vibration of rectangular plates with two parallel pinned boundaries while the other two boundaries can have any combination of free, fixed or pinned boundary conditions. Warburton [25] has produced a very comprehensive analytic paper on such plates. Melosh, Papenfuss, Clough, Adini and Tocher have produced [21] similar plate elements of more general application so the use of the plate elements will be left for the coupled system.

2.5 Application of Acoustic Elements

2.5.1 Odd Shaped Room

A problem was required to test a combination of triangular

and rectangular acoustic elements. The Mechanical Engineering Building on the University of Alberta campus, which was under construction at the time, had a reverberation room which offered an excellent model. Being placed directly under a sloped roof section, required that one half of the room have a sloped ceiling. The exact profile of the room is shown in Fig. 2.6 (c), its depth being 22.0 ft.

One problem, exemplified by this room, is what boundary conditions exist at a corner such as shown in Fig. 2.6 (a). Any node along the sloped edge has the boundary condition

$$\frac{\delta p}{\delta x} = - \cot \eta \frac{\delta p}{\delta y} \quad \text{or} \quad \frac{\delta p}{\delta y} = - \tan \eta \frac{\delta p}{\delta x}$$

while along an upright edge

$$\frac{\delta p}{\delta x} = 0$$

Right at the corner node, there is a discontinuity, as there would be in a mathematical analysis (unless certain transforms were undergone). Using finite element methods there are three logical possible choices of how to approximate this boundary condition as shown in Fig. 2.6 (b). The first two are not correct, but on element refinement they will converge to nearly the correct result. This occurs by virtue of the fact that as the elements get smaller the effect of the elements containing the incorrect nodal value diminishes

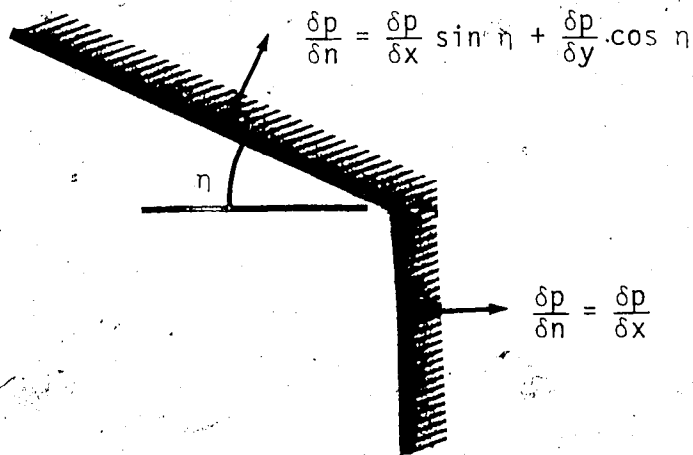


Figure 2.6 (a) CORNER DISCONTINUITY

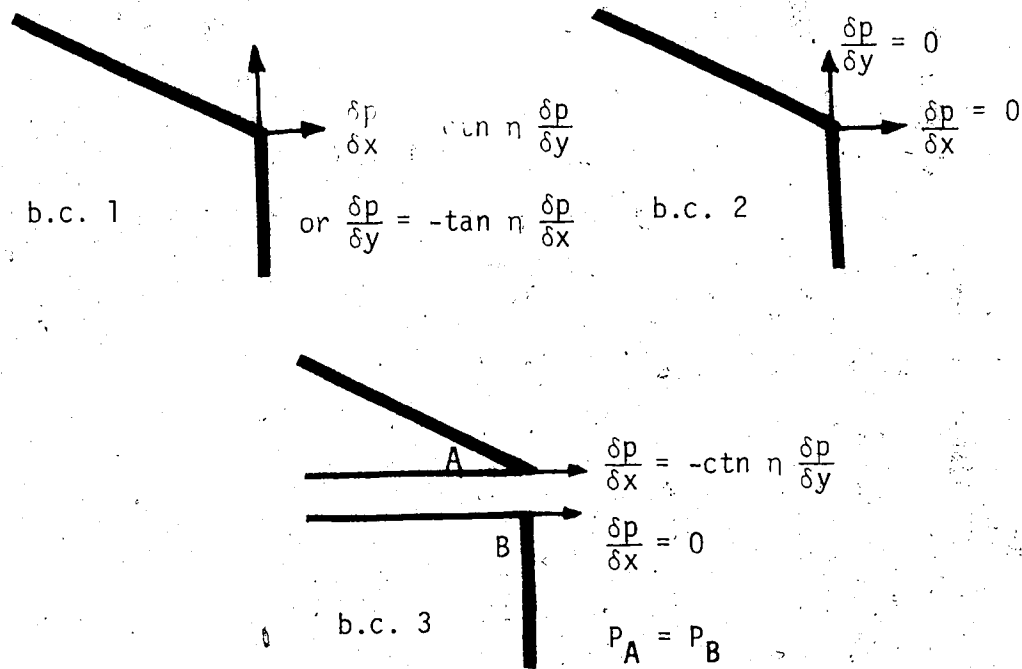
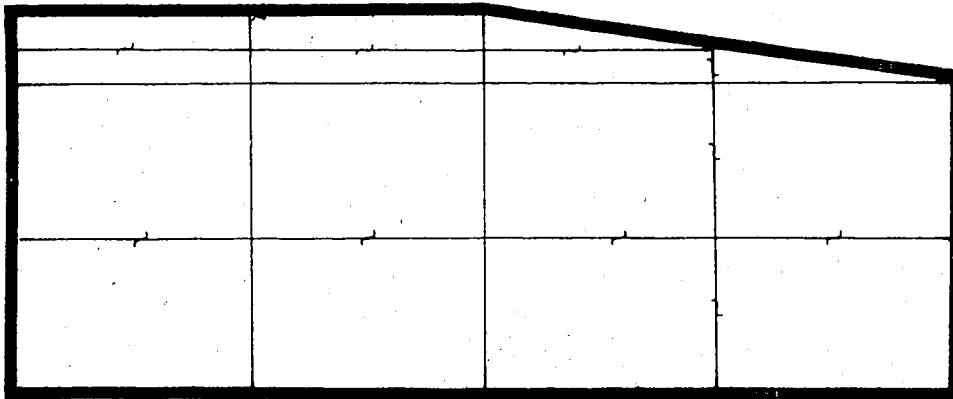


Figure 2.6 (b) APPROXIMATING BOUNDARY CONDITIONS



Scale: 1 in. = 6 ft.

Depth: 22 ft.

————— coarse grid

————— 1st grid refinement

Figure 2.6 (c) FINITE ELEMENT GRIDS

Figure 2.6 SLOPED CEILING REVERBERATION CHAMBER

Table 2.1 CONVERGENCE OF FOUR LOWEST EIGENVALUES
FOR SLOPED CEILING REVERBERATION CHAMBER

Segmentation of Sloped Edge (No. of Parts)	Corresponding (x,y,z) Mode Shape to That for a Rectangular Room			
	(0,0,1)	(1,0,1)	(2,0,1)	(0,1,1)
1	.02039	.03274	.06710	.08987
2	.01976	.03215	.06766	.09128
3	.01992	.03202	.06724	.09027
Exact Results for 22 x 29 x 12 Rect. Room	.02040	.03212	.06730	.08895

in terms of the overall acoustical kinetic and strain matrices. Method 3 could converge to the exact result, but it entails larger partitioning operations on the overall matrices (described in Appendix C2) and is therefore more prone to numerical divergence. If looked at from a potential energy viewpoint, 1 and 2 are respectively slightly weaker and slightly stronger than the correct boundary condition 3 giving respectively lower and higher eigenvalues than 3 for any particular grid configuration. Since the approximate solution converges on the exact solution from above, it was deemed interesting to see the effect on convergence of using boundary condition 1. Because of its "relaxing" effect on the overall energy matrices, it is reasonable to assume that for a relatively coarse grid pattern, boundary condition 1 will give eigenvalues closer to the exact solution than a finer grid using the other boundary conditions. The concept of "flexibility" of a system is quite often used to describe deviation from classical results. A more flexible system has less ability to store strain energy and thereby results in a lower natural frequency.

Grid patterns for the coarse grid and refined grid are shown superimposed on one another in Fig. 2.6 (c). There were other grids used including a finer one that divided the sloped surface into three equal sections, but these would only complicate the figure given. The effect of boundary condition 1 is most exemplified for the coarse grid where the entire slope edge has the "relaxed" boundary condition. For computational convenience c , the velocity of sound, was taken as unity.

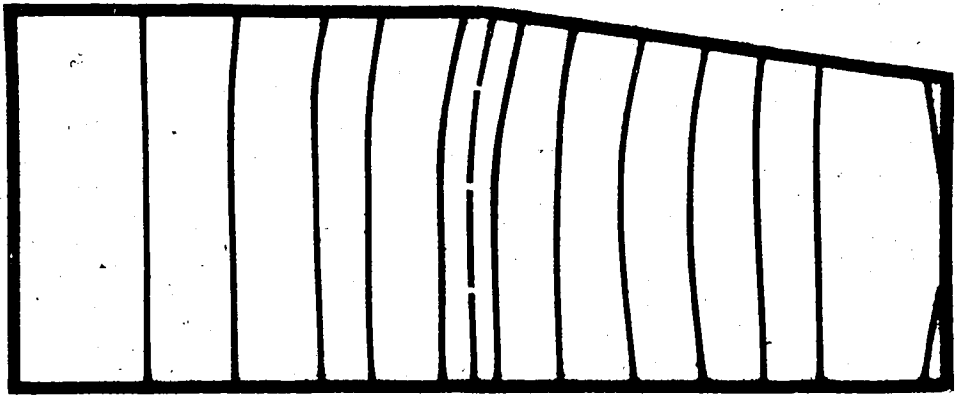
By close examination of each column of Table 2.1 it is easily

seen that the results for the slope ceiling room are very close to the exact solution for a hard rectangular room that would bound the reverberation room. This is logical since the reverberation room does not deviate much from the classical rectangular form. Column one shows the $(0, 0, 1)$ mode, which is independent of the actual profile of the room, and should therefore converge exactly to the classical result. In accordance with the energy approximation method, the results actually start higher than the correct value, drop below, then start upwards again. This can be explained by the "flexibility" of the structure; the more "flexible" the structure, the lower the eigenvalues. Initially the grid was not flexible enough to approximate the mode shape, but after the first refinement the structure became overly flexible because of b.c. 1. Ensuing refinement would lead to closer convergence because the system has sufficient flexibility to closely approximate the mode shape, while each further subdivision of the sloped ceiling lessens the effect of b.c. 1 (until one enters the region where numerical errors become significant). Similar analysis can be done on the remaining three columns, noting that the sloped roof has almost no effect on the $(x, 0, 1)$ modes but is quite important in the $(0, y, 1)$ modes.

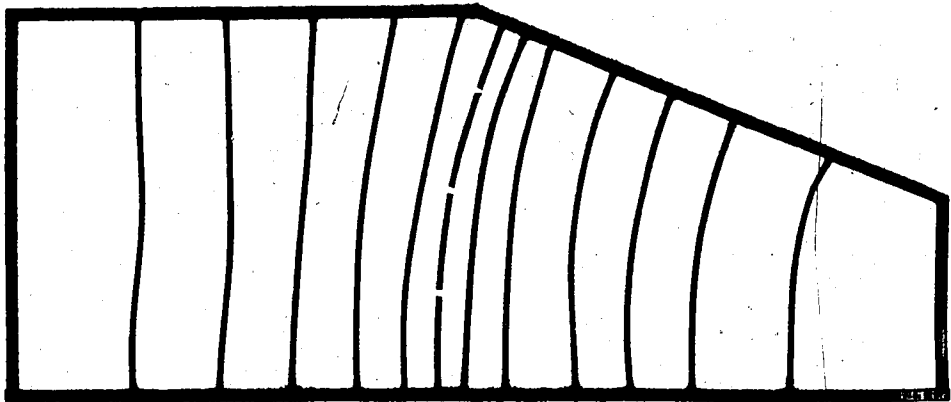
Figures 2.7 through 2.9 show the principal mode shapes of three rooms of different dimension but with the same basic shape. The (a) figures are the actual profiles for the reverberation chamber, whereas the (b) and (c) figures show the changes due to substantially increasing the effect of the sloped wall on the x-direction and x-y directions, respectively. The points of no pressure variation

within the room are of importance when making sound measurements. For a hard rectangular room the zero-pressure nodal line occurs at positions that are simple fractions of the overall dimension, i.e. $1/2$, $1/3$, etc. Figure 2.7 shows how the zero-pressure node line deviates from the classical position for a rectangular room. The narrowing of the enclosure at one end changes the volume distribution as well as causing localized compression and rarefaction of the sound wave near the roof. A wave travelling in the x-direction, is given an unbalanced y-component of force, tending to bend it into a path where uniform compression (or rarefaction) occurs on both ceiling and floor. In Fig. 2.7 the reflection off the narrow end wall, floor and ceiling, at non-zero angles of incidence, causes "focusing" of the pressure waves in the lower right-hand corner of the room, giving maxima in pressure levels in this region.

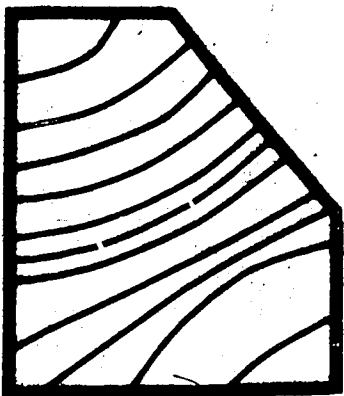
Figure 2.8 is actually very similar to Fig. 2.7 except there are now two node lines, i.e. two maxima and a minima, that are substantially affected by the sloped roof. It is interesting that the maxima along the full height wall in Fig. 2.8 moves from the lower left to upper left corner as the slope angle of the roof, η , becomes more than 45° . Figure 2.8 (c) has a higher eigenvalue than Fig. 2.9 (c) so it could be said that the diagram ordering is incorrect, but it is of greater interest to show the development of a mode shape.



(a)



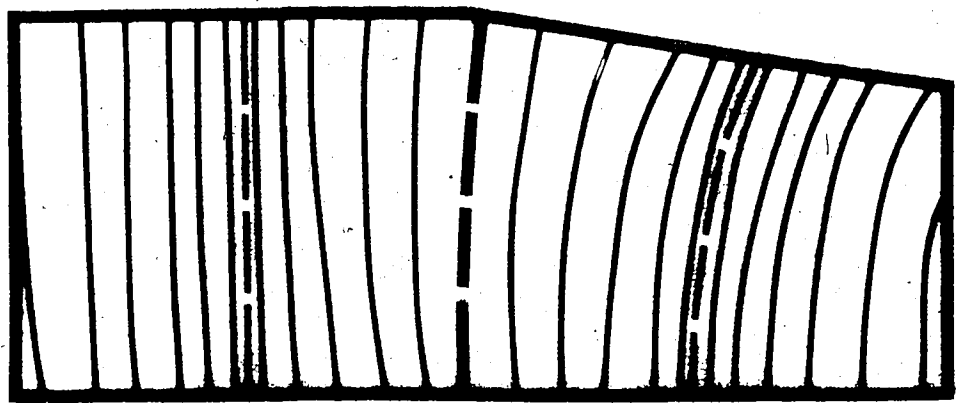
(b)



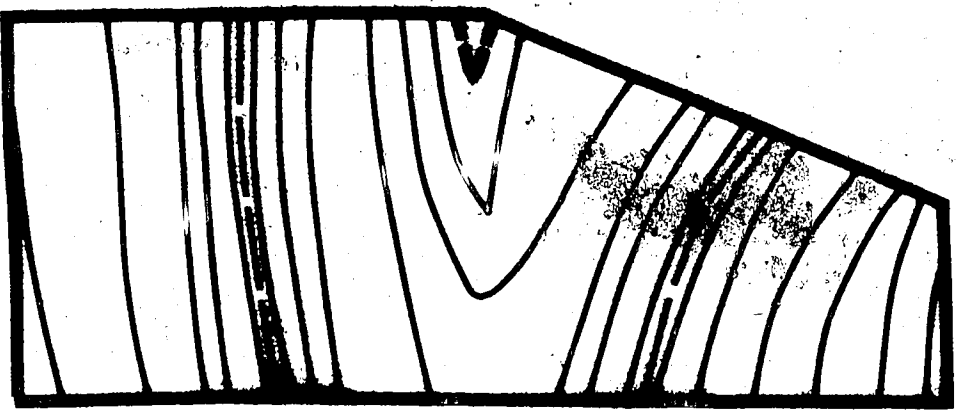
(c)

Scale: 1" = 6'
Isobar
Absolute Minima

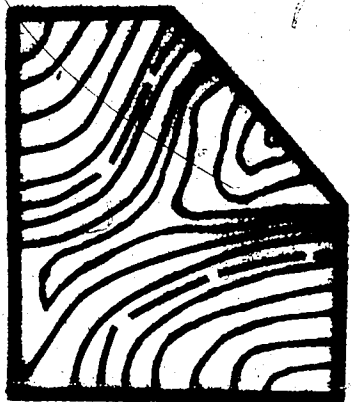
Figure 2.7 FIRST MODE - ROOMS WITH SLOPED CEILING



(a)



(b)

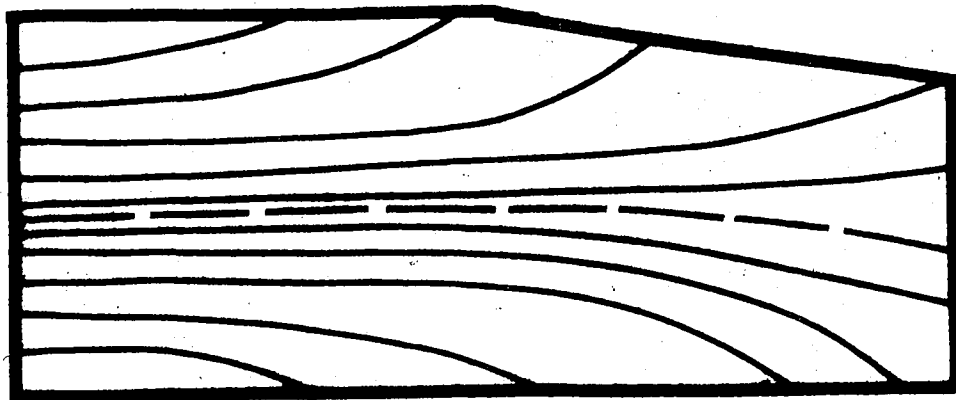


(c)

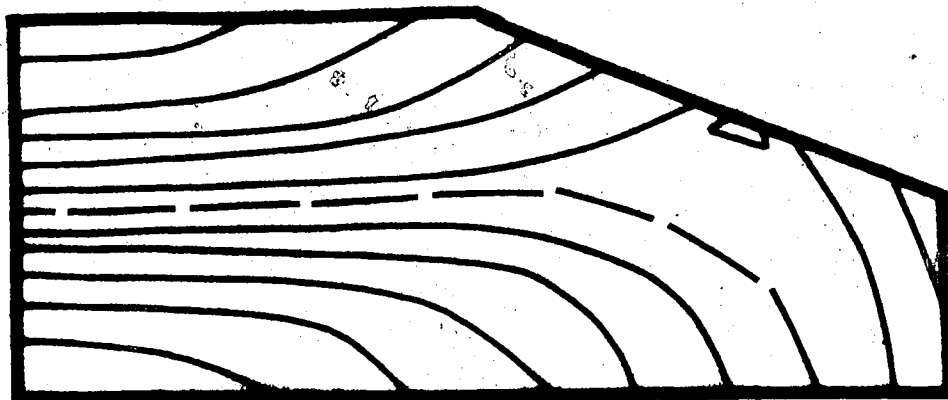
Scale: 1" = 6'

- Absolute Maxima
- Isobar
- Absolute Minima

Figure 2.8 SECOND MODE - ROOMS WITH SLOPED CEILING



(a)



(b)



(c)

Scale: .1" = 6'

Isobar

Absolute Minima

Figure 2.9 THIRD MODE - ROOMS WITH SLOPED CEILING

CHAPTER III

COUPLED ELEMENTS

The elements produced thus far have their independent applications, but have not yet been intercoupled, i.e. a displacement of the plate must cause a pressure change in the fluid and vice versa.

3.1 The Coupling Matrix

Former work by Warburton [26] and Pretlove [27] approached coupling by using the exact acoustic equation with a normal mode representation of the plate. Zimmerman and Gladwell [28] did a very complete treatment of coupled plate-acoustic systems, but encountered difficulties because they formulated the acoustic and plated elements entirely in terms of displacement or force quantities which, if nothing else, cause conceptualization problems. Using the pressure acoustic formulation and the displacement plate formulation described by Mason [29, 30] and the coupling concept advanced by Craggs [31], the ensuing formulation is easily conceptualized and relatively efficient.

To satisfy equilibrium, the forces due to the flexed panel and the pressure distribution over the surface area of the plate must be conserved. Terms whose first variation satisfies the boundary condition at the interface must be included in the respective functionals. This boundary condition is simply that the normal velocity of the fluid must be the same as the transverse velocity of the plate over the entire plate surface.

$$\dot{w} = \dot{\underline{u}} \cdot \vec{n}$$

where $\dot{u} \cdot \vec{n}$ is the normal velocity component of the fluid. By differentiating with respect to time and using equations (A8) and (A11)

$$\text{grad } p_1 \cdot \vec{n} = -\rho \ddot{w}_p = -\rho \text{grad } \dot{\phi} \cdot \vec{n} \quad (3.1)$$

where ρ is the acoustic density and ϕ , of course, is the velocity potential. Recalling the form of the acoustic functional, and adding to it a term whose first variation with respect to ϕ satisfies the dynamic boundary condition

$$J = \int_{t_1}^{t_2} \frac{\rho}{2} \left[\iiint_V \{ \text{grad } \phi \cdot \text{grad } \phi - \frac{\dot{\phi}^2}{c^2} \} dV - \iint_{S_c} \rho w_p \dot{\phi} dS_c \right] dt$$

where S_c is the interface surface. This last term can be physically interpreted as the pressure displacement work, B_a , at the coupling interface

$$B_a = - \iint_{S_c} \rho \dot{\phi} w_p dS_c = + \iint_{S_c} p_1 w_p dS_c \quad (3.2)$$

It must have a stationary value and satisfy the dynamic boundary conditions. This can easily be seen by following the procedure of Appendix A3 including the extra term.

The energy added to (or extracted from) the acoustic element in the form of work, must come from (or go to) the adjacent plate element. Therefore, the work term must occur in the energy equations for the plate, but with the opposite sign. External forces, other than the acoustic pressure, can act on the plate elements but they will be excluded from this study because it is the free vibration problem which is of interest.

To form the coupling matrix proper, Θ , it is now necessary to recall the approximations for pressure and displacements used in Chapter II.

$$p_e = \{f(x^*) \ f(y^*)\}^T \{p_n\} \cos \frac{n\pi z}{d} \quad (3.3)$$

where

$$x^* = x/a$$

$$y^* = y/b$$

for the rectangular acoustic elements

$$p_e = \{g(x', y')\}^T \{p_n\} \cos \frac{n\pi z}{d} \quad (3.4)$$

where

$$x' = \frac{\epsilon + b}{a + b}$$

$$y' = \frac{\eta}{h}$$

for the triangular acoustic element. Note the coordinate system indicated here is the localized system because this will be the system

the plate will be associated with initially.

$$w_p = \{f(\ell^*)\}^T \{w_n\} \sin \frac{k\pi z}{d}$$

where

$$\ell^* = \frac{\epsilon}{l_p} \quad 0 \leq \epsilon \leq l_p$$

Depending on the element to be coupled to the plate element, one of the two pressure approximations will be used. The pressure formulation for the rectangular acoustic elements will be used in the following excursion because the experiments and examples to follow are based on this element.

$$B_a = \iint_{S_c} p_1 w_p dS_c$$

For this example, assume that the line plate element is coupled to edge 1 - 3 of Fig. 2.1 (a) where y and y^* are identically zero. Also, $\ell^* = x^*$ and $\epsilon = x$, respectively. So

$$B_a = \{p_n\}^T \left[\int_0^1 \{f(x^*) f(0)\} \{f(x^*)\}^T dx^* l_p \right. \\ \left. \cdot \int_0^d \cos \frac{m\pi z}{d} \sin \frac{k\pi z}{d} dz \right] \{w_n\}$$

where Θ_{rect} is the integral within the square brackets.

The integrals with respect to x^* can be found in Appendix B2, while the integrals with respect to z are in Appendix B1.

Careful examination of Appendix B1 shows that the integrals are taken over one-half harmonic interval. This alters the orthogonality of the sine - cosine product from the standard full interval form of Fourier [32], whereas the sine - sine and the cosine - cosine product integrals are unchanged. It is obvious then when $n + q$ is an even sum of integers, there is no coupling integral produced by this method. This would tend to indicate that in the z -direction an odd order acoustic mode would be driving an even order plate mode or vice versa. This is readily explained in such a coupling situation because for $n + q = \text{even integer}$, the net $p - v$ work is zero giving an unexcitable configuration.

The integrals with respect to x^* ($y^* = 0$) were for coupling for side 1 - 3 of the rectangular element. These integrals will alter when another edge of the element is used, i.e. $y^* = 1$, $x^* = 0$ or $x^* = 1$ but all can be handled by the aforementioned Appendices. The coupling formulation for a triangular acoustic element is the same; substitute (3.4) and (3.5) in equation (3.2) and multiply out the entries of matrices for a surface. Because of the random orientation in the $x - y$ plane of any edge, it is exceedingly difficult to do the ensuing line integrals. It is initially chosen that the surface to be coupled, is co-incident with the localized x -axis, as shown in Fig. B1. The integration can then be performed with relative ease as a form of

$$(a + b) \int_0^1 x^{*m} f(x^*) dx \quad m = 0, 1, 2, 3$$

$$x^* = \frac{x + a}{a + b}$$

These integrals can be done by hand (some of which are shown in the latter parts of Appendix B2). The resulting localized coupling matrix $[\theta]_{\text{TRI}}'$ must be rotated by pre-multiplying by an acoustic rotational matrix $[\theta]_a$ and post-multiplying by a plate rotational matrix $[\theta]_p$ before it can be placed in the overall coupling matrix.

$$[\theta]_{\text{TRI}} = [\theta]_a^T [\theta]_{\text{TRI}}' [\theta]_p$$

This completes the formulation of the coupling matrix.

Including the present discussion, the coupled energy functionals J_a and J_p , for the overall system can be written from equations in Appendix A4 and Chapter 2, Section 4.

$$J_a = \int_{t_1}^{t_2} \left\{ \frac{\rho_a}{2} \{\dot{\phi}\}^T [S] \{\dot{\phi}\} + \frac{\rho_a}{2} \{\dot{\phi}\}^T [P] \{\dot{\phi}\} - \rho_a \{\dot{\phi}\}^T [\theta] \{w_p\} \right\} dt$$

$$J_p = \int_{t_1}^{t_2} \left\{ \frac{1}{2} \{\dot{w}_p\}^T [M] \{\dot{w}_p\} + \frac{1}{2} \{w_p\}^T [K] \{w_p\} \right.$$

$$\left. + \rho_a \{\dot{\phi}\}^T [\theta] \{w_p\} \right\} dt$$

Noting that $p = \rho \dot{\phi}$

By taking the first variation of both functionals (the first with respect to ϕ and the second with respect to w_p) and equating them to zero, the coupled equations of motion can be arrived at. To give more physical significance to $\delta J_a = 0$, this functional variation should be differentiated with respect to time and the pressure formulation substituted. Then,

$$[P] \{\dot{p}\} + [S] \{p\} - [\Theta] \{\ddot{w}_p\} = 0 \quad (3.6)$$

$$[M] \ddot{w}_p + [K] \{w_p\} + [\Theta]^T \{p\} = 0 \quad (3.7)$$

These equations of motion are for a coupled plate-acoustic system with no external force $\{\bar{F}\}$ acting on the plate elements. These external forces could be included by simply placing them in nodal form on the right hand side of (3.7). $\{p\}$ and $\{w\}$ can take any time function desired, so random vibration studies could easily be undertaken. A finite difference approach could be used for stepping through time.

Since this is a steady-state study, this discussion will not be pursued. Equations (3.6) and (3.7) can be written in a more compact matrix form

$$\begin{bmatrix} \Theta^T \\ 0 \\ S \end{bmatrix} - \omega^2 \begin{bmatrix} M & 0 \\ -\Theta & P \end{bmatrix} \begin{Bmatrix} w_p \\ p \end{Bmatrix} = 0$$

where the steady-state time function has been considered to have a frequency ω . The square brackets around the entries have been dropped for

convenience. This equation can be used in eigenvalue solutions but the matrices are unsymmetric, therefore, computation becomes tedious even by numerical methods. Irons [33] advanced an approach that makes these matrices symmetric. By partitioning the matrices and performing some basic matrix operations giving

$$\left\{ \begin{bmatrix} K & 0 \\ 0 & P \end{bmatrix} - \omega^2 \begin{bmatrix} M + \theta S^{-1} \theta & -\theta^T S^{-1} P \\ -P S^{-1} \theta & P S^{-1} P \end{bmatrix} \right\} \begin{pmatrix} w_p \\ p \end{pmatrix} = 0$$

The result is symmetric due to the symmetry of M, K, P and S. This approach is not exactly suitable to this situation, as the M, K matrices are of the order of one-tenth the size of the S, P matrices. To do the inversion of the S matrix would therefore be exceedingly time consuming, not to mention inaccurate (because of the small values of the entries in the matrix). Instead, the M matrix was inverted and Iron's basic procedure was followed giving

$$\left\{ \begin{bmatrix} K M^{-1} K & K M^{-1} \theta^T \\ \theta M^{-1} K & S + \theta M^{-1} \theta^T \end{bmatrix} - \omega^2 \begin{bmatrix} M & 0 \\ 0 & P \end{bmatrix} \right\} \begin{pmatrix} w_p \\ p \end{pmatrix} = 0$$

which again is symmetric and can be used for the eigenvalue problem more simply than its unsymmetric counterpart.

Initial checks were done on a simple coupled system; a cubical room with one flexible boundary (as shown in Fig. 3.1). To simplify things even further the flexible boundary was made almost rigid (i.e. plate eigenvalues are well above acoustic eigenvalues)

so as to deviate only slightly from the exact rigid room case. The computed results of the rigid boundaried room and the room with one slightly flexible boundary, are shown in Table 3.1, along with the exact results for a "rigid" room. The acoustic element is the same grid for both computed cases.

There are two noteworthy items in the results. First, when searching for an exact zero eigenvalue, the IBM eigenvalue - eigenvector routine NROOT sometimes gives a negative result. This is unrealistic for the positive definite problems for which this numerical method is designed. These negative roots must be considered as a measure of the numerical error in the calculations. Secondly, in all cases, the eigenvalues are lowered by the introduction of the slightly flexible wall. Considering only the acoustic equation of motion, this would indicate a slight increase in the potential energy (associated with [P] matrix) with no effective change in the kinetic energy.

$$\omega_a^2 = \frac{\{\psi\}^T [S] \{\psi\}}{\{\psi\}^T [P] \{\psi\}}$$

where $\{\psi\}$ is a principal mode shape.

From this point on it can be said that there are no further independent plane modes, i.e. $(x, 0, 0)$, $(0, y, 0)$, $(0, 0, z)$ modes. This is indicated by the reduction of eigenvalues (square of natural frequency) for cases in which the plane wave is parallel to the flexible boundary. It can also be shown by inspection of the plate eigenvectors, which show deflected plate positions for the above mentioned case. The independent plane wave notation will still be used in

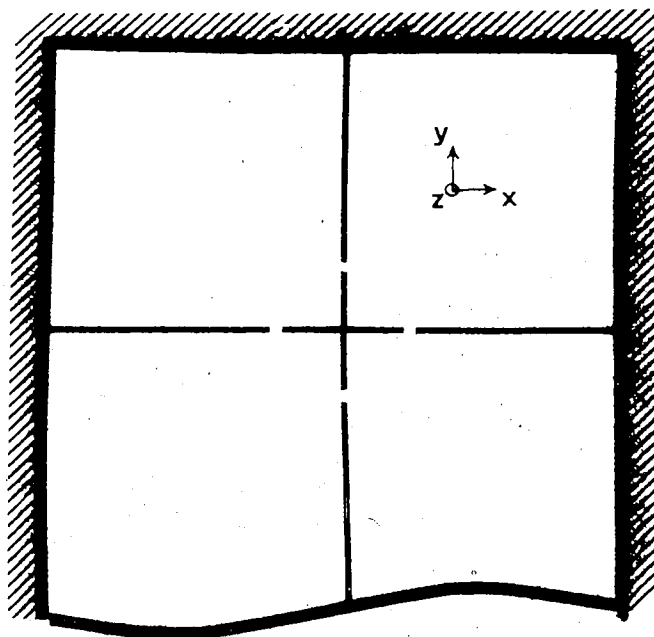


Figure 3.1 TEST ACOUSTIC MODEL

Table 3.1 RESULTS OF TEST MODEL

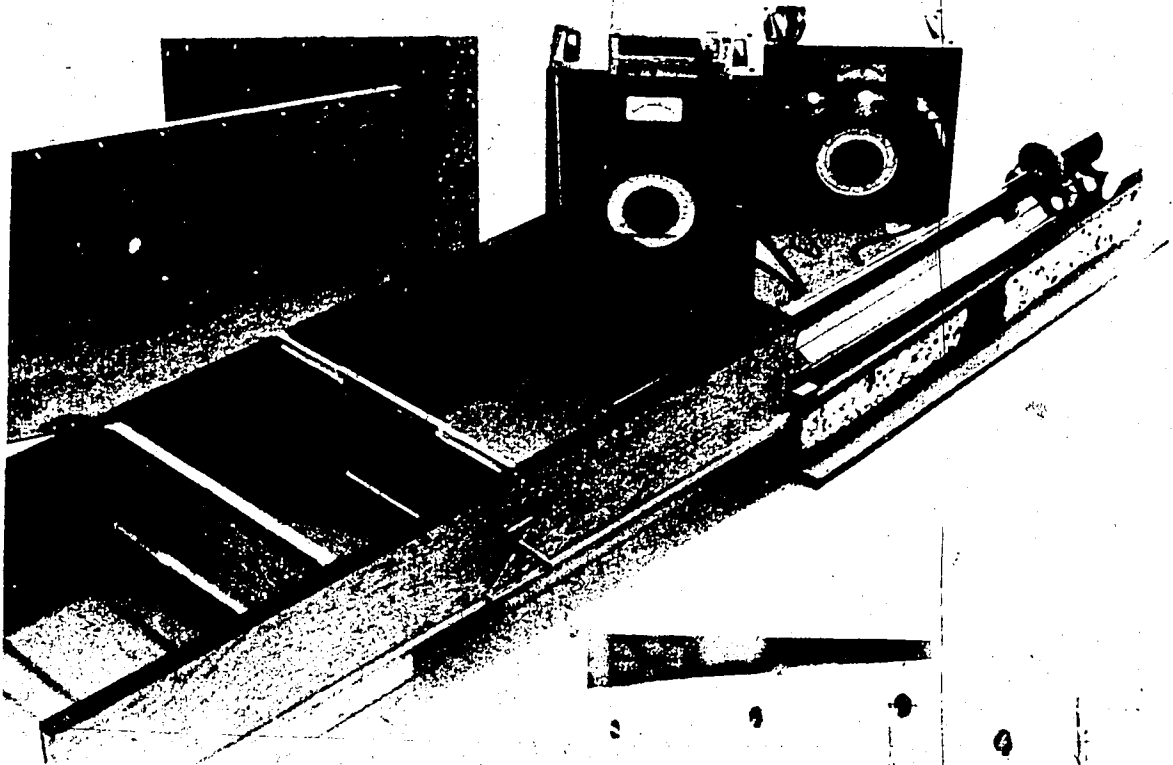
Equivalent Acoustic Mode (x,y,z)	Eigenvalues for a Rigid Room		Eigenvalues for Test Model
	Exact	Calculated	
(0,0,0)	0	-.000000	-.00141
(0,1,0)	9.86960	9.872300	9.70643
(1,0,0)	9.86960	9.872320	9.86831
(1,1,0)	19.73921	19.950510	19.93450
(0,2,0)	39.47842	39.529200	38.77500
(2,0,0)	39.47842	39.529300	39.52610
(1,2,0)	49.34802	49.401200	49.22090
(2,1,0)	49.34802	49.401300	49.36150
(2,2,0)	78.95684	79.058300	78.72000

following discussions, but only for descriptive purposes.

3.2 Sound Transmission Between Panel Coupled Rooms

The culmination of all foregoing work would be applicable in the study of plate-acoustic systems such as general floor areas (with a rigid floor and ceiling) enclosed by or containing flexible floor-to-ceiling panels. This is reasonably broad, and therefore the simple case of direct sound transmission between two rectangular rooms through a variable width floor-to-ceiling panel was carefully analyzed and checked. The widths of the rooms were left unchanged but the length of one room was altered. An experimental apparatus was constructed to approximate the theory. All "rigid" surfaces were made of 3/4 inch fir plywood capped on the inside surfaces with 1/8 inch masonite. A 4 inch speaker was attached to the source room, acoustically exciting the interior of the room through an orifice. Precision oscillators, frequency counters and pressure amplitude monitors were used to measure the standing wave patterns within the receiving and source rooms. The source room had fixed dimensions of 7 inches x 19 inches x 23 1/2 inches depth, while the receiving room had similar cross-sectional dimensions but of variable depth. The components of the apparatus are shown in Fig. 3.2 (a). Figure 3.2 (b) shows the "driver" for the source room as well as the basic hard wall construction of the rooms. Figure 3.3 shows the basic layout of equipment.

Detail "A" in Fig. 3.3 shows the mounting frame for the flexible plate. To approximate a zero deflection boundary condition, a length of 1/2 inch x 1/2 inch aluminum bar stock was accurately machined to



(a)



(b)

Figure 3.2 EXPERIMENTAL APPARATUS

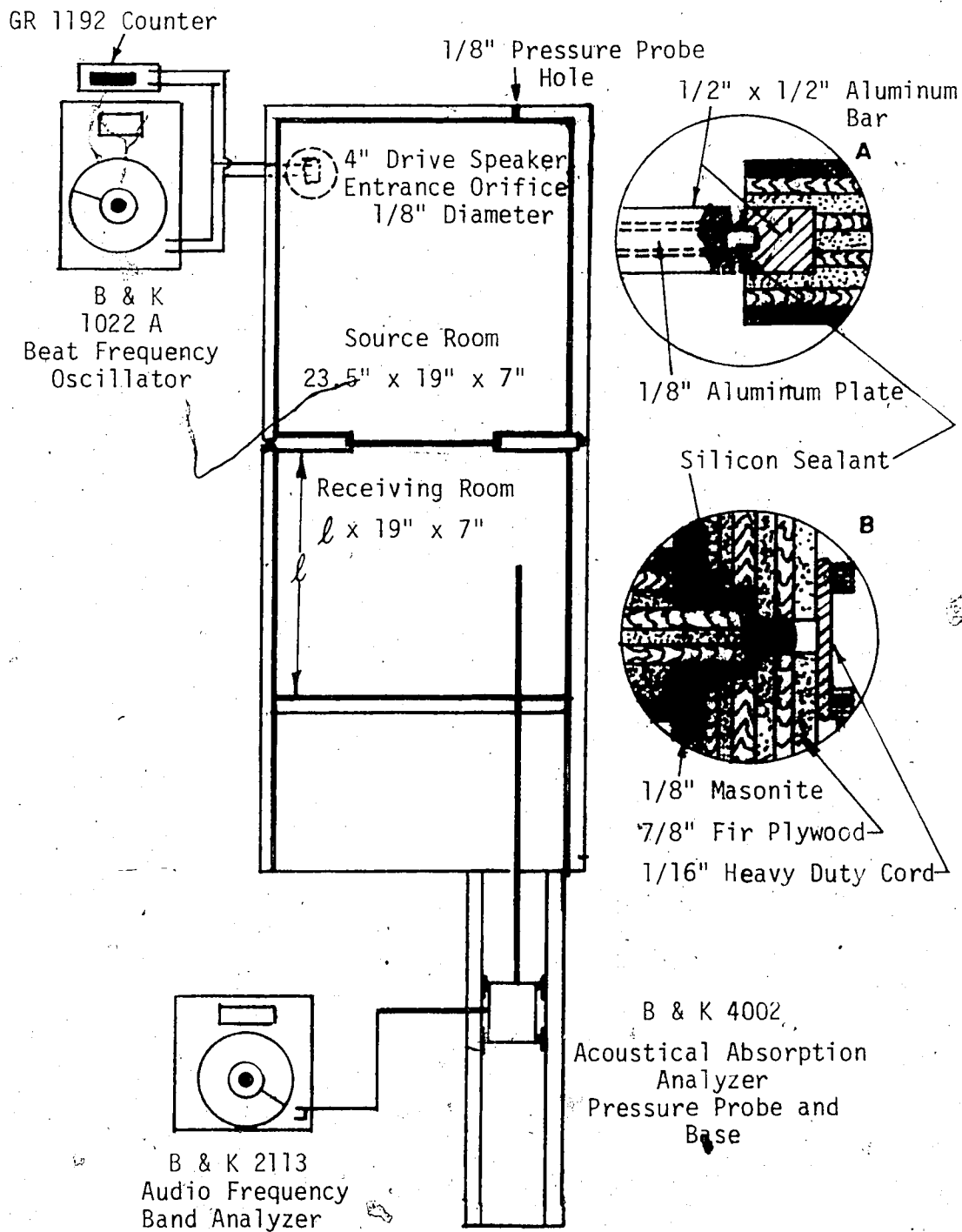


Figure 3.3 PICTORIAL LAYOUT OF COMPONENTS

accept all edges of a 1/8 inch aluminum plate to a depth of 1/16 inch. To assure no air leaks, the bar was carefully fitted to the rigid plywood wall and silicon sealant was used at all connections. Though not shown, the upper and lower bar stock rails were also fitted to the upper and lower panel with sealant. A well defined fixed or pinned boundary condition is not feasible by this construction. It was, therefore, necessary to give both the fixed and pinned analytical result.

Detail "B" is the edge connection between the rooms. Firstly, the rigid interior wall (or aluminum frame, depending on the flexible panel's width) was completely sealed to stop air leakage from one enclosure to another. The sealant and the saw cut isolated either room from structure-borne vibrations in the exterior walls of the other room. This eliminated a large amount of flanking transmission through the exterior boundaries which are not ideally hard. The cord binding, used to align the rooms and accurately seal the boundaries, was sufficiently limp to transmit a minimum amount of vibration. As will be seen in later results, this isolation was ineffective, in a few cases, but on the whole was very satisfactory.

On a more general scale, the entire apparatus was isolated from the laboratory tables by 3 inch foam mats. All boundaries where leaks could occur were either caulked and glued or temporarily caulked with silicon sealant. The holes for the pressure probe were sealed with brass plugs when not being used directly in tests.

It is of note that the various plates were chosen so that their fundamental modes were between 300 Hz and 500 Hz, which is well

within the range of the first few acoustic modes of either room, i.e. the plane standing wave parallel to the plate surface in the y-direction was $355 H_z$.

3.2.1 Theoretical Considerations

To obtain accurate values of ρ_p (plate density) and c (velocity of sound), careful measurements were made in the test laboratory. They are, respectively

$$\rho_p = .003217 \text{ slug/in}^3 \quad (\text{for aluminum})$$

$$c = 13,560 \text{ in/sec}$$

Other constants were accepted at their textbook values

$$\rho_a = 1.376 \times 10^{-6} \text{ slug/in}^3$$

$$E = 10.3 \times 10^6 \text{ lbf/in}^2 \quad (\text{for aluminum})$$

$$\nu = 1/3 \quad (\text{for aluminum})$$

These measurements proved to be valuable because the errors associated with published constants are of the same order as the errors due to the element approximation.

3.2.2 Results

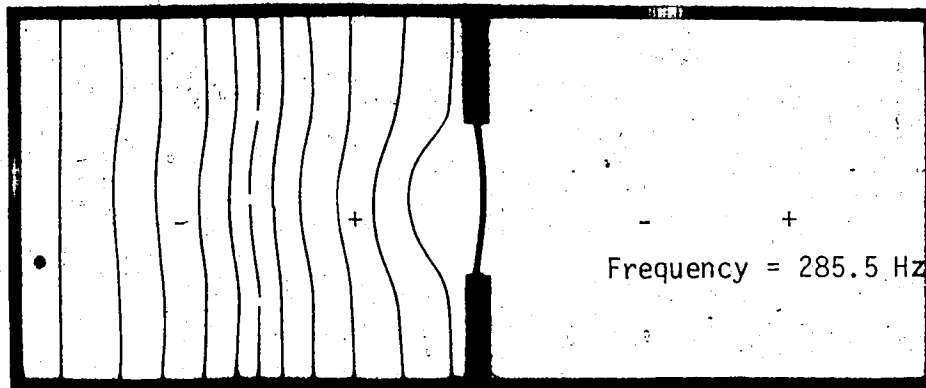
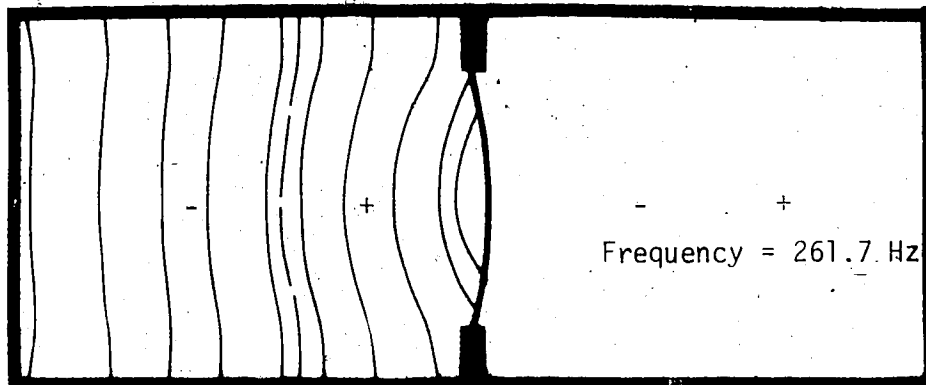
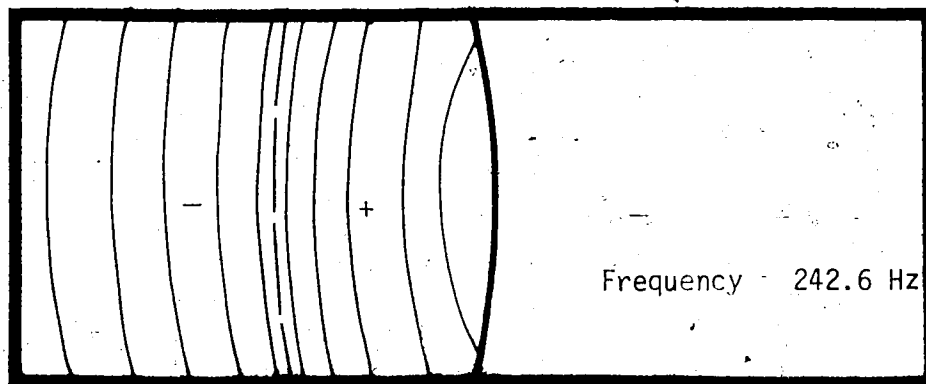
The description of results is broken into two parts:

- i) Effect of changing panel area and stiffness on unchanged room volumes.
- ii) Effect of changing length of receiving room on unchanged source room and panel.

Figure 3.4 through Fig. 3.8 are the five lowest non-zero modes for identical source and receiving rooms. Each of the diagrams in any given figure shows a different panel stiffness and surface area. These panels represent 100 per cent, 73.7 per cent and 42.5 per cent of the coupling wall, respectively. Because the rooms are symmetric about the panel, the principal mode shapes are symmetric, therefore, only one half of the mode shape will be plotted. The positive and negative signs indicate the relative pressures and rarefactions at any given instant. This particular configuration would be equivalent to being on the lines designated as "B" on Fig. 3.13 through Fig. 3.15.

These principal mode shapes can be roughly divided into acoustically and panel dominant types. The acoustically dominant modes are characterized by mode shapes and natural frequencies fairly close to the classical acoustic cases for a hard room. Figure 3.4 is an example of this type of mode. Figure 3.6 shows a panel dominant mode shape which has a natural frequency closely related to the "in vacuo" response for the panel and a highly disturbed acoustical mode shape. For each panel dominant mode there are two acoustical dominants.

Further inspection of the mode shapes show that the nodal lines (zero pressure lines) have moved towards the flexible panel for the acoustically dominant modes and away from the panel for the panel dominant mode. This can be explained in terms of "mass" and



————— Isobar

————— Nodal Line
(Zero Isobar)

Figure 3.4 FIRST MODE - SOUND TRANSMISSION
BETWEEN SYMMETRIC ROOMS

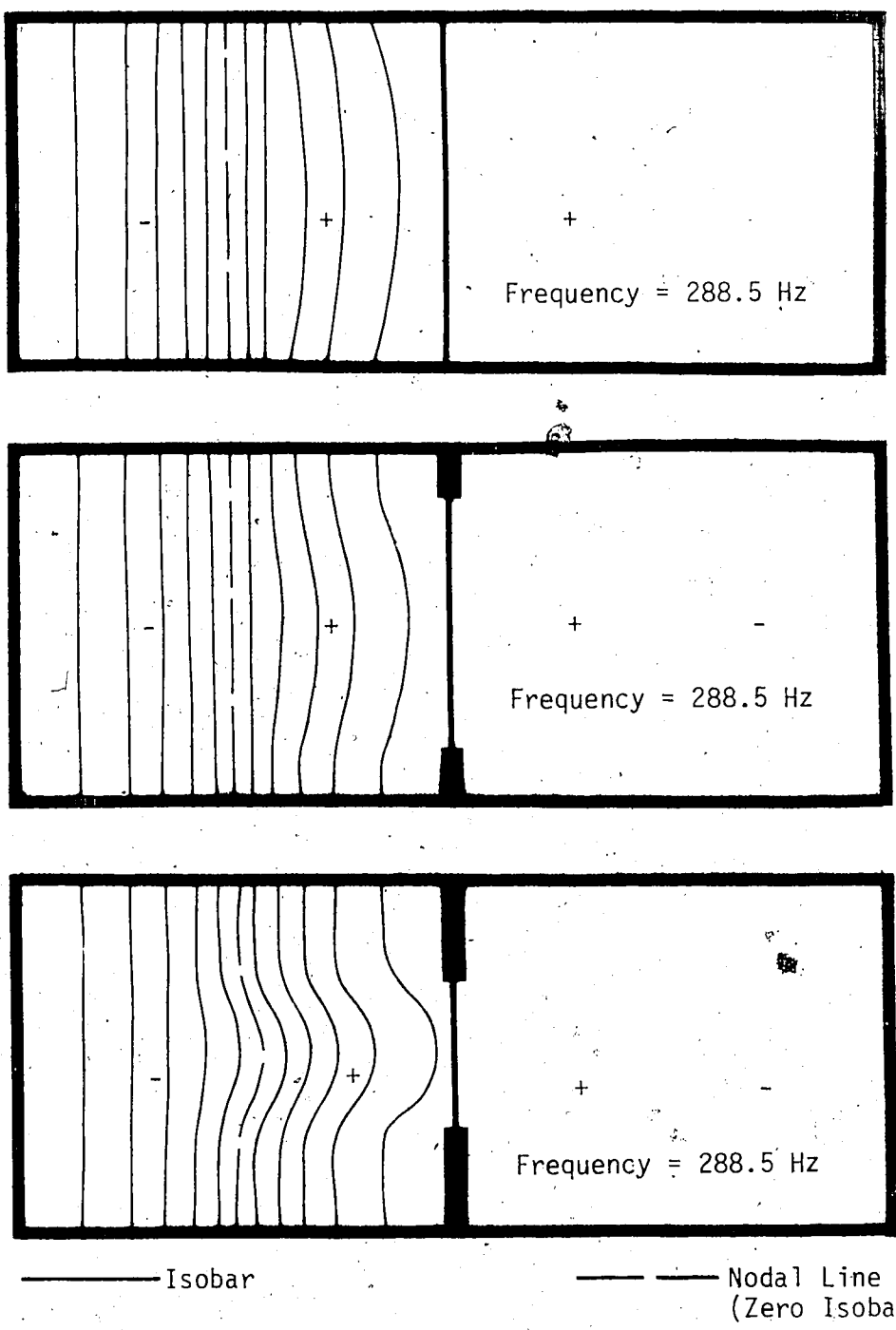
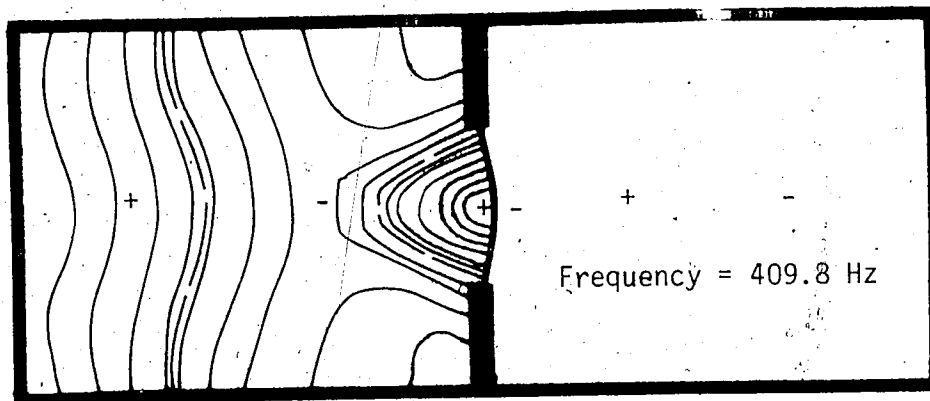
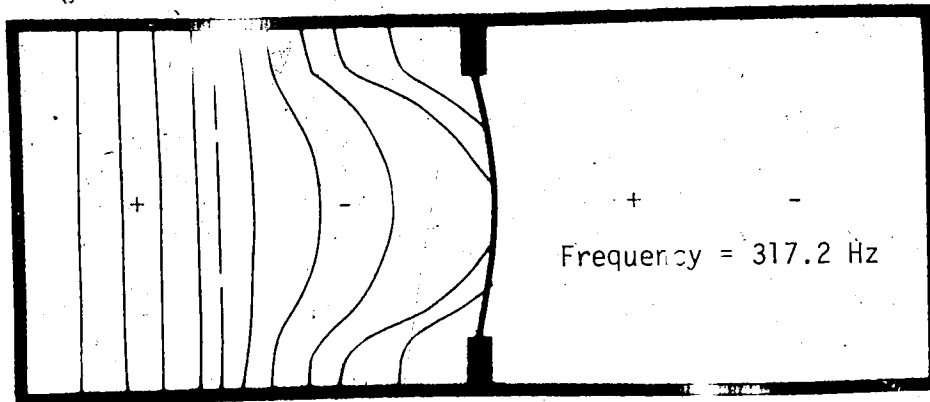
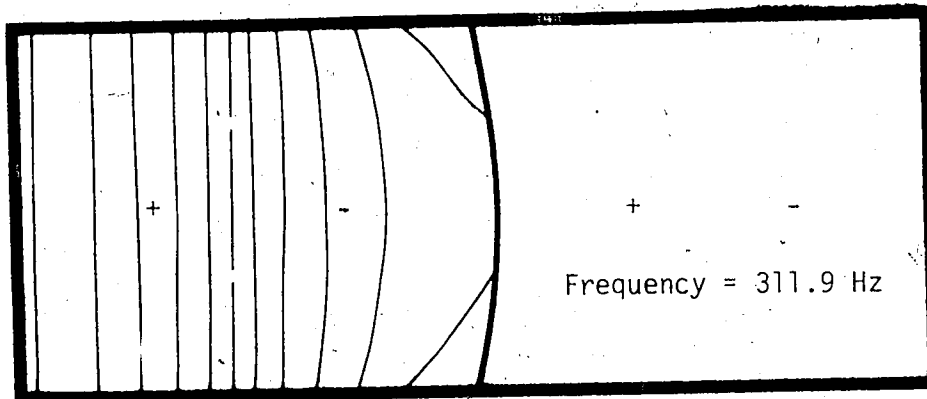


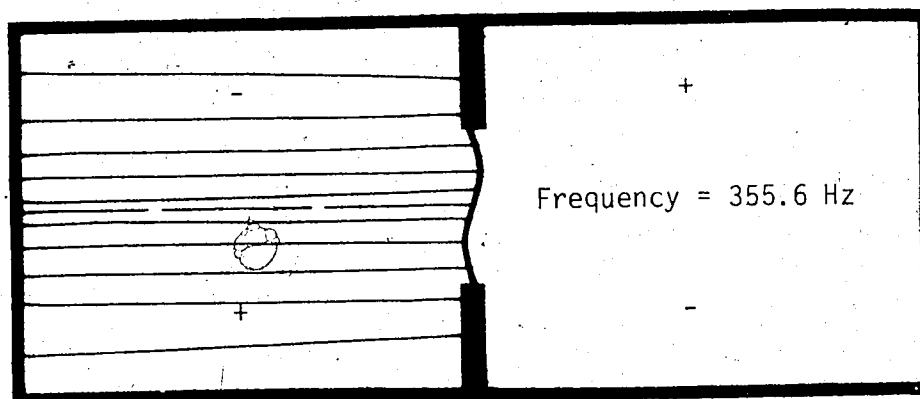
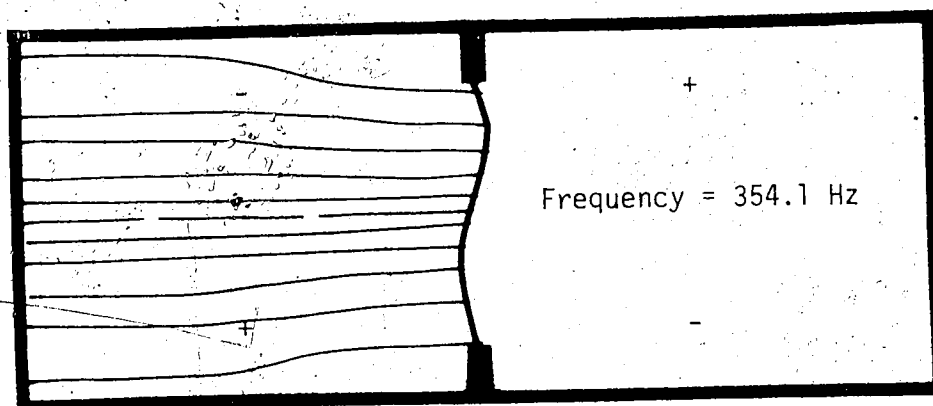
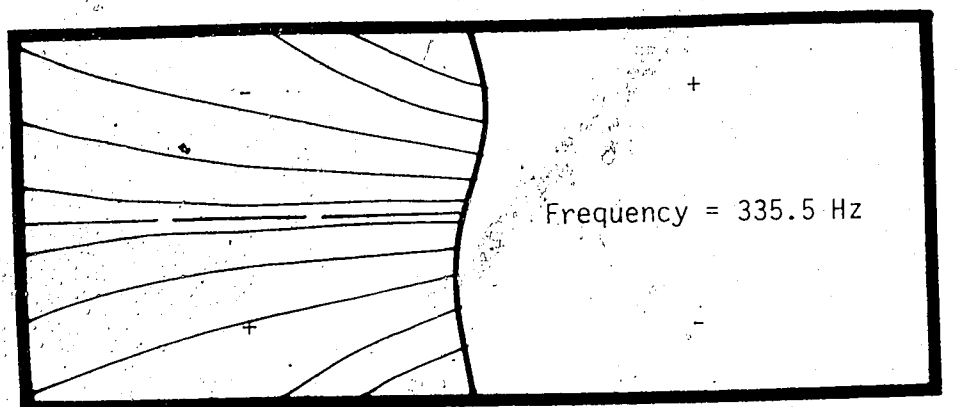
Figure 3.5 SECOND MODE - SOUND TRANSMISSION BETWEEN SYMMETRIC ROOMS



————— Isobar

————— Nodal Line
(Zero Isobar)

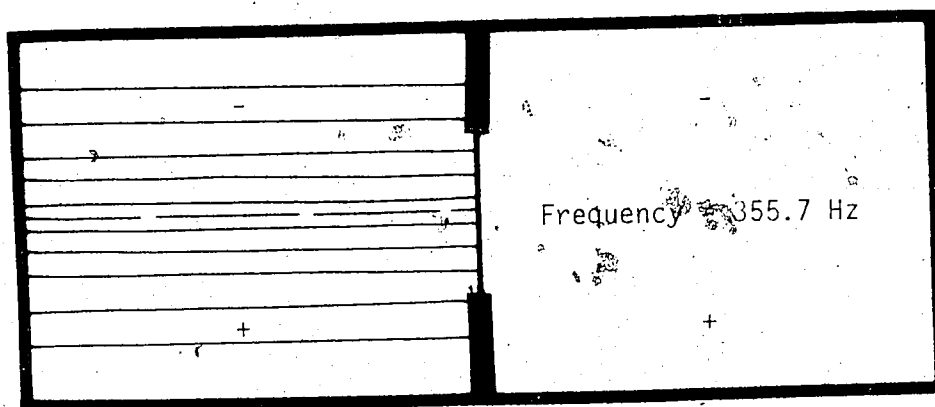
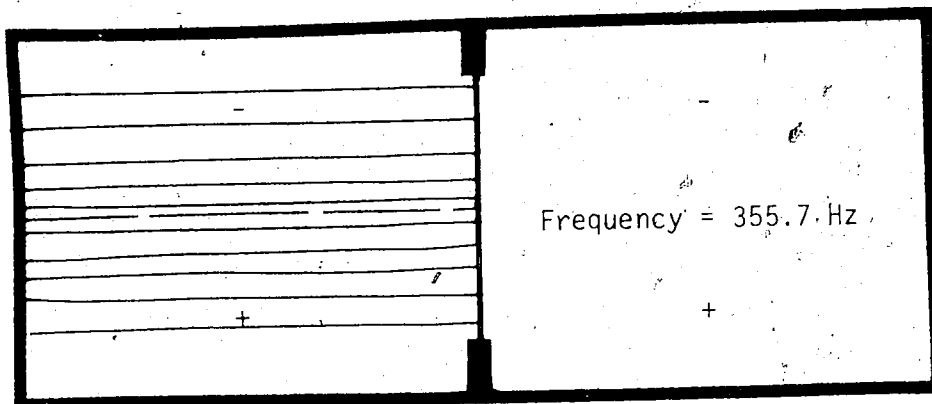
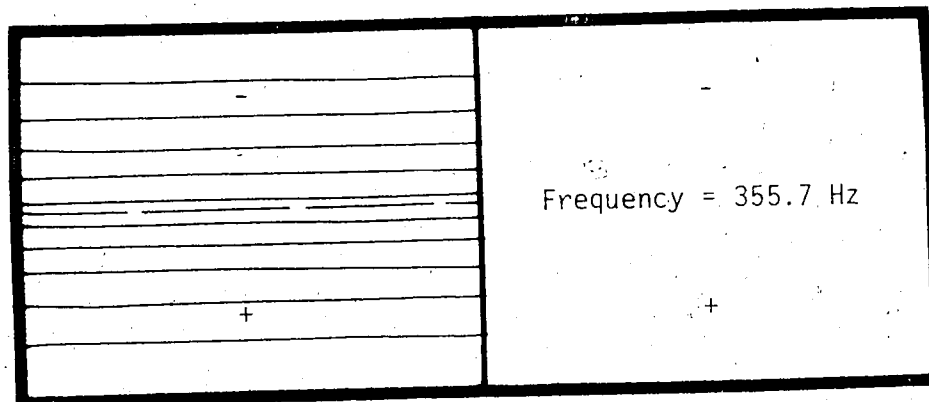
Figure 3.6 THIRD MODE - SOUND TRANSMISSION
BETWEEN SYMMETRIC ROOMS



————— Isobar

----- Nodal Line
(Zero Isobar)

Figure 3.7 FOURTH MODE - SOUND TRANSMISSION
BETWEEN SYMMETRIC ROOMS



————— Isobar

————— Nodal Line
(Zero Isobar)

Figure 3.8 FIFTH MODE - SOUND TRANSMISSION
BETWEEN SYMMETRIC ROOMS

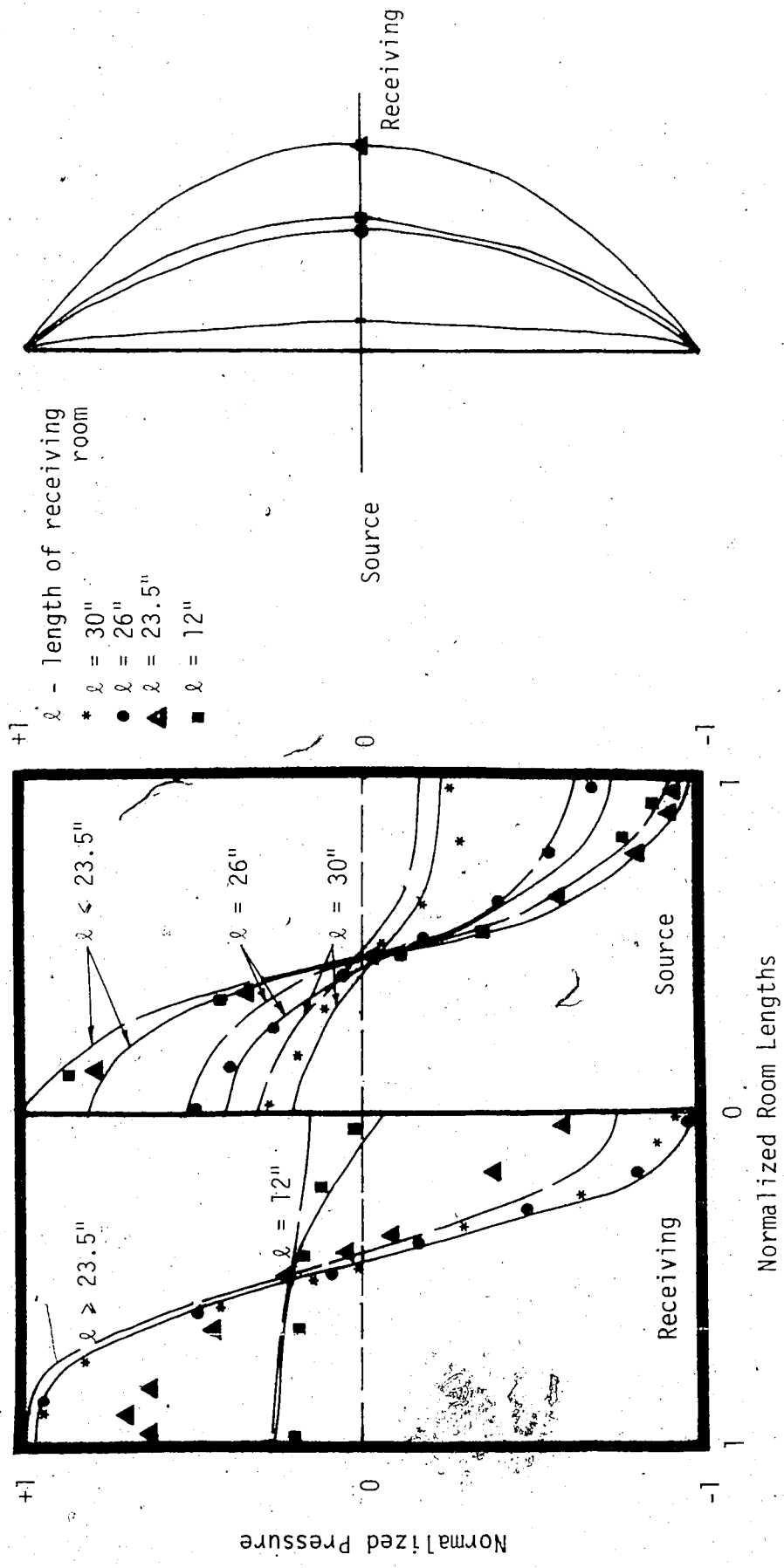


Figure 3.9 FIRST MODE - NORMALIZED LONGITUDINAL PRESSURE VARIATION AND PLATE DISPLACEMENT

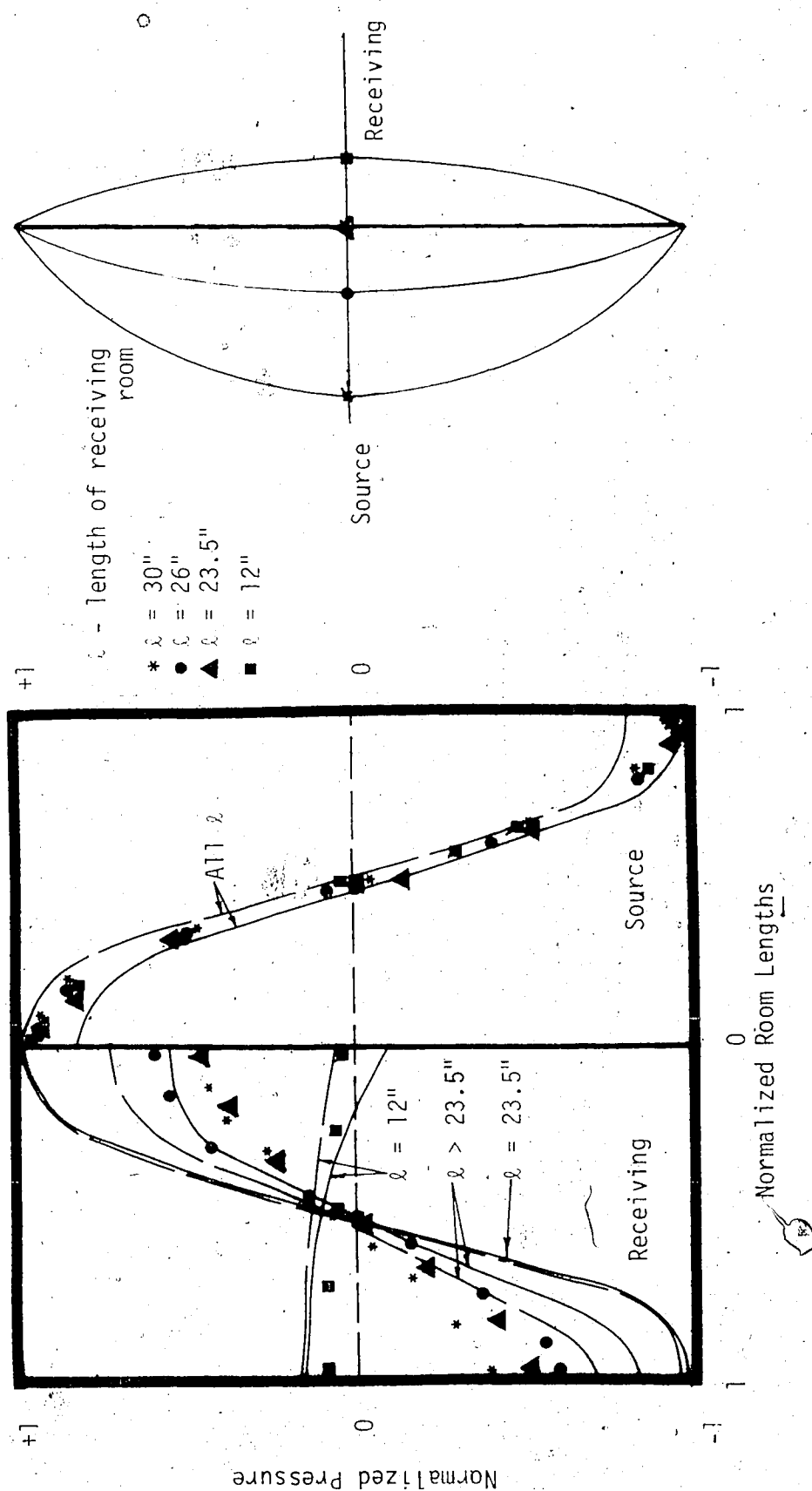


Figure 3.10 : SECOND MODE - NORMALIZED LONGITUDINAL PRESSURE VARIATION AND PLATE DISPLACEMENT

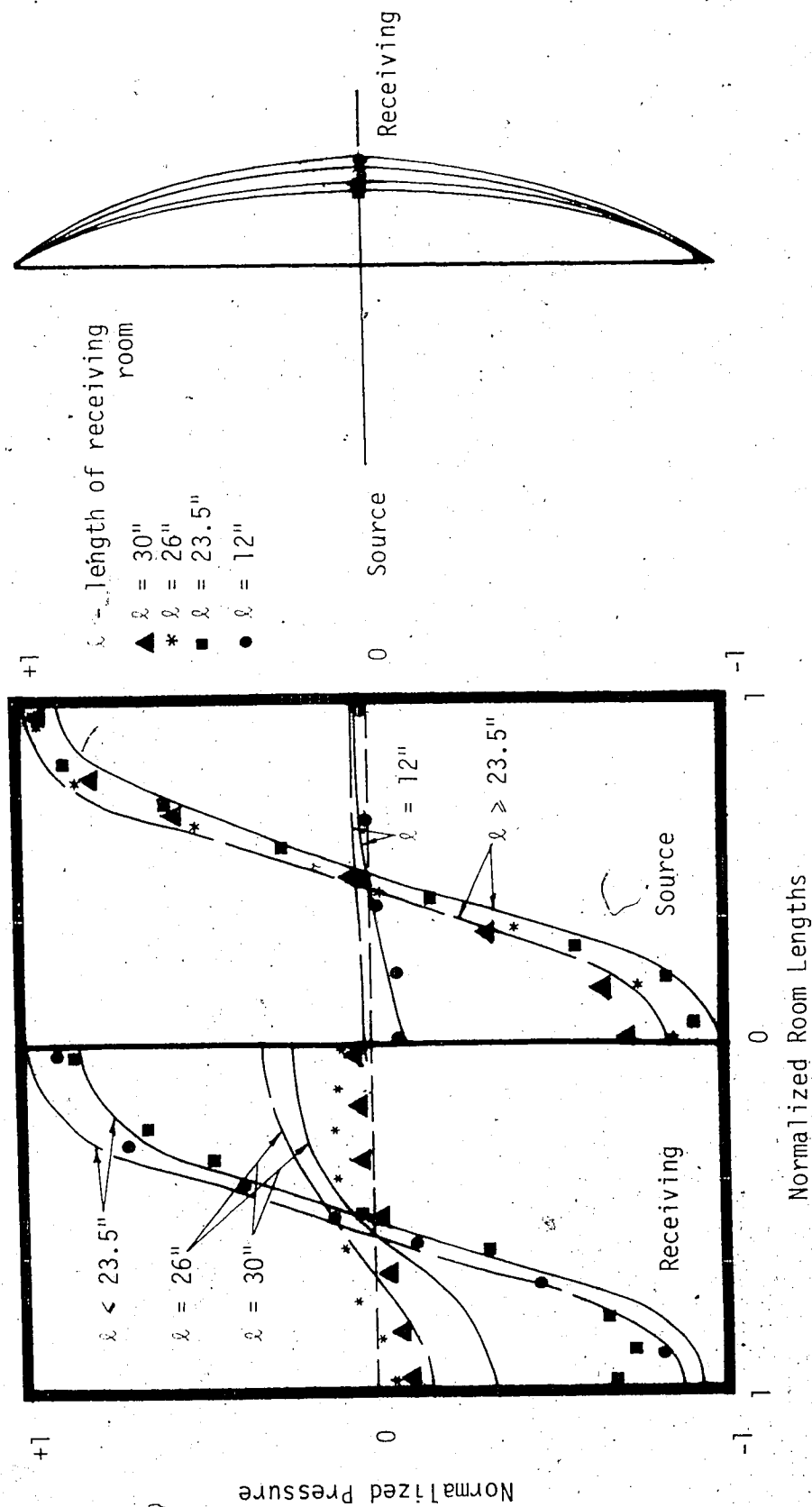
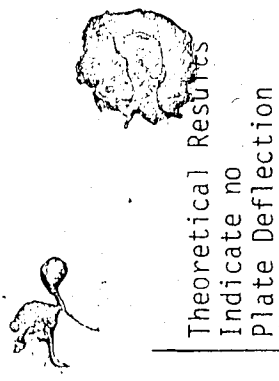


Figure 3.11 THIRD MODE - NORMALIZED LONGITUDINAL PRESSURE VARIATION AND PLATE DISPLACEMENT



Theoretical Results
Indicate no
Plate Deflection

- λ - length of receiving room
- * $\lambda = 30''$
- $\lambda = 26''$
- ▲ $\lambda = 23.5''$
- $\lambda = 12''$

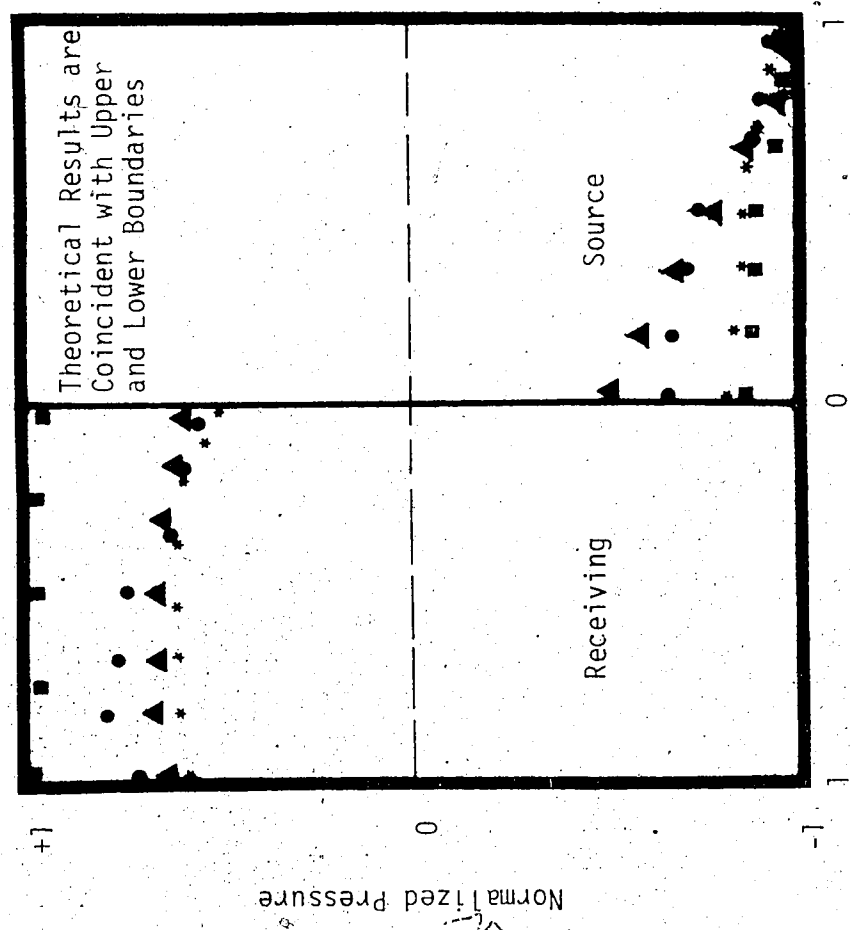


Figure 3.12 FOURTH MODE - NORMALIZED LONGITUDINAL PRESSURE VARIATION AND PLATE DISPLACEMENT

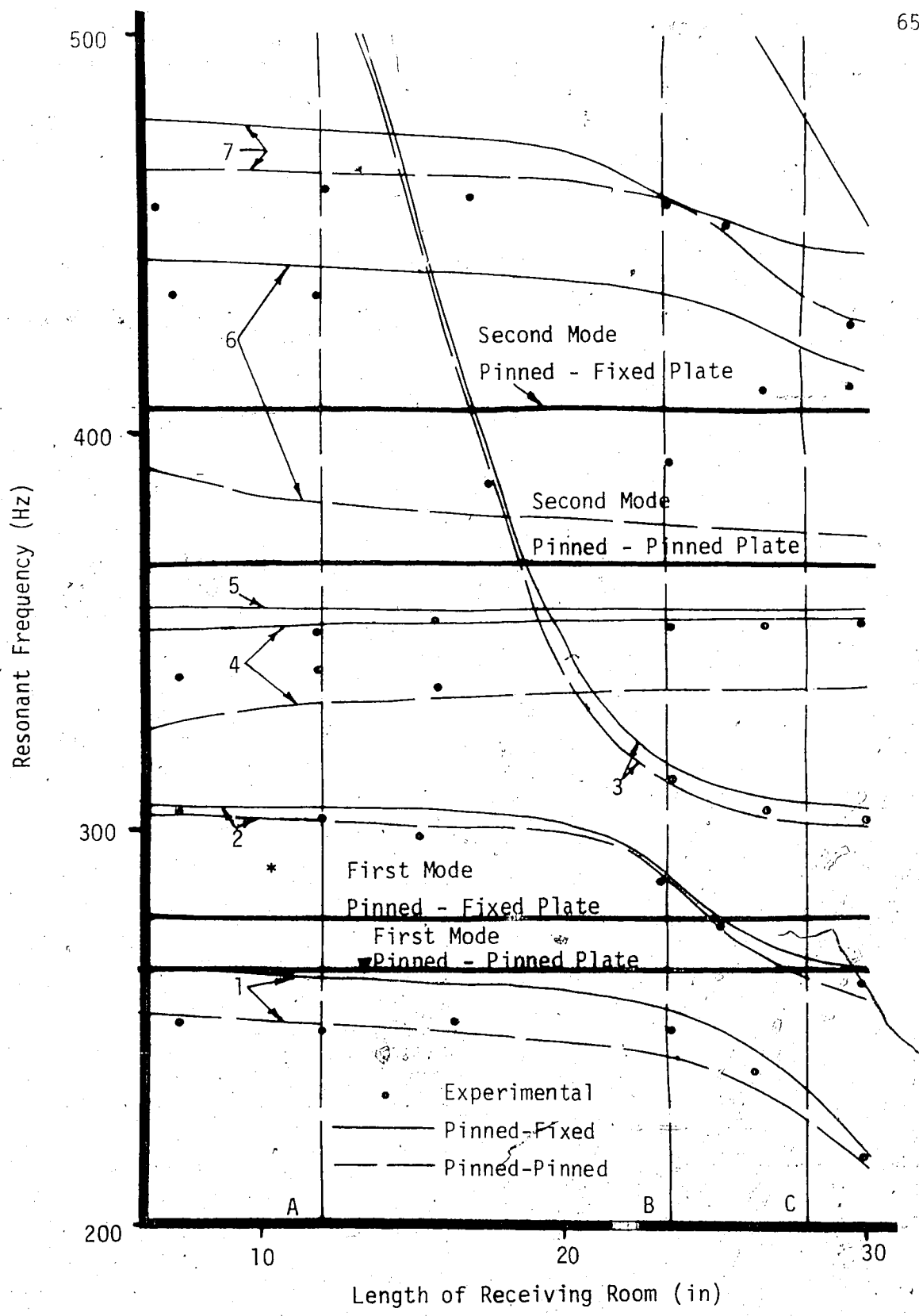


Figure 3.13 FULL COUPLING PANEL - RESONANT FREQUENCIES FOR SOUND TRANSMISSION

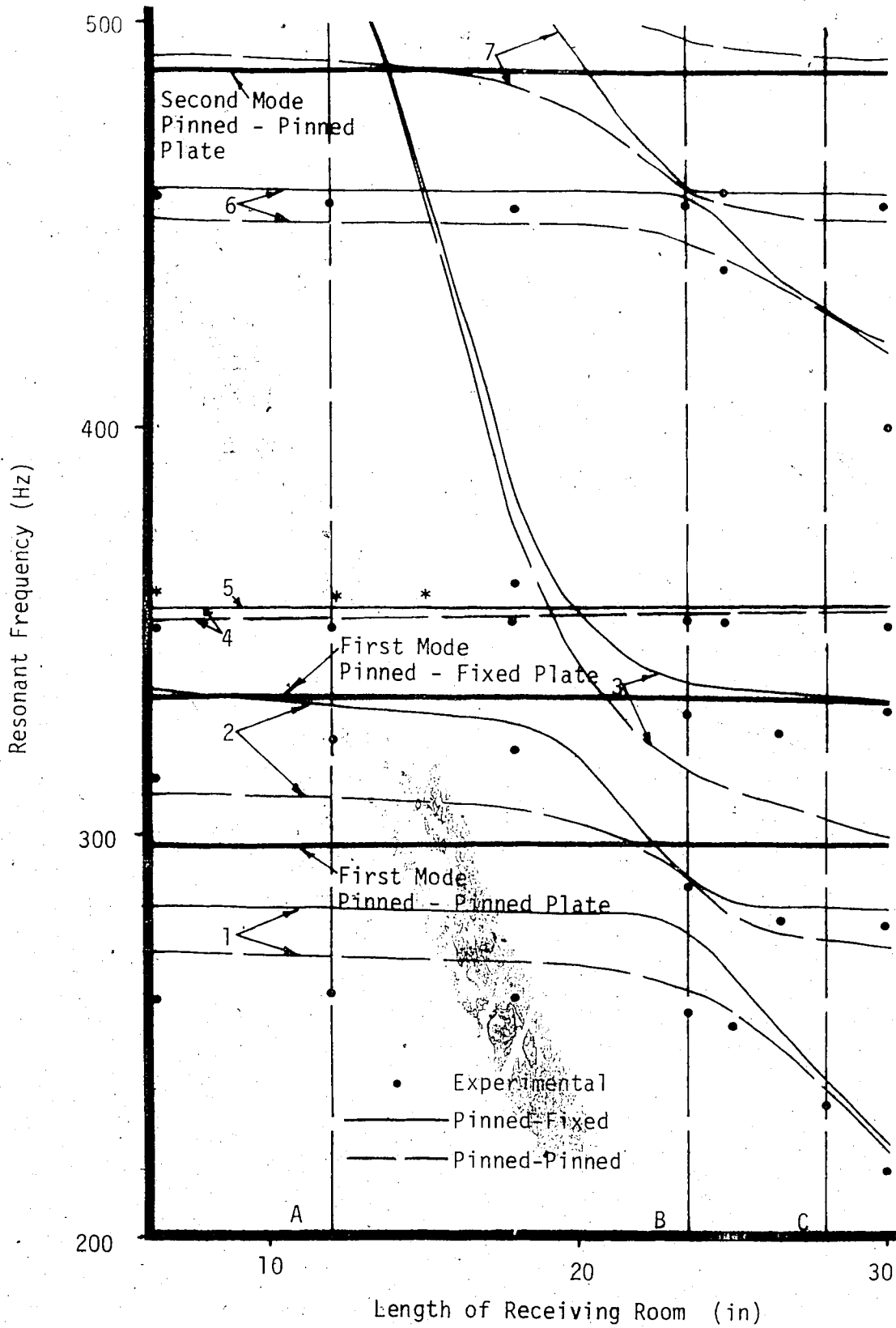


Figure 3.14 73.7 PER CENT COUPLING PANEL - RESONANT FREQUENCIES FOR SOUND TRANSMISSION

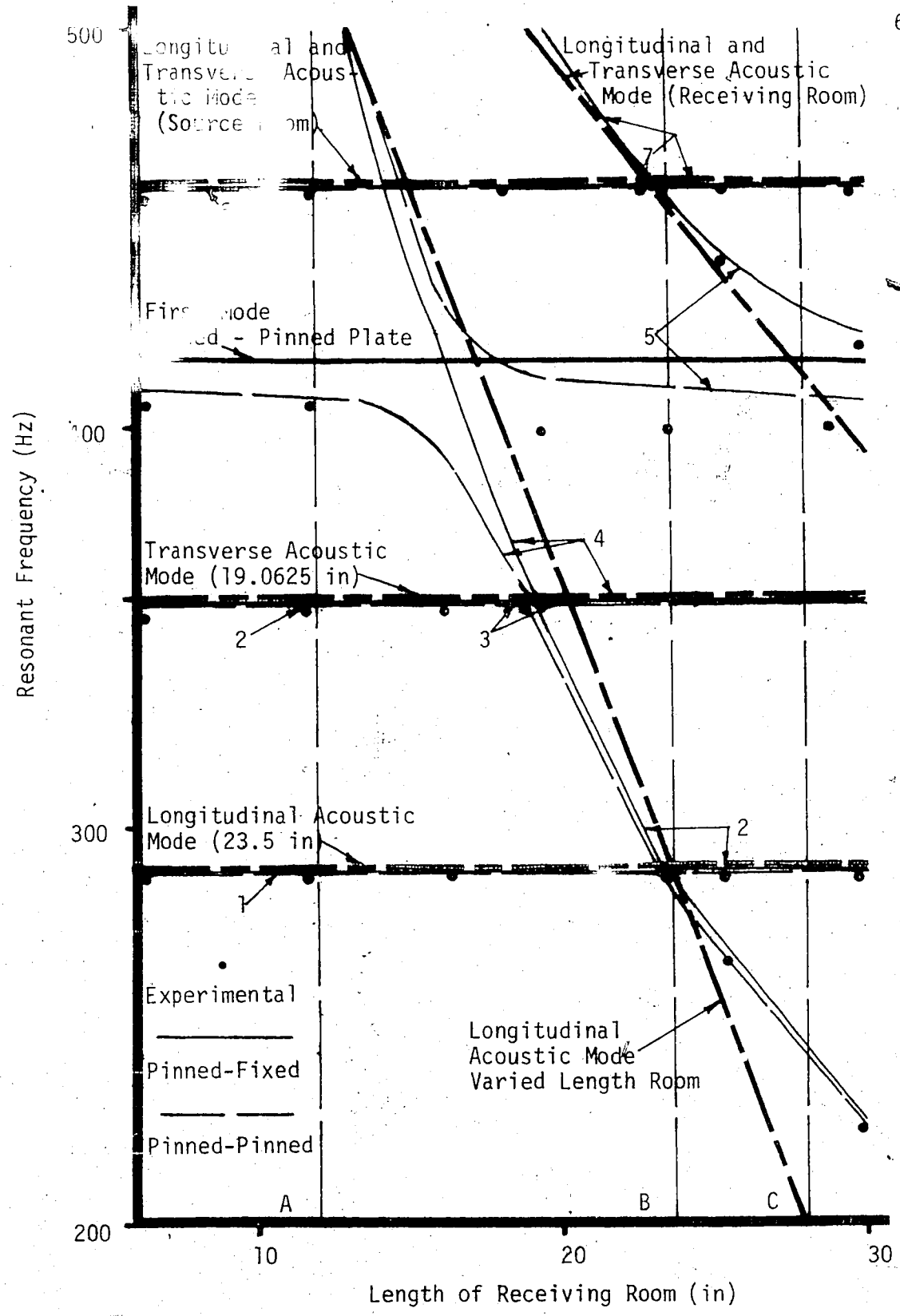


Figure 3.15 42.5 PER CENT COUPLING PANEL - RESONANT FREQUENCIES FOR SOUND TRANSMISSION

"stiffness" effects, as previously described. For any given enclosure the panel and the air in the adjacent room act as a "limp" (i.e. unstiffened) mass on the end of the enclosure to give the lower acoustically dominant mode. The second acoustically dominant mode occurs when the adjacent room reaches a frequency where it acts as a stiffener for the "limp" plate. Panel dominant modes occur at frequencies where the mass or stiffness effects of the rooms respectively decrease or increase the "in vacuo" panel frequency.

It is noteworthy that Fig. 3.5 shows the paradoxical case of sound transmission with no panel motion. Though such a case can not exist with damping present, a natural frequency closely related to the one for this configuration was measured.

Figure 3.9 through Fig. 3.15 relate the effects of changing receiving room length on the natural frequencies and principal mode shapes for any given panel. Figure 3.9 through Fig. 3.12 were scaled with respect to the maximum pressure and the individual room lengths to give a basis for comparison of theoretical and experimental results. It is to be noted that good agreement occurs for all cases except where there is little or no panel motion, i.e. transverse modes and symmetric acoustical modes. These adverse configurations are highly dependent on damping which is not considered in this thesis. To the right of the scaled pressure diagrams are scaled displacement diagrams of the plan view of the coupling panel.

The principal mode shapes within the coupled rooms can basically be described in terms of strain energy or frequency; the higher the strain energy stored, the higher the natural frequency

to maintain the energy level. Acoustically, the lowest strain energy state is the uniform pressure mode in which the room's overall pressure raises and lowers "en mass" while the second lowest is a single noded standing wave in the direction of the maximum room dimension. The panel is at its lowest potential state when unflexed, while the next higher state is a set of half-sine waves in the two planar directions, as previously described. When exciting a coupled system with any given frequency, the individual components will react more violently if the exciting frequency is near one of the components' natural frequencies. The resulting overall natural frequency will therefore be a modification of the components' natural frequencies.

The paragraphs that follow describe each of the lowest five overall natural frequencies as a function of receiving room length starting with a short receiving room. In both the acoustical and flexural sense "mass" effect lowers a component's natural frequency while "stiffness" effect increases it. Also, included is some insight as to the effect of changing the panel area and stiffness on the overall natural frequencies. The vertical lines "A", "B" and "C" in Fig. 3.13 through 3.15 will serve to locate zone points during discussion.

For the lowest overall natural frequency near point A, the receiving room has an almost zero-frequency uniform pressure which acts as a mass in tandem with the mass effect of the panel lowering the component frequency of the source enclosure. As the configuration moves towards "B" the acoustical stiffness of the receiving room drops to equal the stiffness of the source room; the wall still acts as a

Imp mass, lowering the component frequency of either room. Moving towards "C" the receiving room develops a longitudinal single node standing wave, while the source room goes to a uniform pressure state. In this region the frequency is close to but above the component frequency for the receiving room. As the panel frequency increases and the panel forcing area decreases, the plate stiffness tends to raise the acoustic frequency of the system to the point where the source room appears to be acoustically hard and the frequency is that classically calculated (as in Fig. 3.15). It is to be noted that when the source room is shorter than the receiving room, the stiffness of the panel increases the frequency of the total configuration over that which would normally be calculated for the receiving room.

The second mode is extremely dependent on the frequency of the coupling plate for unsymmetric rooms (points A and C). For the first two panel widths the natural frequency is close to the frequency for an "in vacuo" panel with a slight increase due to the acoustic stiffness of both rooms. When the rooms are symmetric, sound transmission with no wall motion takes place (totally independent of the plate frequency) at the natural frequency of the hard bounded source or receiving room. For other configurations, acoustical mass effects of either room tend to lower the frequency of the panel.

Beyond this point the overall natural frequencies and principal mode shapes become disorganized. It is best to discuss Fig. 3.13 and Fig. 3.14 and then Fig. 3.15 separately.

The third principal mode for the two larger panel configurations is governed by a single node longitudinal acoustic wave in

the receiving room in the vicinity of "A" and by the fundamental panel frequency between "B" and "C". The fourth and fifth mode shapes have transverse wave patterns in both source and receiving rooms regardless of receiving room length. In the fourth mode the wave patterns at any point near the coupling panel of one room is 180° out-of-phase with a point immediately adjacent to it in the adjacent room, causing a net force to be incident on any particular section of the panel. Since the fundamental frequency of the plate is below the overall natural frequency, the intercoupled plate-acoustic system has a natural frequency lower than that which would be calculated for similarly dimensioned "hard" rooms. The fifth mode has the adjacent wave patterns in phase so that the panel has no effect.

For the more uncoupled configuration, Fig. 3.15, the second and third modes are degenerate in the region of "A". The frequency of the coupling panel is sufficiently above the frequency of a transverse acoustic wave that the previously independent frequencies associated with the "out-of-phase" and "in-phase" acoustic mode shapes are the same. This would indicate that the rooms are effectively hard. These mode shapes are similar to the fourth and fifth mode shapes for the wider panel configurations. In the region between "A" and "B" the second mode becomes dependent on the longitudinal acoustic mode in the receiving room and from "B" to "C" on the fundamental longitudinal acoustic mode in the source room. In the region of "B" the third and fourth modes are degenerate and remain as such for further lengthening of the receiving room. The fourth acoustic mode is dependent on the "in vacuo" panel frequency near "A" but becomes

dependent on the fundamental longitudinal acoustic mode of the receiving room between "A" and "B". Beyond this, the acoustic and panel modes become coupled as the fundamental frequency of the panel is arrived at.

Cases of "weak" intercoupling produce frequency curves that are almost discontinuous at points of curvature. These lines are almost co-incident with those calculated by "hard" room and "in vacuo" panel theories. One noteworthy exception is the longitudinal standing wave in the receiving room. The panel stiffness has some effect in increasing the lower frequency results and the mass effects of the panel decreasing the higher frequencies.

In Fig. 3.13 through Fig. 3.15 the vertical distance between the pinned-pinned and pinned-fixed lines for any given mode is an indication of the mode's dependency on the panel's boundary conditions. This exemplified itself when measurements were made on the experiment apparatus. Resonances associated with narrow distances between pinned-pinned and pinned-fixed boundary conditions were pronounced over a small band width whereas resonances associated with wider distances between the boundary conditions had a much wider "skirt". An adverse effect of the different "skirt" widths was the disappearance of certain less prominent resonances. Also, a shift occurred in the peaks of two closely adjacent resonances because of the phase plane addition of the respective skirt zones. Examples of this can be seen in Fig. 3.13 and Fig. 3.14 marked with "*".

In Fig. 3.13, a 'v' denotes a resonance situation of the upper "rigid" panel of the receiving room and the coupling wall. It is given

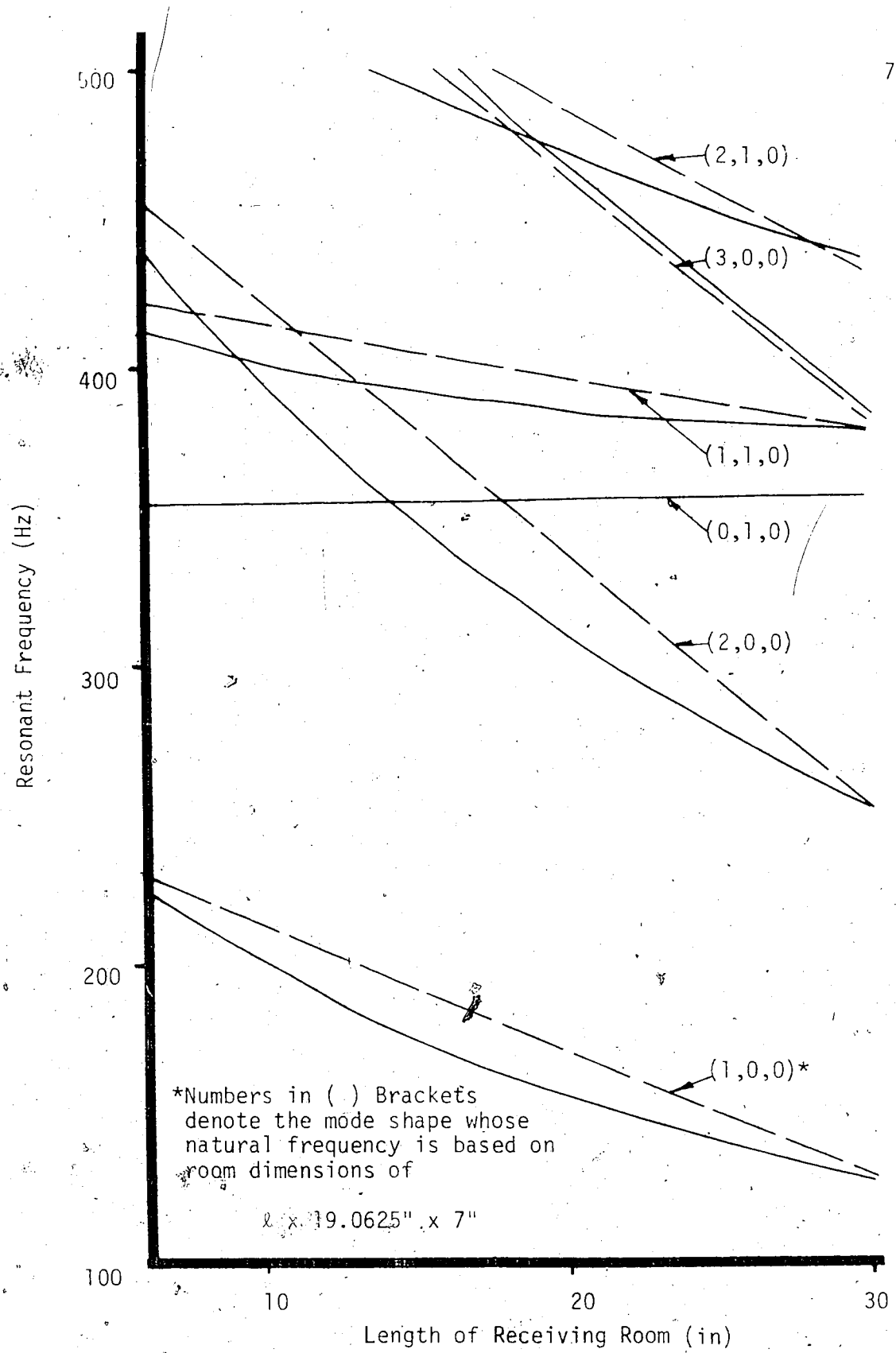


Figure 3.16 42.5 PER CENT ORIFICE COUPLING - RESONANT FREQUENCIES FOR SOUND TRANSMISSION

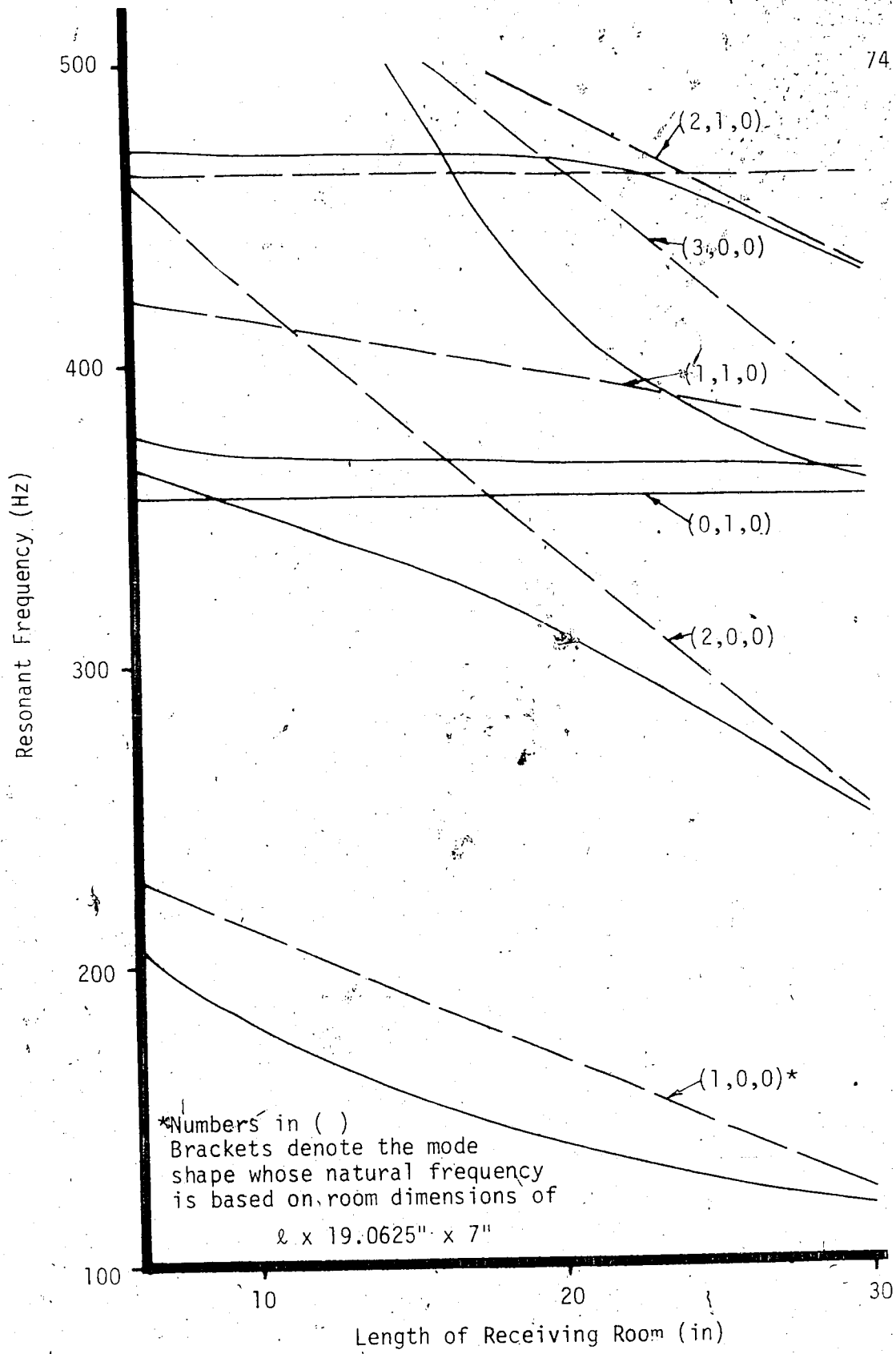
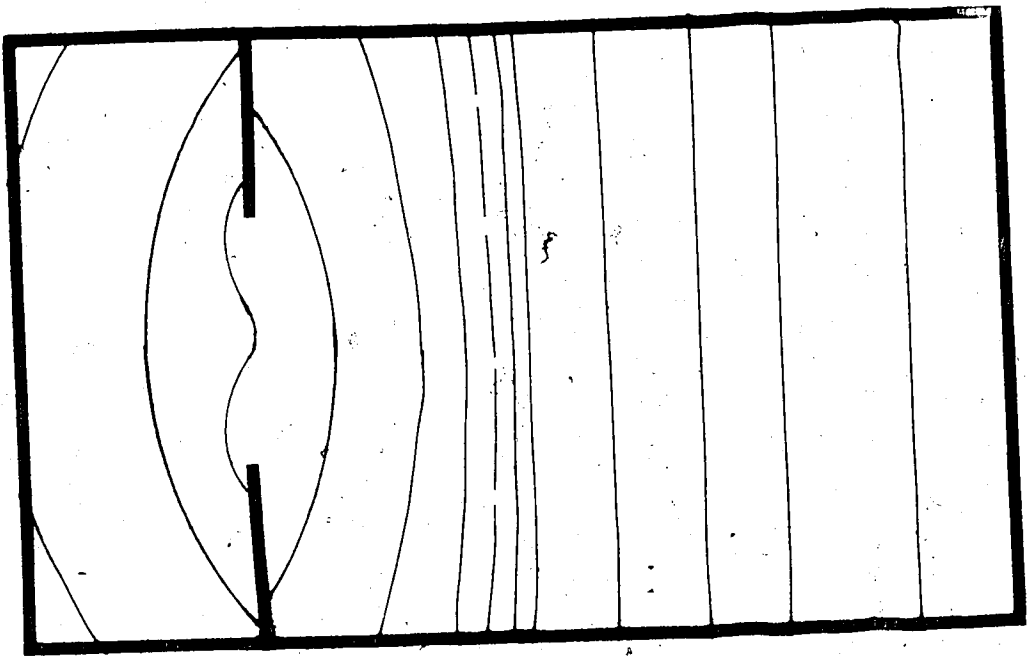
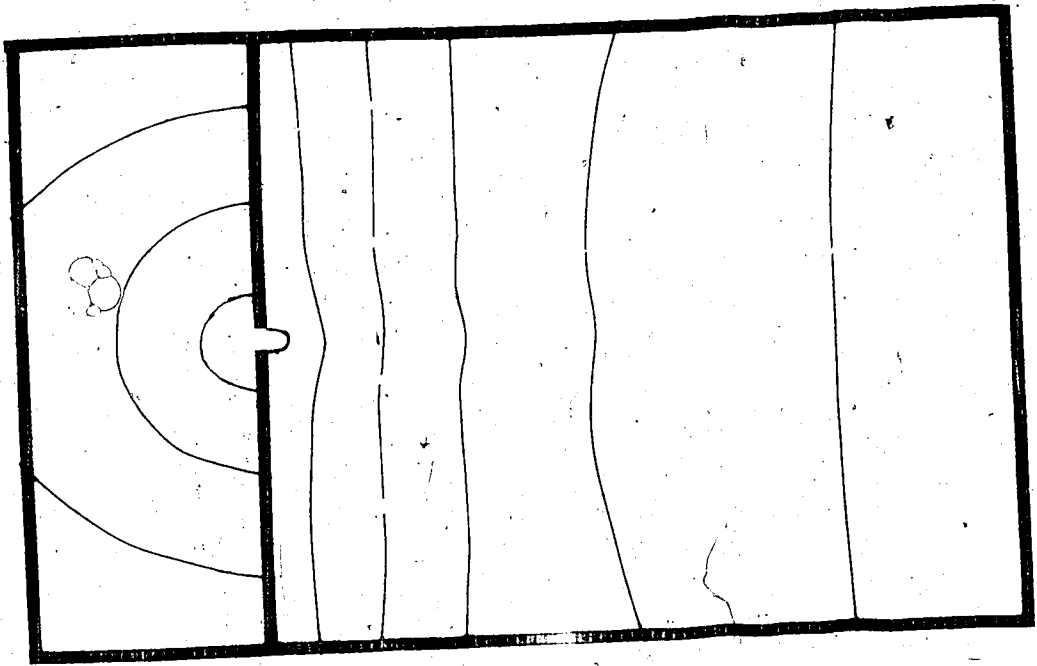


Figure 3.17 4.2 PER CENT ORIFICE COUPLING - RESONANT FREQUENCIES FOR SOUND TRANSMISSION



(a)



(b)

Figure 3.18 EXAMPLE OF ORIFICE COUPLING MODE SHAPES

because it appears as a resonance peak for the given configuration but is not sufficiently large in any of the other configurations.

3.3 Sound Transmission Between Orifice Coupled Rooms

Some interest was shown by Harris and Feshback [34] in the coupling of two rooms by a window. Considering the similarity in rooms studied, a slight diversion was taken to show the natural frequencies for a room with orifice coupling in a panel that represents 43.7 per cent of the coupling wall. A second set of frequencies were calculated for an orifice coupling which represented 4.25 per cent of the coupling wall. These are shown in Fig. 3.16 and Fig. 3.17, respectively.

For the large coupling window there is no extensive change of modal patterns from any given classical principal mode shape due to the excellent acoustic flow between the rooms. The constriction causes local pressure build-up in the corners adjacent to the coupling wall in longitudinal modes (shown in Fig. 3.18), which is common for both widths of constriction. The narrow window is effectively a line source of sound in the shorter room, whether it be the source or receiving room (shown in Fig. 3.18 (b)).

From Fig. 3.16 it is reasonably easy to see that the coupling window has very little effect on the principal frequency. The natural frequencies for a similar room with no window are superimposed with a dashed line and named. The deviation is due to the slight increase in kinetic energy as the flow passes through the common boundary. It is to be noted that the computational error is small, as indicated by

the agreement of slope and only slight reversal of lines for the (3, 0, 0) mode.

For the narrow passage, the natural frequencies and mode shapes vary considerably from classical geometrically based calculations. Again, the frequencies for the lowest mode are close to those for the (1, 0, 0) mode for a similarly dimensioned room with no coupling wall. Larger deviations occur due to greater kinetic energy through the orifice (much similar to two coupled Helmholtz resonators).

For higher modes, there are indications of independence in room characteristics due to a smaller coupling surface. Modes three and four are both transverse wave patterns with the wave "in-phase" and "out-of-phase", respectively, much similar to the panel-coupled rooms. The greater frequency associated with mode four is due to a slight pressure gradient that has its peak at the orifice and declines towards the end walls.

Modes two and six also display this partially uncoupled characteristic. When the receiving room is short the receiving room has a transverse wave pattern, while the source room has a longitudinal standing wave. As the receiving room lengthens, the transverse wave in the receiving room is gradually replaced by a longitudinal wave in mode two. For mode six the transverse wave does not disperse but a longitudinal wave develops in the receiving room.

Mode five has a longitudinal wave pattern much similar to the (3, 0, 0) mode of the equivalently dimensioned uncoupled configuration.

As in mode one, the frequencies are lower because of the Helmholtz resonator effect.

CHAPTER IV
DISCUSSION AND RESULTS

4.1 Discussion

There are several interesting effects which occur when the natural frequencies of the coupling plate are within the range of the natural acoustic frequencies.

- 1) Pressure levels in the receiving room can be higher than those in the source room.
- 2) Acoustically dominant modes occur at frequencies near those classically calculated with only slight deformation of the acoustic mode shapes. In this situation the exciting frequency is sufficiently removed from the natural frequencies of the panel so that the panel acts as a "passive" spring (stiffness) or "limp" mass on an acoustical system.
- 3) Plate dominant modes have natural frequencies that vary as much as 8 per cent from the "in vacuo" classical panel frequencies, though changes in plate mode shapes are not appreciable. The mass and stiffness effects of the adjacent acoustical systems have considerable effect on the overall frequency, but subsequently suffer considerable deformation in acoustical mode shapes.

In the orifice coupled enclosures the effect of the aperture is not significant until the opening is less than 10 per cent of the common wall area. In this range the Helmholtz resonator effect causes the natural frequency to drop considerably, while the rooms become acoustically uncoupled to some extent. As the opening becomes smaller the straight isobars of a classical hard bounded room become distorted into curves because the orifice becomes a stronger "line" source radiating into the room that is the least acoustically excited.

For both types of coupling, the insertion of an intermediate surface, be it a hard boundary with an air slit in it or a coupling panel, causes pressure build ups at these surfaces. This is due to the increase in potential energy and the decrease of kinetic energy because of reduced transverse velocities at a wall.

The principal mode shapes produced give an insight of the acoustic isobars and the deflected form of the panel for a given resonant condition. With the mathematical characteristics of linear combination, visualization as well as calculation of composite sound fields is readily possible.

4.2 Future Research

There are some other possible extensions of the Kantorovich approach in plate-acoustic systems. One would be to study the random dynamic response of the aforementioned rooms and structure. Another would be to change coordinate systems. By developing a cylindrical acoustic element, a circular plate element and a cylindrical shell element (with the θ -direction being used for Fourier approximation)

and the required coupling matrices, the dynamic or resonant response of submerged closed cylindrical sections could be studied. The form of the approximating functions would be

$$r^n F(r,z) (A \cos n \theta + B \sin n \theta)$$

which would lend easily to the approximation of the Bessel Functions used in the solution of classical equations. Notably there would have to be care taken to circumvent the singularity that would occur at the origin ($r = 0$) of the element configuration.

4.3 Results

The finite elements produced give a good approximation of the principal mode shapes and natural frequencies for a coupled plate-acoustic system with two parallel surfaces and perpendicular sides. The agreement is best when the configuration is least dependent on internal hysteretic and viscous damping. Convergence of the approximate results to the exact solution is at a rate of $1/n_e^4$ or $1/n_e^5$ for all cases studied. The use of Kantorovich's approximation and Iron's symmetricization procedure produced a significant saving in computing time and storage.

Such an approach is sufficiently general to allow study of many acoustic panel configurations with little alteration to the major portions of the computing program. If the program is to be used for various problems of varying geometry, the finite element approach is much more attractive than other analytical methods (i.e. finite difference).

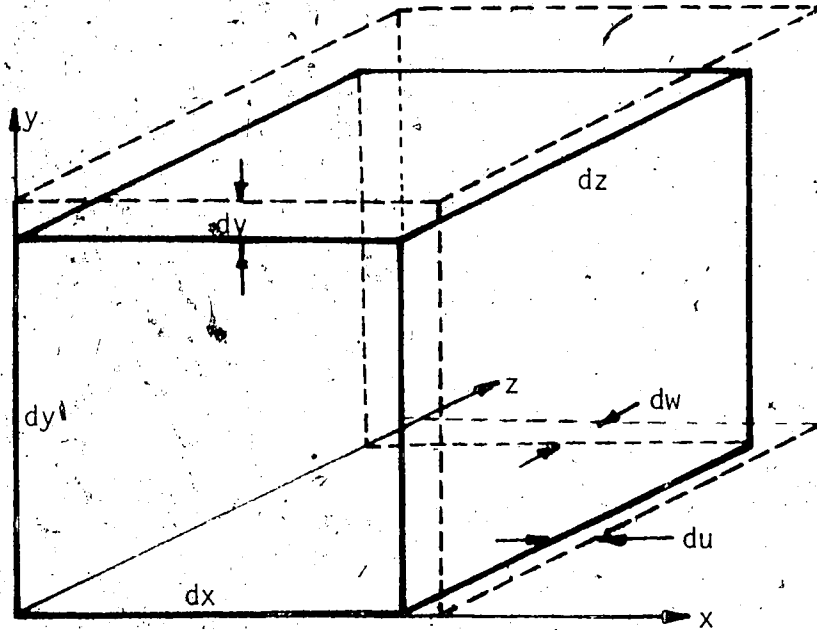
BIBLIOGRAPHY

1. Galilei, G., Dialogue Concerning Two New Sciences (Translated from the Italian and Latin by Henry Crew and Alfonso de Salvio), Evanston and Chicago, 1939.
2. Mersenne, M., "La Theorie et la Pratique de la Musique", Harmonie Universelle, Paris, 1686.
3. Sauver, J., "Système General des Intervalles des Sons", Memoirs of L'Academie Royale des Science, Paris, 1701, pp. 297-299.
4. Knudsen, V. O., "Recent Developments in Architectural Acoustics", Review of Modern Physics, Vol. 6, Sec. 1, 1934.
5. Sabine, P. E., "The Beginning of Architectural Acoustics", Journal of the Acoustic Society of America, Vol. 10, Sec. 1, 1938.
6. Sabine, P. E., "Architectural Acoustics, its Past, its Present and Future", Journal of the Acoustic Society of America, Vol. 11, Sec. 21, 1939.
7. Rayleigh, J. W. S., The Theory of Sound, Vol. 1 & 2, 1896, Dover Publishers, New York.
8. Lamb, H., The Dynamic Theory of Sound, 1925, Dover Publishers, New York.
9. Morse, P. M., "Acoustics and Basic Physics", Journal of the Acoustic Society of America, Vol. 27, Sec. 2, 1955, pp. 216.
10. Morse, P. M. and Bolt, R. H., "Sound Waves in Rooms", Reviews of Modern Physics, Vol. 16, No. 2, 1944, pp. 69-150.

11. Bishop, R. E. D. and Gladwell, G. M. L., "An Investigation into the Theory of Resonance Testing", Philosophical Transactions of the Royal Society of London, Vol. 255, No. 1055, 1963, pp. 241-280.
12. Nilsson, A. C., "Reduction Index and Boundary Conditions for a Wall Between Two Rectangular Rooms", Parts 1 & 2, Acoustica, Vol. 26, 1972.
13. Lyon, R. H., Dietrich, C. W., Ungar, E. E., Pyle, R. W. and Apfel, R. E., "Low-Frequency Noise Reduction of Spacecraft Structures", NASA CR-589, 1966.
14. Pretlove, A. J. and Craggs, A., "A Simple Approach to Coupled Panel-Cavity Vibration", Journal of Sound and Vibration, Vol. 11, No. 2, 1970, pp. 207-215.
15. Craggs, A., "The Transient Response of a Coupled Plate-Acoustic System Using Plate and Acoustic Finite Elements", Journal of Sound and Vibration, Vol. 15, No. 4, pp. 509-528.
16. Craggs, A., "Computation of the Response of Coupled Plate-Acoustic Systems Using Plate Finite Elements and Acoustic Volume - Displacement Theory", Journal of Sound and Vibration, Vol. 18, No. 2, pp. 235-245.
17. Gladwell, G. M. L., "A Finite Element Method for Acoustics", presented at the 5th Congress of Acoustics 1965 (Liege).
18. Jennequin, G., "Is the Computation of Noise Level Inside a Car Feasible?", Institution of Mechanical Engineers, 1971, pp. 132-137.

19. Pin Tong, "The Finite Element Method for Fluid Flow", Recent Advances in Matrix Methods of Structural Analysis and Design, 1971, pp. 787-808, University of Alabama Press.
20. Zienkiewicz, O. C., The Finite Element Method in Engineering Science, 1971, McGraw-Hill, London.
21. Holand, I. and Bell, K., Finite Element Methods in Stress Analysis, 1970, Tapir, Norway.
22. Long, R. R., Engineering Science Mechanics, 1963, Prentice-Hall, pp. 78-88.
23. Timoshenko, S. P., Vibration Problems in Engineering, Third Edition, Van Nostrand, 1955, pp. 442.
24. Timoshenko, S. P. and Gere, J. M., Theory of Elastic Stability, Second Edition, McGraw-Hill, 1961, pp. 319-347.
25. Warburton, G. B., "The Vibration of Rectangular Plates", Proceedings of the Institute of Mechanical Engineering, Vol. 168, 1954, pp. 371-384.
26. Warburton, G. B., "Vibration of a Cylindrical Shell in an Acoustic Medium", Journal of Mechanical Engineering Science, Vol. 1, 1961.
27. Pretlove, A. J., "Free Vibration of a Rectangular Panel Backed by a Closed Rectangular Cavity", Journal of Sound and Vibration, Vol. 2, 1965.
28. Gladwell, G. M. L. and Zimmerman, "Energy Formulations of Acoustic and Structural Vibration Problems", Journal of Sound and Vibration, Vol. 3, 1966.

29. Mason, V., Ph.D. Thesis, University of Southampton.
30. Mason, V., "Rectangular Finite Elements for Analysis of Plate Vibration", Journal of Sound and Vibration, Vol. 7, 1968, pp. 437-488.
31. Craggs, A., Ph.D. Thesis, University of Southampton, 1969.
32. Boas, M. L., Mathematical Methods in the Physical Sciences, 1966, pp. 290-301.
33. Zienkiewicz, O. C. and Newton, R. E., "Coupled Vibration of a Structure Submerged in a Compressible Fluid", Proceedings of the Symposium on Finite Element Techniques, University of Stuttgart, Germany, 1969, pp. 371.
34. Harris, C. M. and Feshbach, H., "On the Acoustics of Coupled Rooms", Journal of the Acoustic Society of America, Vol. 22, No. 5, 1960.



u, v, w - displacements in the x, y, z directions respectively

v_0, v - initial and final specific volumes

ρ_0, ρ - initial and final densities

dx, dy, dz - dimensions of the infinitesimal element in the x, y, z directions respectively

Figure A1 INFINITESIMAL ACOUSTIC ELEMENT

APPENDIX A
ACOUSTIC FORMULATION

1.1 Equations of Motion for Acoustics

A derivation of the equations is given by H. Lamb [8], therefore what is presented here will only represent a condensation of the above author's work.

Considering the element as shown in Fig. A1 (with the included notation) and defining the dilatation Δ as the ratio of the specific volume increment to the original specific volume, we get

$$\begin{aligned}\Delta &= (v - v_0) / v_0 \\ v &= v_0 (1 + \Delta)\end{aligned}\tag{A1}$$

Similarly, condensation s can be defined for densities

$$\begin{aligned}s &= (\rho - \rho_0) / \rho_0 \\ \rho &= \rho_0 (1 + s)\end{aligned}\tag{A2}$$

The density is the inverse of the specific volume, therefore

$$1/v = (1 + s) (1 + \Delta)$$

Considering only small dilatations and condensations, it can be shown that

$$\Delta \approx -s\tag{A3}$$

Looking more closely at the dilatation, it is defined by

$$\frac{(dx + du)(dy + dv)(dz + dw) - dx dy dz}{dx dy dz}$$

Neglecting second order terms, it becomes

$$\Delta = \text{div } \underline{u} \quad (\text{A4})$$

where

$$\underline{u} = (u, v, w) \quad \text{and} \quad \text{div} = \frac{\delta}{\delta x} + \frac{\delta}{\delta y} + \frac{\delta}{\delta z}$$

Poisson and Laplace consider the thermodynamics of sound to be almost adiabatic, which agreed well with experiments. Therefore, from (A2)

$$\frac{p}{p_0} = \left(\frac{\rho}{\rho_0} \right)^\gamma = (1 + s)^\gamma$$

where γ is the ratio of the specific heats. Again, assuming a small dilatation

$$p = p_0 (1 + \gamma s) \quad (\text{A5})$$

By taking a force balance in each of the principal directions, we get

$$\begin{aligned}
 -\rho \frac{\delta^2 u}{\delta t^2} &= \frac{\delta p}{\delta x} \\
 -\rho \frac{\delta^2 v}{\delta t^2} &= \frac{\delta p}{\delta y} \\
 -\rho \frac{\delta^2 w}{\delta t^2} &= \frac{\delta p}{\delta z}
 \end{aligned}
 \tag{A6}$$

with the minus sign indicating the direction of acceleration relative to the pressure gradient. Equation (A6) can be written in more efficient notation as

$$-\rho \frac{\delta^2 \mathbf{u}}{\delta t^2} = \text{grad } p
 \tag{A7}$$

It is worthwhile to note that the velocities in the different coordinate directions within the acoustic element can be directly related to the condensation s by

$$\frac{\delta u}{\delta t} = \frac{-p_0 \gamma}{\rho} \frac{\delta}{\delta x} \int_{-\infty}^{t_2} s \, dt$$

$$\frac{\delta v}{\delta t} = \frac{-p_0 \gamma}{\rho} \frac{\delta}{\delta y} \int_{-\infty}^{t_2} s \, dt$$

$$\frac{\delta w}{\delta t} = \frac{-p_0 \gamma}{\rho} \frac{\delta}{\delta z} \int_{-\infty}^{t_2} s \, dt$$

In acoustics the excess pressure ($p - p_0$), is used rather than the overall pressure p . Rearranging (A5) to get the excess pressure p_1 , and making substitutions from (A3) and (A4)

$$p_1 = -\rho_0 \gamma \operatorname{div} \underline{u} \quad (A8)$$

The excess pressure can be directly substituted into (A6) and upon combination with (A7)

$$\operatorname{div} (\operatorname{grad} p_1) - \frac{\rho}{\gamma p_0} \frac{\delta^2 p_1}{\delta t^2} = 0$$

The divergence of the gradient of a scalar is the Laplacian operator ∇^2

$$\nabla^2 p_1 - \frac{\rho}{\gamma p_0} \frac{\delta^2 p_1}{\delta t^2} = 0$$

which is a standard form of the wave equation

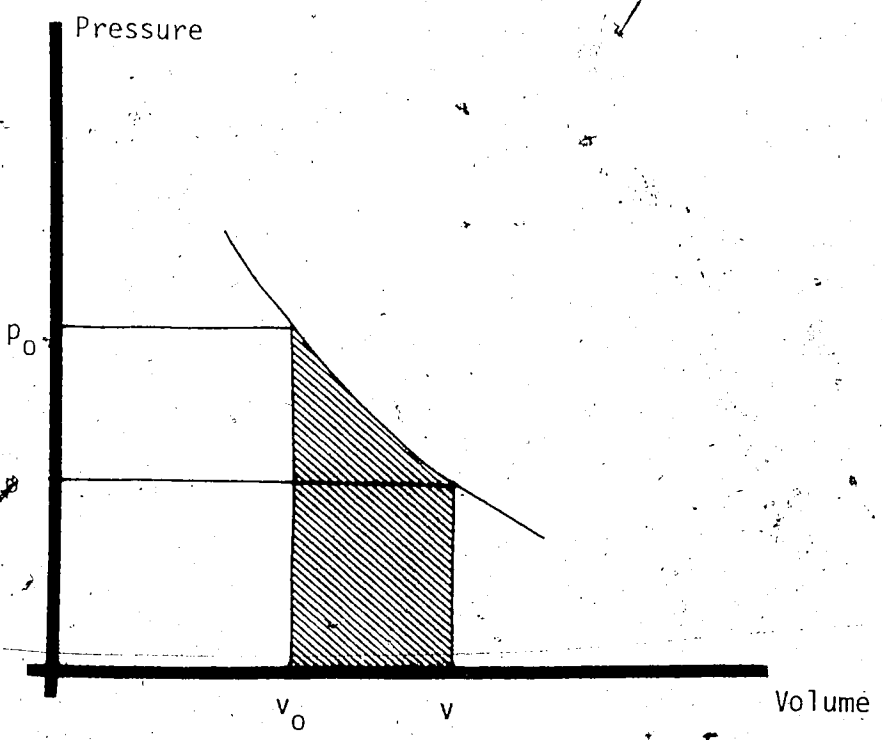


Figure A2 P-V CURVE

and $\frac{\gamma p_0}{\rho}$ is the square of the wave velocity, which from now on is c , the velocity of sound

$$c^2 = \frac{\gamma p_0}{\rho} \quad (A10)$$

A.2 Energy Equations for Acoustics

The kinetic energy T for an infinitesimal element can be written as

$$T = \frac{1}{2} \rho \iiint_V \frac{\delta \underline{u}}{\delta t} \cdot \frac{\delta \underline{u}}{\delta t} dV$$

The potential energy U can be found by integrating the shaded area in Fig. A2 over the whole volume V

$$U = \iiint_V \left\{ p_0 \frac{(v-v_0)}{v_0} - \frac{1}{2} (p_0 - p) \frac{(v-v_0)}{v_0} \right\} dV$$

Since the average volume change over the whole is zero, the first term disappears and by using (A1), (A3), (A8) and (A10), it can be written that

$$U = \frac{\rho c^2}{2} \iiint_V (\text{div } \underline{u})^2 dV$$

To this point no assumptions have been made as to the form of wave motion. Gladwell and Zimmerman [28] assumed a periodic sound wave and continued onto the energy equations. Craggs [15] studied the tran-

sient response and, therefore, his formulation had to be more general but is, in some respects, easier to follow and will be used for the time being.

A velocity potential ϕ must be defined

$$\phi = -c^2 \int_{t_1}^{t_2} s \, dt + \phi_0$$

where ϕ_0 is the value of the integral at time, t_1 .

It can be derived from the previous equations without much difficulty that

$$\frac{\delta \underline{u}}{\delta t} = \text{grad } \phi$$

$$\text{div } \underline{u} = \frac{1}{c^2} \frac{\delta \phi}{\delta t}$$

$$p_1 = -\rho \frac{\delta \phi}{\delta t} \quad (\text{A11})$$

Note that from here on a superscript "." indicates differentiation with respect to time. The value of the potential lies in its ability to define the total character of a vector quantity \underline{u} by a scalar, although at a loss in physical interpretation.

A.3 Derivation of Equations of Motion from Functional Formulation

It is now worthwhile to show that the first variation of the time integral of the Lagrangian, J , actually gives the correct equation. Making substitutions from (A11) in the energy equation,

and knowing that

$$J = \int_{t_1}^{t_2} (T - V) dt$$

$$= \int_{t_1}^{t_2} \left\{ \frac{1}{2} \rho \text{grad } \phi \cdot \text{grad } \phi dV - \frac{1}{2} \frac{\rho}{c^2} \iiint \dot{\phi}^2 dV \right\} dt$$

Looking for variations on δJ .

$$\delta J = \int_{t_1}^{t_2} \left\{ \rho \text{grad } \phi \cdot \text{grad } \delta \phi dV - \frac{1}{c^2} \iiint \dot{\phi} \delta \dot{\phi} dV \right\} dt$$

Integrating the second term by parts with respect to time,

$$= \frac{1}{c^2} \iiint \left\{ \dot{\phi} \delta \phi \Big|_{t_1}^{t_2} - \int_{t_1}^{t_2} \ddot{\phi} \delta \phi dt \right\} dV$$

Applying Greene's theorem, the first term of δJ can be written as

$$\int_{t_1}^{t_2} \rho \left\{ - \iiint \nabla^2 \phi \delta \phi dV + \iint \delta \phi \text{grad } \phi \cdot dS \right\} dt$$

where S is the surface of the volume of interest. But $\delta \phi$ is zero at t_1 and t_2 , therefore

$$\delta J = \int_{t_1}^{t_2} \left\{ \rho \iiint \left(\frac{1}{c^2} \ddot{\phi} - \nabla^2 \phi \right) \delta \phi dV - \iint \delta \phi \text{grad } \phi \cdot dS \right\} dt$$

Since $\delta J = 0$ and $\delta \phi$ is arbitrary between t_1 and t_2 , the integrands must be zero.

$$\nabla^2 \phi - \frac{1}{c^2} \ddot{\phi} = 0$$

$$\text{grad } \phi \cdot \delta S = 0 \text{ on } S \quad (\text{A12})$$

These equations can be derived from (A11) and represent, respectively, the wave equation and the natural boundary condition. It is only right that the "velocity potential" obey the wave equation as does the pressure p in (A9). The natural boundary condition can be translated either as the normal pressure gradient or the normal velocity being zero at a rigid boundary.

A.4 Matrix Formulation of the Functional

Let the velocity potential within an element be written

$$\phi_e = \{F(\underline{x})\}^T \{\phi_n(t)\}_e \quad (\text{A13})$$

where $\{F(\underline{x})\}$ is a column vector (of some length) of functions of \underline{x} , the coordinates used to define the geometry, such that $\{\phi_n(t)\}_e$ (also a column vector of the same length) is the value of ϕ which varies with time at points called nodes. The right-hand side of (A13) may be differentiated and used in the desired equations containing ϕ_e , but it should be realized that the equations are now approximate. Therefore,

$$\text{grad } \phi_e = \{\text{grad } F\}^T \{\phi_n\}_e$$

and

$$\dot{\phi}_e = \{\dot{F}\}^T \{\dot{\phi}_n\}_e$$

neglecting the variables in round brackets. The energy equations for an element can now be written

$$T_e = \frac{\rho^2}{2} \{\phi_n\}_e^T \frac{1}{\rho} \iiint_v \{\text{grad } F\} \cdot \{\text{grad } F\}^T dV \{\phi_n\}_e$$

$$U_e = \frac{\rho^2}{2} \{\dot{\phi}_n\}_e^T \frac{1}{\rho c^2} \iiint_v \{F\} \{F\}^T dV \{\dot{\phi}_n\}_e \quad (\text{A14})$$

The products within the integral signs are now matrices, which can be integrated to give the final form of the energy equations

$$T_e = \frac{\rho^2}{2} \{\phi_n\}_e^T [S_e] \{\phi_n\}_e$$

$$U_e = \frac{\rho^2}{2} \{\dot{\phi}_n\}_e^T [P_e] \{\dot{\phi}_n\}_e \quad (\text{A15})$$

The square of the acoustic density ρ is kept aside for consistency of units in later work where $[S_e]$, $[P_e]$ are the elemental acoustical stiffness and pressure matrices. These matrices can easily be defined by comparison of (A14) and (A15).

Substituting these equations in the functional

$$J = \frac{\rho^2}{2} \int_{t_1}^{t_2} [\{\phi_n\}_e^T [S_e] \{\phi_n\}_e - \{\dot{\phi}_n\}_e^T [P_e] \{\dot{\phi}_n\}_e] dt$$

Taking the first variation of this equation and integrating the second term with respect to time gives

$$\delta J = -\{\delta\phi_n\}_e^T [P_e] \{\dot{\phi}_n\}_e \Big|_{t_1}^{t_2} + \int_{t_1}^{t_2} \{\delta\phi_n\}_e^T [[S_e] \{\phi_n\}_e + [P_e] \{\ddot{\phi}_n\}_e] dt = 0$$

The first term is zero because $\delta\phi$ is zero at t_1 and t_2 . This can be seen from the potential energy equation in (A14), knowing that

$$\delta\phi = \{F(\underline{x})\}^T \{\delta\phi_n\}_e = 0 \quad \text{at } t_1 = 0 \text{ and } t_2 = 0$$

Since $\delta\phi$ is also arbitrary between t_1 and t_2

$$[S_e] \{\phi_n\}_e + [P_e] \{\ddot{\phi}_n\}_e = 0 \quad (A16)$$

The velocity potential lacks physical significance so rather than using the nodal vector $\{\phi_n\}$, (A16) can be differentiated with respect to time and rewritten in terms of the element nodal excess pressures $\{p_n\}_e$ by using (A11)

$$[S_e] \{p_n\}_e + [P_e] \{\dot{p}_n\}_e = 0 \quad (A17)$$

This last formula will be used in the finite element analysis of acoustic enclosures with rigid boundaries.

APPENDIX B

MATHEMATICAL TABULATIONS AND OPERATIONS

B.1 Fourier Approximation and Integrals Over One-Half Period

Let $h(z)$ be a function that satisfies the wave equation and boundary conditions that $\frac{\delta h}{\delta z} = 0$ at $z = 0$ and $z = d$. If it is piecewise continuous and finite within the interval, then

$$h(z) = \sum_{n=0}^{\infty} e_n \cos \frac{n\pi z}{d}$$

where

$$e_0 = \frac{1}{d} \int_0^d h(z) dz$$

$$e_n = \frac{2}{d} \int_0^d h(z) \cos \frac{n\pi z}{d} dz \quad \text{for } n \neq 0$$

The following integrals will be useful in future analysis

$$\int_0^d \sin \frac{q\pi z}{d} \sin \frac{n\pi z}{d} dz = 0 \quad q = n = 0$$

$$= 0 \quad q \neq n$$

$$= \frac{d}{2} \quad q = n \neq 0$$

$$\int_0^d \cos \frac{q\pi z}{d} \cos \frac{n\pi z}{d} dz = d \quad q = n = 0$$

$$= 0 \quad q \neq n$$

$$= \frac{d}{2} \quad q = n \neq 0$$

$$\int_0^d \sin \frac{q\pi z}{d} \cos \frac{n\pi z}{d} dz = 0 \quad \text{for all } q, n.$$

B.2 Hermitian Interpolation Polynomials.

i) Polynomials: $0 \leq e \leq 1$

$$f_1(e) = 1 - 3e^2 + 2e^3$$

$$f_2(e) = e - 2e^2 + e^3$$

$$f_3(e) = 3e^2 - 2e^3$$

$$f_4(e) = e^3 - e^2$$

ii) Characteristics:

	f_1	f_2	f_3	f_4
$f(0)$	1	0	0	0
$f(1)$	0	0	1	0
$\frac{df(0)}{de}$	0	1	0	0
$\frac{df(1)}{de}$	0	0	0	1

iii) Integrals:

$$\int_0^1 f_i(e) f_j(e) de$$

	f_1	f_2	f_3	f_4
f_1	13/35	11/210	9/70	-13/420
f_2		1/105	13/420	-1/140
f_3	Symmetric		13/35	-11/210
f_4				1/105

$$\int_0^1 f_i'(e) f_j'(e) de$$

	f_1'	f_2'	f_3'	f_4'
f_1'	1.2	0.1	-1.2	0.1
f_2'		4/30	-0.1	-1/30
f_3'	Symmetric		1.2	-0.1
f_4'				4/30

$$\int_0^1 f_i''(e) f_j''(e) de$$

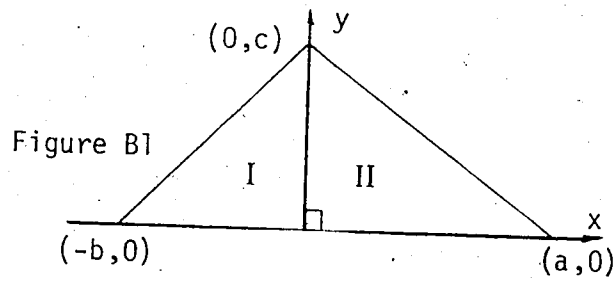
	f_1''	f_2''	f_3''	f_4''
f_1''	12.	6.	-12.	6.
f_2''		4.	-6.	2.
f_3''	Symmetric		12.	-6.
f_4''				4.

Note: $f'(e)$ is the derivative of the function f with respect to the quantity in brackets.

$$\int_0^1 f_i(e) f_j''(e) de$$

	f_2''	f_3''	f_4''	
f_1	-1.2	-1.1	1.2	-0.1
f_2	-0.1	-4/30	0.1	1/30
f_3	1.2	0.1	-1.2	1.1
f_4	-0.1	1/30	0.1	-4/30

B.3 Triangular Integral



Section I:

$$y = \frac{c}{b}(x + b) = c \left(1 + \frac{x}{b}\right)$$

Section II:

$$y = \frac{c}{a}(a - x)$$

$$I = \int_{-b}^0 \int_0^{\frac{c}{b}(x+b)} x^m y^n dy dx$$

$$= \int_{-b}^0 \frac{x^m y^{n+1}}{(n+1)} dx \Big|_0^{\frac{c}{b}(x+b)}$$

$$= \left(\frac{c}{b}\right)^{n+1} \frac{n!}{(n+1)!} \int_{-b}^0 x^m (x+b)^{n+1} dx$$

$$u = (x+b)^{n+1}$$

$$du = (n+1)(x+b)^n$$

$$v = \frac{x^{m+1}}{m+1}$$

$$dv = x^m$$

$$I = (x+b)^{n+1} \frac{x^{m+1}}{m+1} \Big|_{-b}^0 - \left(\frac{c}{b}\right)^{n+1} \frac{1}{(m+1)} \int_{-b}^0 x^{m+1} (x+b)^n dx$$

$$= \left(\frac{c}{b}\right)^{n+1} \frac{n!(-1)^{n+1}}{(m+1+n)!} m! \int_{-b}^0 x^{m+n+1} dx$$

$$= \left(\frac{c}{b}\right)^{n+1} \frac{n!m!(-1)^{n+1}}{(m+2+n)!} x^{m+n+2} \Big|_{-b}^0$$

$$= \frac{(-1)^{2(n+2)+m}}{(m+2+n)!} m! n! (b)^{m+n+2} \left(\frac{c}{b}\right)^{n+1}$$

$$= (-1)^m \frac{m!n!}{(m+2+n)!} b^{m+1} c^{n+1}$$

$$= - \frac{m!n!}{(m+2+n)!} (-b)^{m+1} c^{n+1}$$

$$\begin{aligned}
 \text{II} &= \int_0^a \int_0^{\frac{c}{a}(a-x)} x^m y^n dy dx \\
 &= \frac{1}{n+1} \int_0^a x^m y^{n+1} dx \Big|_0^{\frac{c}{a}(a-x)} \\
 &= \left(\frac{c}{a}\right)^{n+1} \frac{1}{(n+1)} \int_0^a x^m (a-x)^{n+1} dx
 \end{aligned}$$

$$u = (a-x)^{n+1}$$

$$du = -(n+1)(a-x)^n dx$$

$$v = \frac{x^{m+1}}{m+1}$$

$$dv = x^m dx$$

$$\text{II} = \left(\frac{c}{a}\right)^{n+1} \frac{(a-x)^{n+1}}{(n+1)} \frac{x^{m+1}}{(m+1)} \Big|_0^a + \int_0^a \left(\frac{c}{a}\right)^n \frac{x^{m+1}}{(m+1)} (a-x)^n dx$$

after n integrations

$$\begin{aligned}
 \text{II} &= \left(\frac{c}{a}\right)^{n+1} \frac{m!n!}{(m+n+1)!} \int_0^a x^{m+n+1} dx \\
 &= \left(\frac{c}{a}\right)^{n+1} \frac{m!n!}{(m+n+2)!} a^{m+n+2}
 \end{aligned}$$

$$= \frac{m!n!}{(m+n+2)!} a^{m+1} c^{n+1}$$

Total integral over area of triangle

$$\int_A x^m y^n dydx = \frac{m!n!}{(m+n+2)!} c^{n+1} (a^{m+1} - (-b)^{m+1})$$

B.4 Acoustic Rotational Matrix

Since the element is orientated so as to simplify the surface integral, it must be rotated to a position where the nodal characteristics are compatible with adjacent elements. The symmetry of the [P] and [S] matrices can be retained if the invariance of the energy equations are used. The rotation to a new system (x'; y') from the old system (x, y) is a simple one:

p remains unchanged

$$\frac{\delta p}{\delta x'} = \frac{\delta p}{\delta x} \frac{\delta x}{\delta x'} + \frac{\delta p}{\delta y} \frac{\delta y}{\delta x'}$$

$$\frac{\delta p}{\delta y'} = \frac{\delta p}{\delta x} \frac{\delta x}{\delta y'} + \frac{\delta p}{\delta y} \frac{\delta y}{\delta y'}$$

$$\frac{\delta x}{\delta x'} = \cos \theta$$

$$\frac{\delta x}{\delta y'} = -\sin \theta$$

$$\frac{\delta y}{\delta x'} = \sin \theta$$

$$\frac{\delta y}{\delta y'} = \cos \theta$$

Thus, for any given nodal point

$$\begin{Bmatrix} p' \\ \frac{\delta p}{\delta x'} \\ \frac{\delta p}{\delta y'} \end{Bmatrix} = \begin{bmatrix} 1 & 0 & 0 \\ 0 & \cos \theta & \sin \theta \\ 0 & -\sin \theta & \cos \theta \end{bmatrix} \begin{Bmatrix} p \\ \frac{\delta p}{\delta x} \\ \frac{\delta p}{\delta y} \end{Bmatrix}$$

To rotate the total pressure vector for the triangular element, three such rotational matrices must be placed down the diagonal of a large matrix, $[\theta]$, whose remaining entries are zero

$$[p'] = [\theta]^T [p]$$

also $[p] = [\theta]^T [p']$ can be easily proven

B.5. Coordinate Relation Matrix for Triangular Acoustic Elements

$$[A] = \begin{bmatrix} 1 & a & 0 & a^2 & 0 & 0 & 3a^3 & 0 & 0 \\ 0 & 1 & 0 & 2a & 0 & 0 & 3a^2 & 0 & 0 \\ 0 & 0 & 1 & 0 & a & 0 & 0 & a^2 & 0 \\ 1 & b & 0 & b^2 & 0 & 0 & 3b^3 & 0 & 0 \\ 0 & 1 & 0 & 2b & 0 & 0 & 3b^2 & 0 & 0 \\ 0 & 0 & 1 & 0 & b & 0 & 0 & b^2 & 0 \\ 1 & 0 & c & 0 & 0 & c^2 & 0 & 0 & c^3 \\ 0 & 1 & 0 & 0 & c & 0 & 0 & c^2 & 0 \\ 0 & 0 & 1 & 0 & 0 & 2c & 0 & 0 & 3c^2 \end{bmatrix}$$

Let $u = a + b + c$

$\frac{b^2(3a-b)}{(a-b)^3}$	$\frac{-b^2a}{(a-b)^2}$	$\frac{a^2(a-3b)}{(a-b)^3}$	$\frac{-a^2b}{(a-b)^2}$	
$\frac{-6ab}{(a-b)^3}$	$\frac{b(2a+b)}{(a-b)^2}$	$\frac{6ab}{(a-b)^3}$	$\frac{a(a+2b)}{(a-b)^2}$	
$\frac{-6a^2b^2}{c(a-b)^3}u$	$\frac{ab^2(2a+b)}{c(a-b)^2}u$	$\frac{6a^2b^2}{c(a-b)^3}u$	$\frac{a^2b(a+2b)}{c(a-b)^2}u$	$\frac{a(a-c)}{(a-b)u}$
$\frac{3(a+b)}{(a-b)^3}$	$\frac{-(a+2b)}{(a-b)^2}$	$\frac{-3(a+b)}{(a-b)^3}$	$\frac{-(2a+b)}{(a-b)^2}$	$\frac{-ab}{cu}$
$\frac{6ab(a+b)}{c(a-b)^3}u$	$\frac{-b(a+b)(2a+b)}{c(a-b)^2}u$	$\frac{-6ab(a+b)}{c(a-b)^3}u$	$\frac{-a(a+b)(a+2b)}{c(a-b)^2}u$	$\frac{a+b}{cu}$
$\frac{-3b^2(3a-b)(b-c)}{c^2(a-b)^3}u$	$\frac{-ab^2(a+3c-b)}{c^2(a-b)^2}u$	$\frac{-3a^2((a-3b)(a-c) - 3a^2 + b(a+b))}{uc^2(a-b)^3}$	$\frac{a^2b(a-3c-b)}{c^2(a-b)^2}u$	$\frac{3}{c^2}$
$\frac{-2}{(a-b)^3}$	$\frac{1}{(a-b)^2}$	$\frac{2}{(a-b)^3}$	$\frac{1}{(a-b)^2}$	$\frac{-1}{c}$
$\frac{-6ab}{c(a-b)^3}u$	$\frac{b(2a+b)}{c(a-b)^2}u$	$\frac{6ab}{c(a-b)^3}u$	$\frac{a(a+2b)}{c(a-b)^2}u$	$\frac{-1}{cu}$
$\frac{2b^2(3a-b)(b-c)}{uc^3(a-b)^3}$	$\frac{ab^2(2c-b)}{c^3(a-b)^2}u$	$\frac{2a^2((a-3b)(a-c) + ab)}{uc^3(a-b)^3}$	$\frac{a^2b(2c-a)}{uc^3(a-b)^2}$	$\frac{-2}{c^3}$

$[A^{-1}] =$

APPENDIX C
MATRIX FORMULATIONS

C.1 Decreasing the Order of a Matrix

The solution to the eigenvalue problem for a single triangular acoustic element gives ten eigenvectors $\{n\}_i$, of which $\{n\}_{10}$ is of the least interest for this analysis (because of its high eigenvalue). These eigenvectors are orthogonal through the $[S_e]$ or $[P_e]$ matrices of the equation

$$[[S_e] - \omega^2 [P_e]] \{p_e\} = 0$$

This would mean

$$\begin{aligned} \{n\}_i^T [S_e] \{n\}_j &= \text{constant } i = j \\ &= 0 \quad i \neq j \end{aligned}$$

$$\begin{aligned} \{n\}_i^T [P_e] \{n\}_j &= \text{constant } i = j \\ &= 0 \quad i \neq j \end{aligned}$$

where $i, j = 1, \dots, 10$

The orthogonality of the eigenvectors allows any pressure $\{p_e\}$ within the element to be defined by

$$\{p_e\} = \sum_{m=1}^{10} a_m \{n\}_m$$

By adding the constraint that the tenth eigenvector does

not contribute to the pressure distribution, a new pressure vector $\{p_e^*\}$ is arrived at such that

$$\{p_e^*\}^T [A] \{n\}_{10} = 0 \quad (C1)$$

where $[A]$ replaces the $[S_e]$ or $[P_e]$.

By partitioning the vectors and matrix as follows

$$\{p_e^*\} = \begin{bmatrix} p_1^* \\ p_2^* \\ \cdot \\ \cdot \\ \cdot \\ p_9^* \\ \hline p_{10}^* \end{bmatrix} \quad \{n\}_{10} = \begin{bmatrix} n_1 \\ n_2 \\ \cdot \\ \cdot \\ \cdot \\ n_9 \\ \hline n_{10} \end{bmatrix}$$

$$[A] = \begin{bmatrix} A_{11} & A_{12} \\ \hline A_{21} & A_{22} \end{bmatrix}$$

where A_{21} , A_{12} are vectors and A_{22} is a scalar.

Let $\{p_e^*\}_c$ be a vector of the upper nine elements of $\{p_e^*\}$ and $\{n_c\}_{10}$ be the upper portion of $\{n\}_{10}$. Then (C1) can be written as

$$\begin{aligned} & \{p_e^*\}_c^T [A_{11}] \{n_c\}_{10} + \{p_e^*\}_c^T [A_{12}] \{n_{10}\} \\ & + \{p_{10}^*\}^T [A_{21}] \{n_c\}_{10} + \{p_{10}^*\}^T [A_{22}] \{n_{10}\} = 0 \end{aligned}$$

Therefore

$$\{p_{10}^*\}^T = \{p_e^*\}^T [A_c] / B$$

where

$$A_c = [[A_{11}] \{n_c\}_{10} + [A_{12}] \{n_{10}\}]$$

$$B = [A_{21}] \{n_c\}_{10} - [A_{22}] \{n_{10}\} \quad (C2)$$

Again, using orthogonality

$$\{p_e^*\}^T [A^*] \{p_e^*\} = \text{constant}$$

where $[A^*]$ can also be either of the elemental matrices. The matrix can be partitioned

$$\{p_e^*\}^T [A_{11}^*] \{p_e^*\} + \{p_e^*\}^T [A_{12}^*] \{p_{10}^*\}$$

$$+ \{p_{10}^*\} [A_{21}^*] \{p_e^*\} + \{p_{10}^*\} [A_{22}^*] \{p_{10}^*\} = \text{constant}$$

Substituting from (C2)

$$\{p_e^*\}^T \left[[A_{11}^*] + [A_{12}^*] [A_c]^T / B \right.$$

$$\left. + [A_c] [A_{21}^*] / B \right.$$

$$\left. + [A_c] [A_{21}^*] [A_c]^T / B^2 \right] \{p_e^*\}$$

It is now seen that the vector $\{p_e^*\}$ can be looked on as a condensed pressure vector while the result in outer square brackets is a condensed acoustic stiffness or mass matrix depending on the definition of $[A^*]$.

C.2. Applying Boundary Conditions

The overall matrices when initially assembled have no boundary conditions. The system must be "tied down" before the eigenvalue problem can be performed, because the unconstrained matrices are singular.

Several of the nodal characteristics are related to other nodal characteristics, i.e. $\frac{\delta p}{\delta x} = -\cot \eta \frac{\delta p}{\delta y}$, or are zero. The latter characteristics can be handled by simply removing the rows and columns which they (the zero characteristics) multiply with, because they supply nothing to the energy of the system. The zero characteristics are then deleted from the overall nodal characteristic vector $\{p_n\}$, leaving a "shrunk" energy matrix and nodal characteristic vector. The other defined nodal characteristic $\{p^*\}$ can be separated from the undefined ones $\{p_u\}$ by simply shifting rows and columns of the overall matrices so that the calculations remain the same, i.e.

$$\{p_n\}^T [B'] \{p_n\} = \begin{pmatrix} p_u \\ p^* \end{pmatrix}^T [B] \begin{pmatrix} p_u \\ p^* \end{pmatrix} = \text{constant}$$

where the left hand side is the original nodal characteristic vector and original matrix and the right hand side is the re-arranged form.

A relationship exists between $\{p^*\}$ and $\{p_u\}$

$$\{p^*\} = [R] \{p_u\}$$

By partitioning the matrix similarly to the way shown in Appendix C.1, a new overall energy matrix $[B^*]$ can be found in terms of the unknown nodal characters

$$[B^*] = [B_{11}] + [B_{12}] [R] + [R]^T [B_{21}]$$

$$+ [R]^T [B_{22}] [R]$$

17699

NATIONAL LIBRARY
OTTAWA



BIBLIOTHÈQUE NATIONALE
OTTAWA

NAME OF AUTHOR... DONALD B. STEWART.....

TITLE OF THESIS... THE RED TURNIP BEETLE, ENTOMOSCELES
AMERICANA BROWN (COLEOPTERA: CHRYSOMELIDAE)
..... BIOLOGY AND PLANT RELATIONSHIPS

UNIVERSITY OF ALBERTA.....

DEGREE FOR WHICH THESIS WAS PRESENTED... M. Sc.....

YEAR THIS DEGREE GRANTED... 1973.....

Permission is hereby granted to THE NATIONAL LIBRARY
OF CANADA to microfilm this thesis and to lend or sell copies
of the film.

The author reserves other publication rights, and
neither the thesis nor extensive extracts from it may be
printed or otherwise reproduced without the author's
written permission.

(Signed) } Donald B. Stewart.....

PERMANENT ADDRESS:

101, 11470 - 106 Ave
Edmonton
.....

DATED July 20..... 19 73

THE UNIVERSITY OF ALBERTA

THE RED TURNIP BEETLE, ENTOMOSCELIS AMERICANA BROWN

(COLEOPTERA: CHRYSOMELIDAE),

BIOLOGY AND PLANT RELATIONSHIPS

BY



D. BRUCE STEWART

A THESIS

SUBMITTED TO THE FACULTY OF GRADUATE STUDIES AND
RESEARCH IN PARTIAL FULFILMENT OF THE REQUIREMENTS
FOR THE DEGREE OF MASTER OF SCIENCE

DEPARTMENT OF ENTOMOLOGY

EDMONTON, ALBERTA

Fall, 1973

THE UNIVERSITY OF ALBERTA

FACULTY OF GRADUATE STUDIES AND RESEARCH

The undersigned certify that they have read, and recommend to the Faculty of Graduate Studies and Research, for acceptance, a thesis entitled "The Red Turnip Beetle, Entomoscelis americana Brown (Coleoptera: Chrysomelidae), Biology and Plant Relationships" submitted by Donald Bruce Stewart in partial fulfilment of the requirements for the degree of Master of Science.

Brian Hodgson
Supervisor

V. J. L. S.

W. G. Evans

Dated 5 July 1973

ABSTRACT

The life history of *Entomoscelis americana* Brown was followed for the 2 years of the study, 1971 and 1972. Distribution in North America includes the 4 western Canadian provinces, Yukon Territory, Alaska, Washington, Idaho, Montana, Wyoming, Colorado, North Dakota, Wisconsin, and Minnesota. The range of *E. americana* is limited by mean daily July temperatures in excess of 70° F and below 55° F, and by annual precipitation in excess of 32 inches. No evidence of a lower limit of precipitation was found. Diapause was terminated in the laboratory by cold treatment. The larvae and newly-emerged adults are photo-positive. Aestivating adults are photo-negative and show thigmokinesis in conjunction with moist substrate. Following aestivation, the adults are again photo-positive. Dispersal occurs in August, following which, males respond to female odours. *E. americana* is oligophagous and restricted to the Cruciferae. Food plant finding by the larvae is largely by trial and error, although food plant odours act as arrestants at close range and non-food plant odours can act as repellents. Adults respond to food plant odours during August dispersal. Food plant acceptance is determined by at least 2 plant chemicals in the Cruciferae: an aldehyde stimulates larval feeding and synergises with a compound that has phenolic properties to stimulate adult feeding.

ACKNOWLEDGEMENTS

I express sincere thanks to Dr. Brian Hockin, chairman of my committee, for his guidance and many valuable suggestions during this study. I also extend appreciation to other members of the Entomology Department, University of Alberta, especially to Dr. W. George Evans for his helpful comments and critical review of the thesis. Thanks also to Dr. N. Colotelo of the Plant Science Department, University of Alberta for critically reviewing the thesis.

Special thanks are due to Mr. A. Rustemeier of Morinville, Alberta for co-operation in allowing the field studies to be carried out on land leased by him in the St. Albert district of Alberta.

Distribution information from the United States was obtained from the following United States Department of Agriculture, Economic Insect Survey co-ordinators:

W. F. Barr, Department of Entomology, University
of Idaho, Moscow, Idaho.

W. J. Brandvik, North Dakota Department of
Agriculture, Bismark, N.D.

P. J. Clausen, Department of Entomology, Fisheries,
and Wildlife, University of Minnesota, St. Paul,
Minn.

W. D. Frank, Colorado Department of Agriculture,
Denver, Colorado.

- D. L. Keith, College of Agriculture, University
of Nebraska, Lincoln, Neb.
- G. F. Knowlton, Department of Zoology, Utah State
University, Logan, Utah.
- P. A. Jones, Entomology-Zoology Department, South
Dakota State University, Brookings, S.D.
- J. E. May, Arizona Commission of Agriculture and
Horticulture, Phoenix, Ariz.
- G. L. Nielson, New Mexico Department of Agriculture,
Las Cruces, N.M.
- R. Penrose, Oregon Department of Agriculture,
Salem, Ore.
- H. G. Petty, College of Agriculture, University
of Illinois, Urbana, Ill.
- F. M. Philips, United States Department of
Agriculture, Hyattsville, Md.
- R. Pratt, Office of the State Entomologist,
Bozeman, Mont.
- S. O. Ryan, Co-operative Extension Service, Iowa
State University, Ames, Iowa.
- R. J. Sauer, Department of Entomology, Michigan
State University, East Lansing, Mich.
- R. H. Washburn, United States Department of
Agriculture, Palmer, Alaska.

Distribution information for Canada was obtained from the following personnel of provincial and federal departments of agriculture:

- C. F. Barrett, Saskatchewan Department of Agriculture, Regina, Sask.
- G. S. Brown, Canada Department of Agriculture, Ottawa, Ont.
- M. G. Dolinski, Alberta Department of Agriculture, Edmonton, Alta.
- J. A. Doyle, Quebec Department of Agriculture and Colonisation, Quebec City, P.Q.
- A. Hikichi, Ontario Department of Agriculture and Food, Simcoe, Ont.
- A. J. Kolach, Manitoba Department of Agriculture, Winnipeg, Man.

Distribution information for British Columbia was obtained from the Entomology Branch, British Columbia Department of Agriculture, Victoria, B.C.

My thanks are also due to Mr. H. Welling, Plant Science Department, University of Alberta, for providing greenhouse space, soil and equipment for the rearing of the experimental plants used in this study.

Finally, I wish to thank Mrs. M. McLarty, typist of this thesis, for a job well done.

TABLE OF CONTENTS

1. INTRODUCTION	1
2. LITERATURE REVIEW	3
2.A. <i>Entomoseelis americana</i> Brown	3
2.B. Plant selection by phytophagous insects	4
3. <u>ENTOMOSCELIS AMERICANA</u> BROWN	12
3.A. Geographical distribution	12
3.B. Description of stages	16
3.B.i. Egg	16
3.B.ii. Larvae	16
First instar	16
Second instar -	18
Third instar -	18
Fourth instar -	18
Fifth instar -	19
3.B.iii. Pupa	19
3.B.iv. Adult	19
3.C. Life Cycle and habits	22
3.C.i. Hatching	22
3.C.ii. Habits of the larvae	22
3.C.iii. Habits of the adults	22
3.D. Laboratory rearing of <i>E. americana</i>	24
3.D.i. Rearing techniques	24
3.D.ii. Termination of diapause	25

3.E. Adult	27
3.E.i. Materials and methods	27
3.E.ii. Results	29
3.F. Olfactory response of males to females	29
3.F.i. Materials and methods	32
3.F.ii. Results	34
4. FOOD PLANT RELATIONSHIPS OF <u>E. AMERICANA</u>	36
4.A. Food plant finding by the larvae	36
4.A.i. Materials and methods	37
4.A.ii. Results	38
4.B. Food plant finding by the adults	42
4.B.i. Materials and methods	42
4.B.ii. Results	43
4.C. Food plant acceptance	45
4.C.i. Materials and methods	45
4.C.ii. Results	52
5. CONCLUSIONS AND DISCUSSION	59
6. REFERENCES	63
7. APPENDICES	73
I. The photo-response of adults of <i>Entomoscelis americana</i>	73
II. The thigmokinetic response of adults of <i>Entomoscelis americana</i>	75

Appendix	III.	The response of males of <i>Entomoscelis americana</i> to the odour of gravid females.....	76
	IV.	The response of first instar larvae of <i>Entomoscelis americana</i> to the odour of rape foliage in 2-way choice chambers....	77
	V.	The response of first instar larvae of <i>Entomoscelis americana</i> to the odour of food plants and non-food plants in a moving air olfactometer.....	78
	VI.	The response of adults of <i>Entomoscelis americana</i> to odours of rape foliage and blossoms.....	81
	VII.	The response of <i>Entomoscelis americana</i> to lettuce leaf discs treated with chemical fractions of rape foliage.....	83

LIST OF TABLES

Table 1.	The dimensions of all stages of <i>Entomoscelis americana</i>	21
Table 2.	The percent hatch of eggs of <i>Entomoscelis americana</i> following cold treatment	26
Table 3.	The photo-response of adults of <i>Entomoscelis americana</i> in a light-dark choice chamber	31
Table 4.	The thigmokinetic response of adults of <i>Entomoscelis americana</i> in a moist-dry choice chamber	33
Table 5.	The response of males to the odour of gravid females in a moving air olfactometer	35
Table 6.	The response of first instar larvae of <i>Entomoscelis americana</i> to the odours of food plants and non-food plants in a moving air olfactometer	40
Table 7.	The response of first instar larvae of <i>Entomoscelis americana</i> to growing food plants and non-food plants in a choice chamber	41
Table 8.	The response of adults of <i>Entomoscelis americana</i> to odours of rape foliage and blossoms in a double air-stream olfactometer	44

Table 9. The non-cruciferous plants tested for acceptability with *Entomoscelis americana* 49

Table 10. The response of *Entomoscelis americana* to lettuce leaf discs treated with chemical fractions of rape foliage 54

LIST OF FIGURES

Fig. 1. The distribution of *Entomoscelis americana* in North America 15

Fig. 2. The choice chamber used to evaluate moisture and thigmokinetic responses of *Entomoscelis americana* 30

Fig. 3. The moving air olfactometer used to evaluate olfactory responses in *Entomoscelis americana* 30

Fig. 4. The 2-way, food choice chamber used to evaluate the response of *Entomoscelis americana* to food plants, non-food plants, and chemical extracts of rape seed foliage 47

Fig. 5. A flow diagram outlining the procedure used to refine a chemical feeding stimulant from rape seed foliage 57

INTRODUCTION

The red turnip beetle, *Entomoscelis americana* Brown was first collected in Canada in 1825 during Sir John Franklin's second northern land expedition, and until 1941 was considered identical to the Eurasian species, *Entomoscelis adonidis* Pallas. The North American species was re-described as *E. americana* in 1941 by Brown (1942).

Both larval and adult stages of *E. americana* are oligophagous and restricted to cruciferous plants. The adults were first reported attacking cultivated plants at Regina in 1885, and minor outbreaks occurred on the Canadian prairies in 1918, 1927, and 1936. The red turnip beetle is a sporadic pest of cruciferous garden crops in the interior of Alaska, and along the Mackenzie River valley in the North West Territories.

During the past 30 years, *E. americana* received little attention in Canada since it is not a pest of the cereal and forage crops that have been prominent in western Canadian agriculture. It has been largely ignored by American workers as its range in agricultural areas is chiefly restricted to the Canadian North-West.

The preference of *E. americana* for cruciferous plants causes it to be an intermittent, but often severe pest of the increasing rape acreage (*Brassica campestris* L.) in Western Canada. Although the beetle completes its larval stages before most rape crops are sown, the adults emerge when these crops are in the seedling stage, and it is at this time, especially in the parkland areas of the

prairies provinces, that the red turnip beetle is often a severe agricultural pest.

The object of this study is twofold: firstly, to provide a comprehensive description of the stages, life cycle and habits of *E. americana*, and secondly, to investigate the mechanism of food plant selection.

Field studies were conducted in the St. Albert area of Alberta during the growing seasons of 1971 and 1972. Experimental work pertaining to food plant selection, taxes and kineses, embryological development, and the development of rearing techniques were carried out in the laboratories of the Department of Entomology, University of Alberta. The experimental plants used in this study were cultured in the greenhouses of the Plant Science Department, University of Alberta, on the university campus.

2. LITERATURE REVIEW

2.A. *Entomoscelis americana* Brown

The Eurasian red turnip beetle was first noted in the literature by Pallas (1771) as *Chrysomela adonidis*, the specific name derived from the food plant *Adonis autumnalis* L., a herbaceous annual of the family Ranunculaceae. The same insect species was described by J. C. Fabricius in 1777 (Zimsen, 1964) as *Chrysomela trilineata*, and designated *Entomoscelis adonidis* by Redtenbacher (1874). Under this latter designation, adult morphology was described by Linné (1789) and larval morphology by Weise (1893).

The first report of the North American red turnip beetle was from Manitoba, near Latitude 54° N, in 1825; several specimens were collected during Sir John Franklin's second inland expedition, designated *adonidis*, and placed in the genus *Phaedon* Latreille by Kirby (Richardson, Swainson, and Kirby, 1837). Fletcher (1893) and Chittenden (1902) described the life history and both followed Kirby in referring North American specimens of *Entomoscelis* Chevrolat to the Eurasian *adonidis* Pallas. Powell (1941) also used this designation in his description of the genitalia. Because of structural differences between the Eurasian and North American species, Brown (1942) re-described the latter as *Entomoscelis americana*.

The first cultivated crop recorded attacked by *E. americana* was turnip at Regina in 1885 (Fletcher, 1888). The Canadian Insect Pest Review (1924) listed later reports and included the known distribution of the red turnip beetle in Canada. First reports of

attacks on cruciferous vegetable crops in other areas include Manitoba in 1890, 1900, British Columbia in 1905, and the Yukon Territory in 1907. The red turnip beetle attracted attention in Western Canada during minor outbreaks at Edmonton in 1918, (Whitehouse, 1919), Saskatchewan in 1927 (King, 1928), and in the park belt and adjacent prairie regions of Saskatchewan and Alberta in 1936 (Twinn, 1936). Arnason (1948) and Strickland and Hocking (1950) outlined control methods, and a brief description of the red turnip beetle was provided by Beirne (1971).

2.B. Plant selection by phytophagous insects

Early workers recognized that many phytophagous insects are restricted to particular plant taxa for feeding or oviposition. Burmeister (1836) noted that certain flea beetles display a marked preference for cruciferous plants. Fabre (1918) referred to a similar preference in the cabbage butterfly, *Pieris rapae* L. as "botanical instinct", and wrote,

"The botanist, to recognize a crucifer, requires the indication provided by a flower. Here *Pieris* surpasses us ... and she knows this group of plants to perfection." (p. 294, 295).

The classical work of Verschaeffelt (1910) removed part of the mystery of Fabre's botanical instinct by demonstrating that mustard oil glucosides, common in cruciferous plants, are responsible for attracting *Pieris rapae*. Brues (1920) suggested that such botanical instinct may be nothing more than extreme sensitivity to a complex of chemical and physical stimuli provided by the plants. Food plant

discrimination by lepidopterous larvae was shown by Dethier (1937) to involve both gustatory and olfactory stimuli.

The literature from 1864 to 1924, on plant specificity in phytophagous insects was reviewed by Brues (1924). Thorsteinson (1960) provided a review to 1959 and Jacobson (1966) continued the review to 1965.

Person (1931) proposed that volatile components in pine bark such as aldehydes and esters were responsible for attracting the western pine beetle, *Dendroctonus brevicornis* LeConte to its host, however he cited little evidence to support his proposal. As the result of a limited number of tests, Dethier (1941) reported that several essential oils of a number of umbelliferous plants were attractive to larvae of the swallowtail, *Papilio asterus* Cramer.

During later years many botanical compounds, of little importance to insects nutritionally, were reported attractive to various, specialized phytophagous insects. In well-documented studies, Thorsteinson (1953) and Nayar and Thorsteinson (1963) showed that the larvae of the diamondback moth, *Plutella maculipennis* Curtis were stimulated to feed by several mustard oil glucosides extracted from tissues of plant species in the families Crucifereae and Tropaeolaceae. Alcohols and aldehydes in mulberry leaves were reported attractive to larvae of the silkworm, *Bombyx mori* L. (Watanabe, 1958; Hamamura, 1959; Nayar and Fraenkel, 1962). By means of a simple bio-assay method, employing plant extracts on filter paper, Yamamoto and Fraenkel (1959) showed that unidentified, botanical glucosides were responsible for food plant selection by

larvae of the tobacco hornworm, *Protoparce sexta* Johanson, and the Colorado potato beetle, *Leptinotarsa decemlineata* Say. Coumarin, an odorous principle of sweet clover plants, attracted the sweet clover weevil, *Sitona cylindricollis* Fahraeus (Thorsteinson, 1960). Nayar and Fraenkel (1963) provided strong evidence to show that glucosides from the catalpa tree elicit a definite response from the catalpa sphinx, *Ceratomia catalpae* Boisduval.

Feeding stimulants for the boll weevil, *Anthonomus grandis* Boheman include volatile extracts from the leaves of cotton seedlings (Keller *et al.*, 1963; Neff and Vanderzant, 1963), and water extracts from all parts of the cotton plant (Jenkins *et al.*, 1963).

Loschiavo, Beck, and Norris (1963) reported an unidentified feeding stimulant from the American elm attractive to the smaller European elm bark beetle, *Scolytus multistriatus* Marsham. This feeding stimulant was later identified as a pentacyclic triterpene (Baker and Norris, 1967) and represents the first chemical stimulant to be isolated from the woody tissue of a perennial plant. Derr, Randall, and Kieckhefer (1964) extracted an unidentified, non-nutritional component from corn plants that had a stimulatory effect on the corn rootworms, *Diabrotica longicornis* Say and *D. virgifera* LeConte. In a brief report that lacked supporting evidence, Chambliss and Jones (1966) reported that certain tetracyclic triterpenes, bitter principles present in the Cucurbitaceae, were attractive to the spotted cucumber beetle, *Diabrotica undecimpunctata howardi* Barber. In a well-documented study, David and Gardiner (1966) reported that 9 mustard oil glucosides extracted from the Cruciferae elicited a

strong response from the European cabbageworm *Pieris brassicae* L. As the result of an in-depth study involving many field experiments, Feeny, Paauwe, and Demong (1970) demonstrated that allyl isothiocyanate, an aglycone isolated from cruciferous plants, was a powerful attractant for adults of the flea beetle, *Phyllotreta cruciferae* Goeze.

Of the nutritional plant components that have a stimulatory effect, sucrose is one of the most widespread. This effect was demonstrated in the Mexican bean beetle, *Epilachna varivestis* Mulsant (Nayar and Fraenkel, 1963a; Augustine *et al.*, 1964), the European corn-borer, *Pyrausta nubilalis* Hubner (Beck, 1965), and the aphid *Myzus persicae* Sulzer (Dethier, 1966). Amino acids are generally non-phagostimulant, but the exceptions are of interest. Thorpe *et al.* (1947) presented considerable evidence to show that several amino acids caused aggregation in wireworms. In well-designed experiments employing agar-based media, Beck and Hanec (1958) demonstrated that larvae of *Pyrausta nubilalis* were stimulated to feed by several amino acids. A similar effect in the large milkweed bug, *Oncopeltus fasciatus* Dallas was reported by Feir and Beck (1963).

Amino acids also synergise with other compounds. Serine and glucose enhance feeding by larvae of *Pyrausta nubilalis* (Beck and Hanec, 1958); both leucine and methionine increase the acceptability of sucrose by *Myzus persicae* (Mittler and Dadd, 1964). Proline and glutamic acid synergise with sucrose for larvae of the spruce budworm, *Choristoneura fumiferana* Clements (Heron, 1965). Synergism reported among other compounds include sucrose and sinigrin for

larvae of *Plutella maculipennis* (Thorsteinson, 1953; Nayar and Thorsteinson, 1963), glucose and an unidentified plant component for *Protoparce sexta* (Yamamoto and Fraenkel, 1959), and glucose, glucosides, and an unknown volatile plant component for *Epilachna varivestis* (Nayar and Fraenkel, 1963a). As the result of an extensive behavioural, ultrastructural, and electrophysiological study, Chun, (1972) demonstrated that sucrose synergises with mustard oil, glucosides, amino acids, salts, and ascorbic acid for larvae of *Pieris brassicae*.

The fact that both nutritional and non-nutritional plant chemicals have a stimulatory effect gave rise to considerable controversy regarding the mechanism of food plant selection in oligophagous, plant-eating insects. Two subordinate questions from which this controversy arose were cited by Dethier (1966):

"Are the effective stimuli token or nutrient?
Is oligophagy based on the unique acceptance of particular compounds, or rather, general rejection of many?" (p. 48).

Fraenkel (1953, 1959) contended that the leaves of all plants were nutritionally adequate for phytophagous insects, and that food plant specificity was based on the presence of secondary plant chemicals acting as token stimuli. He noted that many plants contained non-nutritional chemicals such as glucosides, alkaloids, and essential oils, and since these chemicals appeared to have no known role in basic plant metabolism, he referred to them as secondary chemicals. As the result of criticism of his generalization regarding food plant specificity (Thorsteinson, 1960; Waldbauer, 1962;

Beck, 1965; Kennedy, 1965), Fraenkel (1969) conceded that nutritional values may vary slightly in plants. He also admitted that certain plant nutrients may act as attractants, but maintained that this could not explain plant specificity in the specialized insects since plant nutrient composition varied greatly with season, soil, age, and light conditions, yet plant specificity was relatively unaffected by such variations.

Jermy (1966) contended that plants developed secondary chemicals as deterrents to herbivores, and insect sensitivity to such deterrents was more important in determining food plant range than adaptation to specific token stimuli. Kennedy (1958) favoured a "dual discrimination" theory of food plant selection involving response to both nutrient and token stimuli. Thorsteinson (1960) maintained that food plant finding was by chance, and plant acceptance initiated by secondary chemicals that act as arrestants and also lower response thresholds to nutrient phagostimulants that release feeding activity.

No single theory of food plant selection can be satisfactorily applied to all the specificities existing between phytophagous insects and plants. Fraenkel's (1959) token stimuli theory may explain plant selection in several lepidopteran species (Ehrlich and Raven, 1964), but does not explain the relationships between many aphids and their food plants where nutritional components play a significant role (Kennedy, 1958). Jermy's (1966) chemical deterrent theory may explain the comparative immunity enjoyed by certain plants, but does not explain food plant selection *per se*.

Kennedy's (1958) dual discrimination theory has the advantage of flexibility with regard to the role of physiological changes in the insect and its food plant, however it assumes that all phytophagous insects are capable of nutritional assessment of food plant value. Verification of Thorsteinson's (1960) theory that secondary chemicals lower response thresholds to sapid nutrients will require detailed electrophysiological analyses of receptor systems as suggested by Schoonhoven (1968) and then may only apply to certain plant-feeding insects.

Much of the controversy regarding the mechanisms of plant selection by oligophagous insects stems from the fact that most research into factors regulating quality discrimination emphasizes nutritional rather than ecological factors. From an ecological viewpoint, the plant may often be considered a place to live as well as a feeding substrate (Kennedy, 1953; Dethier, 1970). Plant selection may be a compromise between meeting the nutritional requirements of the insect, and such ecological considerations as habitat selection (Holloway, 1964), predators (Brower, 1958; Brower and Brower, 1964; Alpin, Benn, and Rothschild, 1968), and parasitization (Downey, 1962; Stride and Straatman, 1962).

Dethier (1954) contended that the diverse patterns of feeding habits in phytophagous insects represented a dynamic equilibrium between two evolving systems, the plants and the insects. The effects of such co-evolution on particular adaptations in plants and insects was discussed by Breedlove and Ehrlich (1968) and Muller (1969). Plants are evolving in an atmosphere of

multiple selective pressures of which insect predation is but one, and respond to these pressures by developing morphological modifications, emigration to new habitats, and the elaboration of new chemicals. Phytophagous insects are evolving new feeding habits as a result of structural modifications, metabolic modifications that overcome plant toxins such as glucosides, alkaloids, and tannins, and neural modifications that permit behavioural diversity (Dethier, 1970). The types of insect-plant relationships will vary as the evolutionary pathways which culminate in them vary. Consequently, no single theory of plant selection will apply to all the specificities existing between insects and plants, and many of these must be investigated separately.

3. ENTOMOSCELIS AMERICANA BROWN

3.A. Geographical distribution

Prior to 1942, the geographical distributions of *Entomoscelis americana* and *E. adonidis* were combined, as these species were then considered identical.

LeConte and Horne (1883) described the range as the boreal regions of North America and Eurasia. Hamilton (1894) reported the North American distribution as everywhere through the Rocky Mountains to 11 thousand feet, as well as Montana, the Hudson's Bay region, Alberta, Manitoba, and the North-West British provinces, and the Eurasian distribution as Southern Europe, France and Germany, and west and east Siberia to Turkestan. Chittenden (1902) reported that the range consisted of the boreal parts of both the Old and New Worlds. Leng (1920) gave the North American distribution as the Hudson's Bay Territory, Montana, Alberta, and Colorado. Essig (1926) listed the distribution as boreal North America, Siberia, and Europe, with the North America distribution including Colorado, Montana, Washington, British Columbia, and Alaska. Beller and Hatch (1932) reported that the Eurasian range extended from Southern France and Bavaria to Persia and Siberia, and showed the North American range as extending from Alaska and the Hudson's Bay region to Montana, Colorado, and Washington.

Figure 1 shows the known distribution of *E. americana* in North America, and was compiled from data received from United States Department of Agriculture, Economic Insect Survey Co-

ordinators, and from federal and provincial departments of agriculture in Canada.

The distribution of *E. americana* in British Columbia is confined to the central portion of the province and has not been reported from the coastal regions. In the southern, interior portion of British Columbia, distribution is restricted to higher elevations. Such distribution in British Columbia suggests a preference for a cool, fairly dry climate, so that the range of *E. americana* may be limited by high summer temperatures and high precipitation. Absence from areas of high summer temperatures is also evident in Washington, Idaho, Montana, Wyoming, and Colorado, where distribution is restricted to higher elevations. In the Dakotas, *E. americana* is only reported from the extreme northern portion of North Dakota, where the average daily July temperature does not exceed 70° F. *E. americana* has not been reported from Ontario, although its range does extend to Minnesota and Wisconsin where annual precipitation is comparable to that of Western Ontario. Although *E. americana* has not been reported from Western Ontario, it is probably present in this region, especially in settlements where market gardens are present.

Figure 1 shows the known distribution of *E. americana* in relation to mean daily July temperature and to average annual precipitation. The July isotherm was chosen since, in Alberta, *E. americana* spends this month in aestivation. The southern limit of *E. americana* does not extend below the 70° F July isotherm, suggesting that its range is restricted by high summer temperature.

The limit of northern distribution coincides with the July 55° F isotherm which also lies fairly close to the permafrost line in Northern Canada. The known range of *E. americana* also appears limited by annual precipitation in excess of about 32 inches, which may explain its apparent absence from Eastern Canada and the coastal regions of British Columbia.

The 70° F July isotherm and the isohyets plotted on Figure 1 are from Chapman and Sherman (1967). The Alaskan 55° F July isotherm is from Watson (1959), and the Canadian 55° F July isotherm is from Thomas (1953).

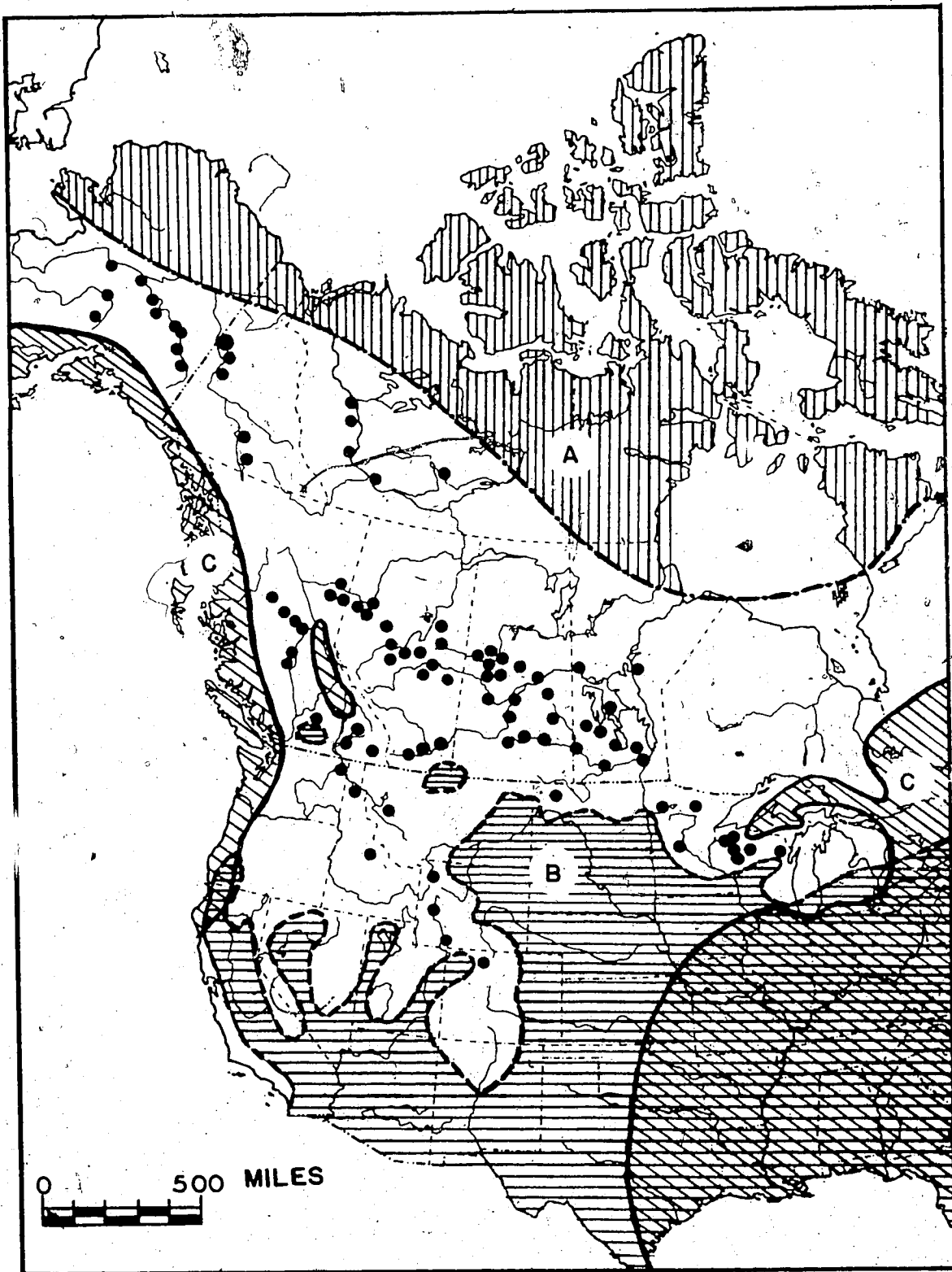


Fig. 1. The distribution of *Entomoscena americana* Brown in North America in relation to temperature and precipitation: A, mean daily July temperature below 55° F; B, mean daily July temperature above 70° F; C, annual precipitation in excess of 32 inches.

3.B. Description of stages

3.B.i. Egg

When first laid, the eggs are bright orange-red, gradually darkening to dark brown. The egg surface is finely reticulated with small hexagonal areas of about 0.15 mm diameter. The egg shape is a prolate spheroid with the length about twice the diameter. Length and diameter measurements are of the order reported by Chittenden (1902), 1.5 X 0.7 mm (Table 1).

3.B.ii. Larvae

There are 5 larval instars, the average measurements of which are shown in Table 1. Larval length measurements vary because of the extendable abdomen and, accordingly, were taken from specimens preserved in 70% ethanol. Head capsule widths were also recorded. The average ratio of increase of head capsule width in successive instars is approximately 1.34.

First Instar - The newly-hatched larvae are orange-yellow, except for the mouthparts, antennae, stemmata, thoracic legs, and a pair of laterally-placed tubercles on each thoracic segment, which are all black. The dorsal surface darkens to near black within 6 hours of hatching; the ventral surface also darkens but retains a slight orange hue. The first instar larva is wedge-shaped; about 2.0 mm in length by about 0.75 mm in width at the head capsule which is the widest part.

The mouthparts are of the generalised, chewing type. A wide, curved clypeus largely overlies a narrower, bi-lobed labrum. Each

of these structures bears 4 large bristles. The mandibles are wide between the condyle and ginglymus, and each bears a well-developed retinaculum as well as 2 large bristles. The laciniae are short and have cuticular spines at their apices. The maxillary palpi are dome-shaped, 4-segmented, and each has 24 basiconic sensilla at the apex. The labium is short and narrow and is equipped with 6 short bristles at the distal end and 2 longer bristles at the posterior end. The labial palpi are 2-segmented and each bears 12 basiconic sensilla at the apex. The antennae are wide-set and each consists of a single article or scape set in a well-defined antennal socket. Each antenna has 4 trichoid sensilla at the distal end. The stemmata are laterally-placed and located immediately behind the antennal sockets. There are 6 stemmata on each side of the head capsule, 4 of which are arranged in a square and lie slightly above a subordinate pair. The thoracic legs are all 3-segmented, each bearing numerous hairs and terminating in a single, simple claw. Each thoracic segment bears a pair of dorsal, transversal rows of fuscous tubercles, with from 6 to 8 tubercles in each row. Also located on each thoracic segment is a pair of laterally-placed, prominent tubercles just above the stigmatal line. Smaller tubercles are also located laterally on each thoracic segment below the stigmatal line, and 2 smaller series on the ventral surface. There are 7 abdominal segments. The first 4 have a pattern of tubercles similar to the thoracic segments, except that the prominent, lateral tubercles are lacking. The 5th and 6th abdominal segments taper abruptly to terminate in a bi-lobed, prehensile structure used in locomotion.

Second Instar - After the first moult, the body remains wedge-shaped, with an average length of about 3.3 mm. The width of the head capsule is about 0.98 mm. The body is flattened on the ventral surface and rounded above. The head is sub-rotund, slightly depressed at the apex, and abruptly truncate at the anterior end. The appendages, mouthparts, and stigmata are the same as in the previous stage. The dorsal surfaces of the abdominal and thoracic segments are divided by transverse folds. The ecdysial suture is apparent as a narrow, slightly-depressed, dorsal groove running from the apex of the head to the posterior abdominal segments, and is more distinct where it crosses the thoracic tergites. The colour of the body is velvet-black on the dorsal surface and blackish-orange on the ventral surface. The tubercle pattern is the same as in the previous stage.

Third Instar - After the 2nd moult, the body is less wedge-shaped and more elongate. The head capsule and thoracic segments are approximately the same width - about 1.28 mm, and the body length is about 5.2 mm. Tubercle pattern, colour, and appendages are the same as in the previous stage.

Fourth Instar - The body length is about 8.1 mm, and the head capsule width about 1.67 mm. The head capsule is slightly narrower than the thoracic segments, providing the body with a more elongate shape. The ornamentation is the same as in the previous stage, except that the cuticle on the ventral surface is more translucent, providing a dull, orange hue in this region. A pair of small, indistinct projections is present on the ventral surface of

the 4th, 5th, and 6th abdominal segments.

Fifth Instar - The length of the final instar is about 12.0 mm, and the width of the head capsule about 2.17 mm. The body is more elongate in this stage, with the head capsule noticeably narrower than the thorax. The small projections on the 4th, 5th, and 6th abdominal segments are more pronounced in this stage and appear as 3 pairs of translucent, bag-like pseudopodia that can be extended from median slits in the ventral surface. These serve as prolegs and are used in conjunction with the bi-lobed, terminal abdominal segment during locomotion. The remaining ornamentation and colour is the same as in the previous stage, except that the ventral surface is yellow in many specimens.

3.B.iii. *Pupa*

The average pupal dimensions are 6.1 X 3.1 mm. The colour is chiefly bright orange, with the antennae, elytra, and leg cases yellowish-orange. The spiracles are rotund and fuscous. The elytra cases each bear 3 longitudinal striae. The ecdysial suture is a shallow, median groove on the dorsal surface of the metathorax. The thorax is covered with fine, short bristles and similar bristles are arranged as median, transverse ridges on each abdominal segment.

3.B.iv. *Adult*

The form and colour pattern were described by Chittenden (1902), Fletcher (1905), and Brown (1942). The outline of the body,

from the dorsal aspect, is elongate oval. Average female body dimensions are 9.1 X 4.9 mm, while the males are smaller at 7.6 X 4.2 mm (Table 1).

The colour pattern is the same in both sexes. The dorsal surface of the head is red, and bears a small, black triangle on the median line at the posterior margin. The mouthparts, clypeus, antennae, and small areas surrounding the eye are black. The pronotum is red with a broad, black median area as well as a small spot on each side also in black. The black median area on the pronotum is bell-shaped, widest at the posterior edge, and covers about two-fifths of the tergite. The scutellum is a small, black triangle. The elytra are red, each with a narrow, black, sutural margin except near the scutellum, and a wider sub-median vitta that is pointed at each end and approaches, but does not meet, the base and apex of each elytron. The punctures of the pronotum, elytra, and sterna are fine, dense, and scattered.

The tarsal segments of the anterior and middle legs are wider in the male than in the female, and are probably of advantage to the males during copulation. The terminal, abdominal segments are flattened at the middle. The posterior margin of the abdomen is bisinuate in the male, and simply truncate in the female.

Table 1. The dimensions in mm of all stages of *Entomoscelis americana* Brown. Egg and larval measurements based on 10 observations, pupal and adult measurements based on 20 observations.

Stage	Length [†]	Width [†]
Egg	1.5 ± 0.11 (1.3 - 1.7)	0.7 ± 0.12 (0.6 - 0.9)
First instar larva	2.1 ± 0.12 (1.9 - 2.2)	0.75 ± 0.013* (0.73 - 0.76)
Second instar larva	3.3 ± 0.10 (3.2 - 3.4)	0.98 ± 0.023* (0.96 - 1.01)
Third instar larva	5.2 ± 0.07 (4.8 - 5.3)	1.28 ± 0.043* (1.22 - 1.31)
Fourth instar larva	8.1 ± 0.43 (7.6 - 8.7)	1.67 ± 0.056* (1.59 - 1.73)
Fifth instar larva	12.0 ± 0.73 (11.1 - 12.9)	2.17 ± 0.059* (2.09 - 2.25)
Pupa	6.1 ± 0.91 (5.2 - 7.4)	3.1 ± 0.45 (2.3 - 3.7)
Female Adult	9.1 ± 0.67** (7.8 - 9.7)	4.9 ± 0.30 (4.3 - 5.4)
Male adult	7.6 ± 0.49** (6.8 - 8.2)	4.2 ± 0.23 (3.7 - 4.5)

*head capsule width
**excluding antennae

† mean ± S.D.
(range)

3.C. Life cycle and habits

3.C.i. Hatching

E. americana is uni-voltine and overwinters as eggs in the soil. In 1972, eggs in the Edmonton area hatched during the first week of May. Muscular contractions in the embryo begin within 6 hours before hatching and are readily observed through the egg chorion. Eclosion is accomplished by means of a rupture of the vitelline membrane and chorion that originates anteriorly and then extends along the dorsal side of the egg. No cuticular hatching spines are evident on newly-hatched larvae.

3.C.ii. Habits of the larvae

The first instar larvae are strongly photo-positive and climb up plant stems soon after hatching. While no cultivated cruciferous crops are available in early May, the larvae feed on such cruciferous weeds as volunteer rape, *Brassica campestris* and shepherd's purse, *Capsella bursa-pastoris* (L.) Medic. The larvae feed both during the day and night. When disturbed, they drop to the soil, where their coloration blends well with that of the soil. The 5 larval instars are completed in about 3 weeks. The mature larvae then enter the soil to a depth of about 1 inch and form small, smooth cavities within which they pupate. The pupal stage lasts from 2 to 3 weeks.

3.C.iii. Habits of the adults

Most field studies were conducted on 2 adjoining, one-

quarter section fields in the St. Albert area, located on the North $\frac{1}{2}$, Section 12, Township 53, Range 35, West of the 4th Meridian. One field contained roughly one acre of volunteer rape at one corner which was left intact during the 2 years of the study. In 1972, the adults began emerging in the volunteer rape during the first week of June and populations were highest during the second week of June. Feeding activity is greatest during the first 3 weeks after emergence, and it is at this time that *E. americana* can cause considerable damage to cultivated rape crops.

At the beginning of July, *E. americana* begins a period of aestivation that lasts for about one month. During this period, the beetles are found under plant debris, in soil crevices, or buried in loose soil to a depth of about one inch. When the aestivation period ends, the beetles disperse by walking and flying, and are then found in previously uninfested rape fields or on patches of cruciferous weeds. The plants that served as food prior to aestivation are producing seed and have lost most of their leaves.

The 2 fields where much of this study was conducted were both sown in barley during the spring of 1972, and most of the weeds later destroyed with a herbicide. Many small, isolated patches of volunteer rape persisted in both fields however, these having sprouted from seed in late May. Such later growth has an abundance of blossoms and leaves, and appears to be an attractive source of food for the dispersing beetles. The isolated growths of volunteer rape in both

fields were checked twice-weekly during August and the beetles were found progressively further into the barley fields at each check. Three weeks after dispersal began, both fields were infested throughout, and at the end of August the beetles were discovered in a previously uninfested rape field one mile distant.

Immediately after dispersal, copulation occurs. Oviposition begins during the first week of August and continues for about one month. The eggs are deposited in masses of up to 80 on the soil beneath food plants and are found under leaf litter, in soil crevices, or buried in loose soil to a depth of about one-quarter inch. The abdomens of the females remain swollen after oviposition and these when dissected, are found to contain no eggs but rather, a yellow haemolymph. In the field, many specimens of *E. americana* die shortly after oviposition, while others persist until mid-October.

3.D. Laboratory rearing of *E. americana*

3.D.i. Rearing techniques

Larvae and adults were reared both directly on cabbage leaves and on potted rape plants in rearing cages. Openings in the floor of the rearing cage permitted the use of plastic planters that were suspended in trays of water beneath the cage. This system simplified watering of food plants and also provided that the soil in the planters and the floor of the rearing cage were at the same level, allowing easy access to food plants by the larvae.

Detached rape leaves are unsuitable as food, since such leaves, when detached for 3 days, are toxic to the larvae. A

naturally-occurring enzyme, such as a glucosidase, may be present in rape foliage. Although mustard oil glucosides are non-toxic, cleavage of such glucoside molecules will yield glucose and mustard oils. Many mustard oils, according to Ettliger and Kjaer (1968) are strongly irritant and can cause damage to animal tissue.

Egg-gathering was simplified by maintaining copulating couples in small containers that were lined at the bottom with layers of paper towelling. The females oviposited between these layers, and the egg masses were easily brushed off when the paper towelling was changed.

3.D.ii. *Termination of diapause*

Daily, microscopic examination of freshly-laid eggs revealed that embryological development progresses for about 3 weeks. The late embryos then enter diapause which lasts, in the field, until the first week of May. Several thousand eggs that had completed embryological development were stored in a cold room at 15° C. After one week, all but 500 eggs were transferred to a cold room at 10° C, and one week later, all but 500 of these transferred to a cold room at 5° C. In this fashion, the eggs were successively introduced to lower temperatures until a minimum of -15° C was reached. Each week, 50 eggs were removed from each cold storage unit and returned to room temperature. These were placed on moistened discs of paper towelling in covered, Pyrex glass petri dishes and checked daily to determine the percentage hatch.

Table 2. The percent hatch of eggs of *Entomoscelis americana* Brown following temperature treatment to terminate diapause.

Temperature (°C)	Duration of treatment in weeks									
	(1)	(2)	(3)	(4)	(5)	(6)	(7)	(8)	(9)	(10)
20	-	-	-	-	-	-	-	-	-	-
15	-	-	2	-	-	1	-	1	1	1
10	-	1	-	4	3	5	6	8	3	4
5	-	-	-	4	2	6	12	14	16	12
0	-	4	14	60	84	90	87	90	84	86
-5	-	-	-	14	16	10	20	18	14	17
-10	-	-	-	-	-	1	-	-	2	-
-15	-	-	-	2	-	-	1	-	①	-

Table 2 shows the results of the cold treatment. Diapause was most effectively terminated by cold treatment at 0° C, with maximum hatch occurring after 6 weeks exposure to that temperature.

Most of the eggs hatched between 24 and 36 hours after removal from the cold storage unit.

3.E. Adult taxes and kineses

While the photo-positive response of the larvae is obvious and requires no experimental confirmation, a similar, but discontinuous response that varied with time was observed in the adults. Experiments were designed to evaluate the photo-response of newly-emerged and aestivating adults. Other experiments were conducted to test the response of aestivating adults to moist substrate and also to determine if they showed thigmokinesis.

3.E.i. *Materials and methods*

The response of field-collected, newly-emerged adults to light was investigated by means of an opaque, plastic, cylindrical choice chamber (30.0 X 4.0 cm) that admitted light at one end only. The lighted end of the choice chamber was covered with a 5.0 cm, Pyrex glass petri dish and illuminated from above by a fluorescent light fixture equipped with a single, 15-watt daylight type, 16-inch tube. The light source was suspended 6 inches above the choice chamber and provided approximately 260 foot-candles of incident light at the lighted end of the chamber. Five groups of 20 adults were placed in the choice chamber for 2-hour

periods and the numbers in the lighted and darkened regions recorded at the conclusion of each trial. The intensity of reaction was determined from the ratio of the percentage in the lighted end to the percentage in the darkened end (L/D). Photo-responses were similarly investigated at the beginning, during, and at the end of the aestivation period.

The response of aestivating adults to moist substrate was determined by placing groups of 20 in a rectangular choice chamber (17.0 X 9.0 cm) that was lined at the bottom with a single layer of paper towelling. Five groups were placed in choice chambers with dry substrate, their positions recorded after 30 minutes, and then placed in choice chambers with one-half the paper substrate moistened, for a further 30 minutes. During these tests, the choice chambers were kept in a darkened container that was rotated 90° between trials to discount the effects of any stray light entering the system.

A thigmokinetic response in conjunction with moist substrate was investigated in aestivating adults by repeating the moist substrate tests with one-half the paper towelling folded to provide parallel, tunnel-shaped openings between the paper towelling and the floor of the test chamber (Figure 2). Five groups of 20 adults were placed in choice chambers with dry substrate for 30-minute periods, their positions recorded, and then placed in test chambers with the folded substrate moistened, for further 30-minute periods.

3.E.ii. Results

Table 3 shows the results of the tests with the light-dark choice chamber. The recordings are totals of 5 trials listed in Appendix I. Of the newly-emerged adults, a total of 94 were found at the lighted end of the chamber. At the beginning of the aestivation period, only 10 were found at the lighted end, and the response was roughly neutral when the aestivation period was about 75% complete. At the end of aestivation, a total of 89 were found at the lighted end.

In trials employing moist substrate, all the aestivating adults responded positively to the moistened paper towelling, while in trials employing dry substrate the beetles were located randomly in the chamber.

The results of the tests to determine thigmokinetic response to openings in moist substrate are shown in Table 4 which lists the totals of 5 trials listed in Appendix II. In trials employing dry substrate, the beetles were dispersed randomly in the test chamber and a total of 9 were found in the openings provided by the folded paper substrate. When the folded paper substrate was moistened all the beetles were found at the moist end of the test chamber and a total of 77 were found within the openings.

3.F. Olfactory response of males to females

Approximately one week after completion of the aestivation period, copulation begins. Experiments were conducted in the laboratory to determine if the males, at this time, would respond to the

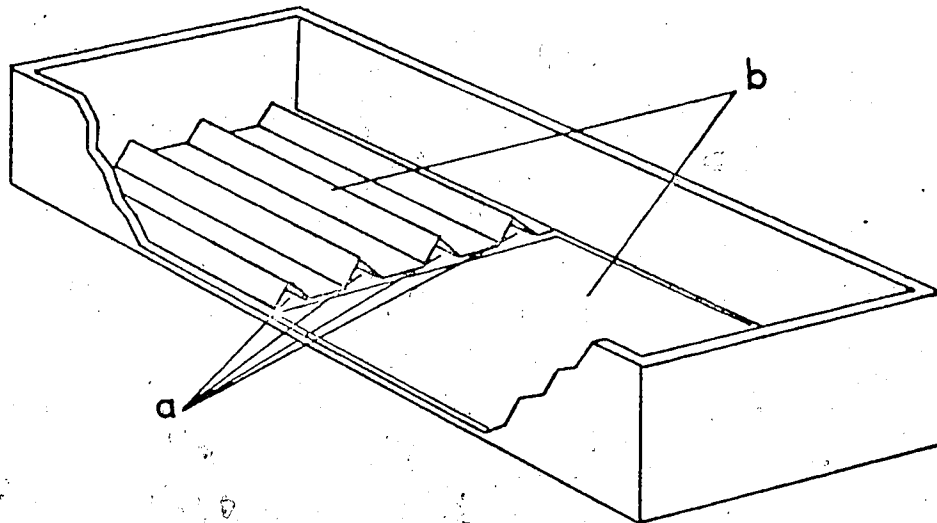


Fig. 2. The choice chamber used to evaluate moisture and thigmokinetic responses of aestivating adults of *Entomoscelis americana* Brown: a, tunnel-shaped openings between paper towelling and the floor of the test chamber; b, paper towelling.

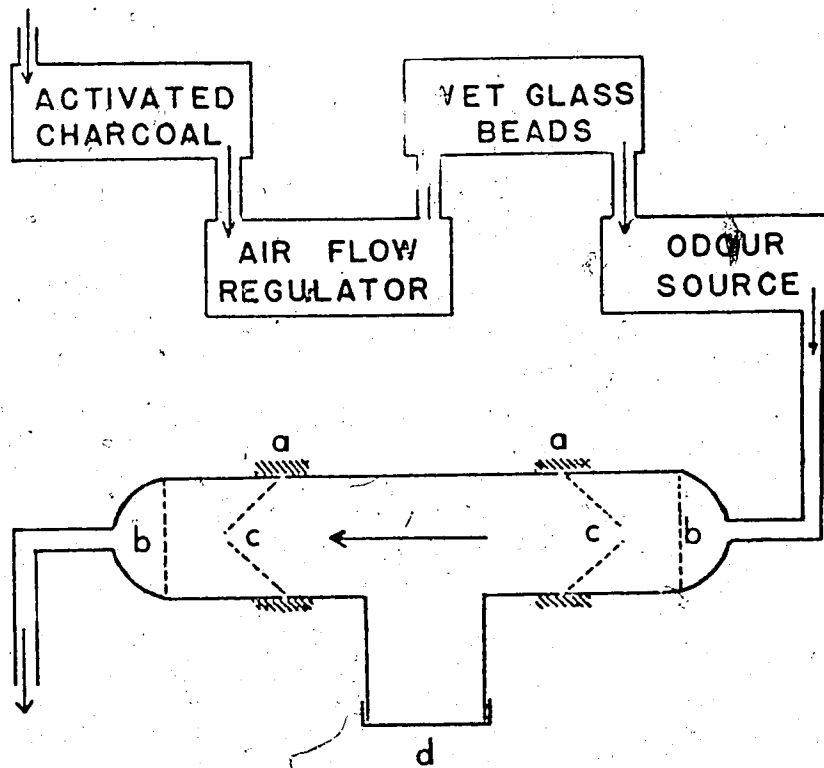


Fig. 3. A T-tube apparatus used to evaluate olfactory responses of *Entomoscelis americana* Brown: a, plastic tube couplings; b, flat 20-mesh, saran screen discs; c, 75°, 20-mesh saran screen cones; d, opaque plastic cover.

Table 3. The photo-response of adults of *Entomoscelis americana* Brown in a light-dark choice chamber. The results are totals of 5 trials.

Level of Maturation	Light	Dark	L/D ratio	L.S.*
Newly-emerged adults (June 6th)	94	6	15.66	0.005
Beginning of aestiv- ation (July 5th)	10	90	0.11	0.005
Aestivation 75% com- plete (July 25th)	51	49	0.96	0.5 - 0.9
Aestivation complete (July 31st)	89	11	8.09	0.005

*level of significance from chi-square tests

odour of the females.

3.F.i. *Materials and methods*

The response of males to the odour of gravid females was evaluated by placing groups of 36 males in a darkened, moving-air olfactometer and employing 6 females as an odour source. The olfactometer (Fig. 3) is similar to that used by Hocking and Lindsay (1958) and consists of a Pyrex glass T-tube, 34.0 X 3.4 cm, including the end pieces. The outer surface was covered with black, vinyl tape to exclude light. The end pieces contained insect traps made from 20-mesh brass screen and were joined to the T-tube by means of polyvinyl chloride coupling sleeves which, according to the manufacturer, are odourless (Hocking and Lindsay, 1958). Laboratory service air was deodourized by passage through a 250 ml tower containing activated carbon, and moistened in a similar tower containing wet, 3mm glass beads. The air flow to the olfactometer was adjusted to 7 litres/minute (7.7 meters/minute) by means of a tapered-tube flow meter. The temperature of exhaust air from the system ranged between 19 and 21° C, while the relative humidity ranged between 70 and 80%. Test specimens were placed in the main body of the T-tube by means of the stem, and a strip of paper towelling served as a walking substrate for the beetles.

Before tests were conducted with females as an odour source, groups of 36 males were first subjected to 2 preliminary runs in moist air, one run with the air flow in one direction, the second run with the air flow reversed. These runs were of 1-hour duration each, and the numbers of beetles in upwind and

Table 4. The thigmokinetic response of aestivating adults of *Entomoscelis americana* Brown to openings in moist substrate in a moist-dry choice chamber. (Results are totals of 5 trials).

	End of chamber with no openings in substrate	End of chamber with openings in substrate:	
	In substrate	In openings	Not in openings
Chamber with dry substrate (control)	50	9	41
Chamber with moist substrate openings	0		23

(Level of significance from chi-square test: 0.005)

down-wind traps were recorded at the conclusion of each run. Beetles that did not enter the insect traps were listed as neutral. Following the pairs of runs in moist air, 6 females were placed in the odour source tower and the pairs of runs repeated. The tower containing the females was washed and the system purged for 15 minutes with moist air between alternate runs to remove odour traces. A total of 10 pairs of runs was conducted with 5 groups of males: 5 pairs in moist air, and 5 pairs in moist air plus the odour of the females.

3.F.ii. Results

Table 5 shows the results of the tests in the moving air olfactometer. The results are the totals of the 10 pairs of runs listed in Appendix III. When moist air with no odour source was used, a total of 237 males remained in the main body of the olfactometer and were listed as neutral, while 62 entered the upwind trap and 61 entered the downwind trap. When gravid females were used as an odour source, a total of 133 remained in the main body of the olfactometer, while 198 entered the upwind trap and 29 entered the downwind trap.

Table 5. The response of males of *Entomoscelis americana* Brown to the odour of gravid females in a moving air olfactometer. (Results are totals of 5 trials).

	Neutral	Trap #1*	Trap #2
Moist air only	237	62	61
Moist air plus odour of females	133	198	29

(Level of significance from chi-square test: 0.005)

*odour source trap

4. FOOD PLANT RELATIONSHIPS OF E. AMERICANA

In oligophagous insects, successful utilisation of food plants depends largely upon properly co-ordinated interaction between the insect and the host plant (Dethier, 1954; Thorsteinson, 1960). While the behaviour that is involved in food plant selection has been divided into several components by a number of workers (Dethier, 1953; Thorsteinson, 1953; DeWilde, 1958), two major components were considered in this study:

- (1) Orientation and movement toward the food plant, or food plant finding.
- (2) Recognition of the food plant, or food plant acceptance.

4.A. Food plant finding by the larvae

The newly-hatched larvae need not search far for proper food plants since the adults deposit their eggs on soil beneath cruciferous plants. The proximity of hatching larvae to food plants gives rise to two distinct possibilities regarding food plant finding: (1) food plant finding is by trial and error and the larvae cannot recognize the proper plant until actual contact has been made or, (2) food plant finding is not random and the larvae will orientate and move toward the plant from a limited distance, by response to a stimulus such as odour. Experiments were conducted to evaluate the response of larvae to the odour of food plants, non-food plants, and to growing plants.

4.A.i. *Materials and methods*

Two groups of 10, newly-hatched larvae were placed in a pair of choice chambers in a darkened container. The choice chambers measured 23.0 X 12.0 cm, were covered with 20-mesh, brass screening, and were designed to fit over a pair of 10.0 cm diameter Pyrex glass petri dishes. In one choice chamber, fresh, whole rape leaves were placed in one petri dish and moistened paper towelling in the other. The second choice chamber acted as a control and fresh lettuce leaves were used in place of rape foliage. Previous tests revealed that the larvae will not eat lettuce. The two tests were run simultaneously and the location of the larvae in the choice chambers recorded 10 times at 15-minute intervals. The darkened container that held the choice chambers was rotated 90° at each check to discount the effects of light and laboratory air currents.

Five groups of 60, newly-hatched larvae were placed in the moving air olfactometer described in section 3.F.i. (Figure 3) for 1-hour periods. Each group of larvae was subjected to 2 pairs of runs in the olfactometer. The first pair of runs involved moist air only with the air flow direction reversed between runs, followed immediately by a pair of runs using freshly-picked, whole rape leaves as an odour source.

Groups of 100, newly-hatched larvae were each subjected to two runs in the olfactometer, each of 1-hour duration, to evaluate their response to the odour of non-food plants. Each group was first tested in moist air only, followed by a run using fresh, whole leaves of non-food plants as an odour source, and with the

air flow direction reversed. The non-food plants tested included leaf lettuce, *Lactuca sativa crispa* L., dandelion, *Taraxacum officinale* Weber, lamb's quarters, *Chenopodium album* L., and white Dutch runner beans, *Phaseolus coccineus albus* B.

One-hundred, newly-hatched larvae were offered a choice of growing food plants and non-food plants. Two plastic planters were used, one containing six, 6-inch rape plants, the other containing six, 6-inch lamb's quarters plants. The planters were set 10 cm apart in openings cut in the floor of a cardboard container that measured 60.0 X 30 cm at the floor and with walls 60 cm high. The container was open at the top and illuminated from above by a fluorescent light fixture equipped with four, 40-watt daylight type, 48-inch tubes. The incident light reaching the floor of the test chamber was measured with a photometer and the light source adjusted to provide even coverage. The larvae were placed on the floor of the test chamber at a point midway between the two planters. At 15-minute intervals, the locations of the larvae were recorded, and the test chamber rotated 90° to discount light direction and laboratory air currents. At each check, larvae climbing up the inner walls of the test chamber were returned to the floor, midway between the planters.

4.A.ii. Results

The tests with the 2-way, screened choice chambers did not indicate a positive larval response to the odour of rape foliage, and their distribution in the chambers was fairly even at the end

of the ten recordings (Appendix IV).

Table 6 shows the results of the tests in the moving air olfactometer and lists the totals of runs entered in Appendix V. In trials employing rape leaves as an odour source, significantly more larvae remained in the main body of the olfactometer than when moist air alone was used. When rape leaves were used, equal numbers of larvae were found in the insect traps at the conclusion of the runs, indicating that larval response to the odour of rape leaves is not orientated movement toward the odour source, but rather that larval movement is arrested in the presence of such odour. In the trials with lettuce, dandelion, and lamb's quarters, significant numbers of larvae moved away from the odour source when compared with runs in moist air, and were found in the down-wind insect traps. When bean foliage was used as an odour source, no significant difference was detected in larval movement when compared to runs in moist air.

Table 7 shows the numbers of larvae on food plants and non-food plants at 15-minute intervals during the tests with growing plants. Although approximately equal numbers of larvae climbed up both types of plants at the beginning of the test, those on rape plants soon settled down to feed, while the larvae on lamb's quarters plants continued climbing and walking on the leaves until most had fallen back to the soil. Very few larvae fell from the rape plants and the number of larvae on these plants increased at each 15-minute interval, while the number on the lamb's quarters plants correspondingly decreased.

Table 6. The response of first instar larvae of *Entomoscyllis americana* Brown to the odours of food plants and non-food plants in a moving air olfactometer.

Type of Foliage	Moist air only (control)		Moist air plus plant odours		L.S.**		
	Neutral	Trap #1	Trap #2	Neutral		Trap #1*	Trap #2
Rape	125	236	239	190	205	205	0.005
Lettuce	102	220	178	72	48	380	0.005
Dandelion	128	210	162	96	72	332	0.005
Lamb's quarters	110	197	193	100	119	281	0.005
Bean	103	189	208	111	196	193	Not significant

*odour source

**level of significance from chi-square tests.

Table 7. The response of 100, newly-hatched larvae of *Entomoscelis americana* Brown to growing food and non-food plants in a choice chamber.

Time (mins)	Numbers on		Numbers on		Numbers on walls	
	rape plants	lamb's quarters plants	rape plants	lamb's quarters plants	and floor of choice chamber	choice chamber
15	18	20				62
30	26	24				50
45	28	21				51
60	37	18				45
75	36	16				48
90	41	12				47
105	42	14				44
120	49	9				42
135	56	12				32
150	58	10				32

4.B. Food plant finding by the adults

At the conclusion of the aestivation period, the beetles actively disperse and are then found on late-growth cruciferous plants that have an abundance of foliage and blossoms. Dispersing, field-collected adults were returned to the laboratory and tests conducted to determine their response to the odour of fresh rape foliage and blossoms.

4.B.1. *Materials and methods*

Groups of 20 adults, unfed for 24 hours, were placed in the moving air olfactometer described in section 3.F.i. (Figure 3) and tested in moist air only. Many of the test specimens entered the stem of the T-tube during the runs in moist air, and in order to overcome this difficulty the olfactometer was modified to provide two, separate air streams entering at the ends of the apparatus, and both exiting through the stem. This method was successful in that it provided air movement in the stem and very few specimens then entered the stem. A second 250 ml tower was added as an alternate odour source and the apparatus supplied with a second tapered tube, air flow-meter. The air flow entering each end was adjusted to 7 litres/minute (7.7 meters/minute). Five groups of 20 adults were each subjected to a pair of runs in the olfactometer, one run in moist air only, followed immediately by a run in which rape foliage or blossoms were employed as an odour source. Freshly-picked, whole leaves or blossoms were used. Runs were of 1-hour duration, and after each pair of runs, the odour source tower was

washed and the system purged with moist air for 15 minutes to remove odour traces. The odour source was placed in alternate towers in consecutive pairs of runs. In this fashion, 5 series of trials were conducted to evaluate the the olfactory response of:

- (1) Males and females (mixed) to foliage;
- (2) Females to foliage;
- (3) Males to foliage;
- (4) Females to blossoms;
- (5) Males to blossoms.

4.B.ii. Results

Table 8 shows the results of the tests in the double air-stream olfactometer and lists the totals of 5 pairs of runs recorded in Appendix VI. When moist air alone was used, a large number of specimens remained in the main body of the olfactometer, while those that entered the insect traps displayed no distinct preference for either trap. When mixed males and females were exposed to the odour of rape foliage, 60% entered the odour trap. However, since these were mostly females, the sexes were separated in succeeding trials. When their response to the odour of rape foliage was checked separately, 75% of the females entered the odour trap, while the males showed no distinct preference. When the odour of rape blossoms was used, 87% of the females and 77% of the males were found in the odour trap.

Table 8. The response of adults of *Entomoscelis americana* Brown to odours of rape (*Brassica campestris* L.) foliage and blossoms in a double air-stream olfactometer.

	Moist air only (control)		Moist air plus plant odours		L.S.**
	Neutral Trap #1	Trap #2	Neutral Trap #1	Trap #2	
Foliage:					
Mixed adults	22	44	13	27	0.05
Females	38	27	14	11	0.005
Males	33	31	32	35	N.S.***
Blossoms:					
Females	63	20	9	4	0.005
Males	35	31	17	6	0.005

* odour source

** level of significance from chi-square tests

*** not significant

4.C. Food plant acceptance

While phototaxis plays a major role in directing the larvae to the proper environment for feeding, and plant odours direct the adults to the proper plants, it is assumed that the ultimate forces that determine food plant acceptance, or final recognition, are largely gustatory response to chemicals in food plant tissue.

Although *E. americana* was not observed feeding on non-cruciferous plants in the field, tests were conducted to determine if the larvae or adults would feed on such plants. Other tests were conducted to determine if chemicals in rape seed foliage were responsible for food plant acceptance by *E. americana*, and whether both larvae and adults responded to the same chemicals. Finally, larval and adult responses to sinigrin, a mustard oil glucoside common to the Crucifereae, were tested.

4.C.i. Materials and methods

Bio-assay method - Figure 4 illustrates the test chamber used to evaluate the response of *E. americana* to the non-cruciferous plants, to chemical fractions of rape foliage, and to sinigrin. Leaf discs of 2.0 cm diameter were prepared with a stainless steel punch and mounted on insect pins that were equipped with 0.5 cm diameter plastic discs to support the leaf discs. The insect pins were imbedded in a 1.0 cm layer of styrofoam plastic that was covered by a single layer of moist paper towelling and contained in a 10.0 cm diameter Pyrex glass petri dish. The leaf discs were held about 3 mm above the paper towelling during adult testing, and

about 1 mm for larval testing. The entire arrangement was covered with a stoppered, glass funnel.

Non-cruciferous plants - Groups of 10 adults, unfed for 24 hours, and groups of 50, newly-hatched larvae were offered non-cruciferous leaf discs in the test chambers for 4-hour periods. At the end of these periods, rape leaf discs were added to the test chambers, providing a choice of leaf discs for a second 4-hour period. Thirteen species of non-cruciferous plants, representing 5 families, were tested (Table 9).

Chemical fractions of rape foliage - Neither larvae nor adults of *E. americana*, starved for one day, will eat lettuce. In order to evaluate their response to chemical fractions of rape foliage, they were offered a choice of lettuce leaf discs treated with the chemical fractions, and untreated lettuce leaf discs. Choice trials involved groups of 10 adults, unfed for 24 hours, in the test chambers for 4-hour periods, and groups of 50, newly-hatched larvae for 12-hour periods. The adults were field-collected, and tested during the first 3 weeks after emergence. The larvae were from eggs hatched in the laboratory.

All chemical fractions from the plant extraction process were evaporated to dryness and dissolved in minimal amounts of methanol. Lettuce leaf discs were treated by immersion in the methanol solutions for one minute, and then air-dried. Control lettuce discs were immersed in methanol for one minute, and then air-dried. Immediately following each trial, the leaf discs were removed and their outlines accurately recorded on graph tracing

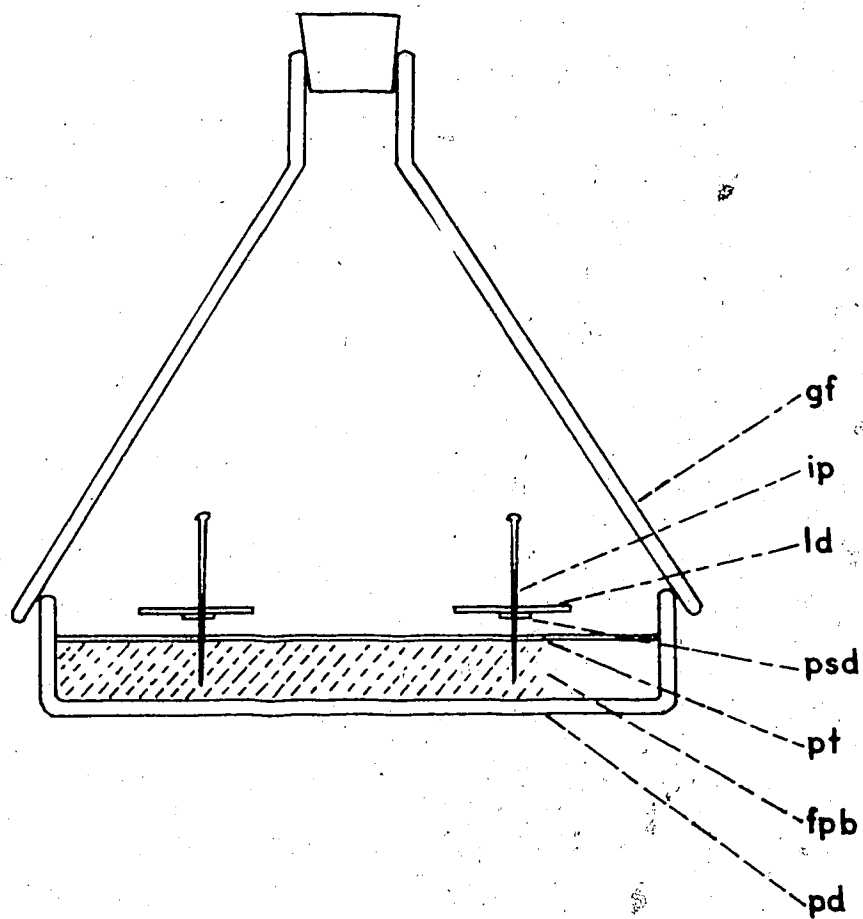


Fig. 4. The choice chamber used to evaluate the response of *Entomoscelis americana* Brown to food plants and non-food plants: gf, glass funnel; ip, insect pin; ld, leaf disc; psd, plastic supporting disc; pt, paper towelling; fpb, foam plastic bottomlayer; pd, petri dish.

Table 9. The non-cruciferous plants tested for feeding acceptability with *Entomoscelis americana* Brown.

Test plant	Common name
CHENOPODIACEAE	
<i>Chenopodium album</i> L.	lamb's quarters
<i>Beta vulgaris</i> L.	garden beet
<i>Beta vulgaris cicla</i> L.	Swiss chard
<i>Spinacia oleracea</i> L.	spinach
LEGUMINOSEAE	
<i>Pisum sativum</i> L.	garden pea
<i>Medicago sativa</i> L.	alfalfa
TROPAEOLACEAE	
<i>Tropaeolum majus</i> L.	large nasturtium
SOLANACEAE	
<i>Solanum tuberosum</i> L.	potato
<i>Lycopersicon esculentum</i> Mill.	tomato
<i>Nicotiana tabacum</i> L.	tobacco
COMPOSITAE	
<i>Taraxacum officinale</i> Weber	dandelion
<i>Cirsium arvense</i> (L.) Scop.	Canada thistle
<i>Lactuca sativa crispa</i> L.	leaf lettuce

paper. These were then reproduced by direct contact on Kodalith photographic film (Canadian Kodak Co., Toronto, Ont.), and enlarged 5.66 times with a projector. The enlarged image provided a circle with an area of 100 cm^2 which, when traced with a polar planimeter (Hughes and Owens Co., Toronto, Ont.) gave a reading of 100 when the instrument was set to yield a 1:1 ratio. The ratios of the areas of the partially-consumed discs to their original areas were determined, and the areas consumed expressed as percentages of the whole.

Two methods of chemical fractionation of rape foliage were carried out in this study. The first method involved the fractionation of solvent extracts by means of ion-exchange chromatography. This system was abandoned since it failed to concentrate the chemical feeding stimulants in definite fractions. The second fractionation method was designed, with minor modifications, after the method used by Nayar and Thorsteinson (1963) to isolate mustard oil glucosides from plant tissues of species in the families Crucifereae and Tropaeolaceae. Fig. 5 is a flow diagram of the fractionation procedure employed in this study.

Fresh rape leaves were dried in an electric, ventilated oven (Cenco Instruments Corp., Toronto, Ont.) set at 80° C , this temperature selected to inactivate naturally-occurring plant enzymes that may tend to break down compounds. (As noted in section 3.D.i., rape leaves detached for 3 days are toxic to the larvae.) The dried leaves were ground to a powder in a Sorval Omni-Mixer and stored in glass jars at 0° C . A 100-gram sample of the leaf powder was extracted 3 times in petroleum ether with a Sorval Omni-Mixer.

Each extraction was for 30 minutes in 300 ml of petroleum ether that was removed by filtration between extractions. The temperature during the extraction procedure was held near 20° C by means of an ice-water bath. The liquid fractions were combined, reduced by evaporation, and tested for a feeding stimulant with *E. americana*. Larvae and adults were each subjected to 5 trials in test chambers to evaluate their response to this fraction.

The residue from the petroleum ether extraction process was then extracted 3 times in 80% ethanol, following the same procedure employed in the petroleum ether extraction, and was similarly tested with *E. americana*. Since the ethanol solution contained a feeding stimulant, it was reduced to 10 ml by evaporation, and chromatographed on a 2.0 X 36.0 cm column of Adsorption Alumina, 80-200 mesh (Fisher Scientific Co., Fair Lawn, N.J.), packed and eluted with 80% ethanol. Column flow was adjusted to 30 ml/hour and 10-ml fractions collected with an automatic rotary fraction collector (Buchler Instruments Corp., Fort Lee, N.J.). Each 10-ml fraction was tested for a feeding stimulant with the larvae and adults of *E. americana*. Since a feeding stimulant was present in fractions 6-25, these were combined, reduced to 10 ml by evaporation, and chromatographed on a 2.0 X 36.0 column packed with a cellulose slurry in, and eluted with, 70% ethanol. 10-ml fractions were again collected and, when tested with *E. americana*, a feeding stimulant was detected in fractions 5-16. These fractions were combined, reduced to dryness by evaporation, dissolved in 20 ml of distilled water, and placed on a 2.0 X 36.0 column of activated

carbon (J. T. Baker Chemical Co., Phillipsburg, N.J.). This column was eluted with 250 ml of distilled water, followed by like amounts of ethanol solutions in concentrations 30, 60, and 90%, respectively. Each of the 4 resulting fractions was tested 5 times with the larvae and adults of *E. americana*. Since a feeding stimulant was present in the water and 60% eluates, these were combined, evaporated to dryness, and dissolved in 100 ml of distilled water at 50° C. The water solution was cooled to 21° C and shaken for 10 minutes in a separatory funnel with 100 ml of diethyl ether. The resulting 2 fractions were each tested 5 times for a feeding stimulant with the larvae and adults. Finally, the 2 fractions were re-combined and again tested with *E. americana*.

Tests with sinigrin - A 0.1 gm sample of sinigrin (Nutritional Biochemical Corp., Cleveland, Ohio) was dissolved in 10 ml of distilled water at 21° C. The larvae and adults were each tested 5 times in choice chambers, employing lettuce leaf discs that had been immersed in the sinigrin solution for one minute and air-dried. Control discs were immersed in distilled water for one minute and air-dried.

4.C.ii. Results

Non-cruciferous plants - Of the 13 species of non-cruciferous plants tested, none were accepted by *E. americana*. In all tests, when fresh rape leaf discs were added during the second 4-hour period, these were readily accepted by both larvae and adults.

Chemical fractions of rape foliage - Table 10 lists the results of the tests with chemical fractions of rape foliage. The control leaf discs remained intact during all tests and are not included in the table. *E. americana* did not accept leaf discs treated with the petroleum ether fraction; however, both larvae and adults accepted leaf discs treated with the 80% ethanol extract and each consumed about 49.8% of the leaf areas. The results of individual trials with the ethanol extract fraction are listed in Appendix VII.

Of the fractions collected from the adsorption alumina column, the larvae accepted fractions 11-17, the adults, 6-25. Greatest acceptance by both larvae and adults was detected in fractions 13-15. The larvae accepted fractions 7-14 from the cellulose slurry column, the adults, 5-16. Greatest response was to fraction 9, for leaf discs treated with this fraction were entirely consumed by both larvae and adults. *E. americana* did not accept leaf discs treated with the 90 and 30% eluates from the activated carbon column. Of the leaf discs treated with the distilled water and 60% ethanol eluates, the larvae consumed an average of 72.6 and 30.6%, respectively, the adults, 34.8 and 30.8%, respectively. These averages are computed from a total of 5 trials each for the larvae and adults, listed in Appendix VII.

Both larvae and adults accepted leaf discs treated with the water layer from the separatory funnel, although larval response was greater. As the result of 5 trials each (Appendix VII),

Table 10. The response of *Entomoscelis americana* Brown to lettuce leaf discs treated with chemical fractions of rape (*Brassica campestris* L.) foliage.

Fraction	Approximate area of discs consumed (%)	
	Larvae	Adults
Petroleum ether extract (Result of 5 trials)	0	0
80% ethanol extract (Average of 5 trials)	49.8	49.8
Adsorption alumina column		
Fraction No:		
5	0	0
6	0	6
7	0	13
8	0	19
9	0	19
10	0	25
11	8	38
12	13	36
13	18	29
14	61	84
15	32	61
16	23	47

Table 10 (continued)

Fraction	Approximate area of discs consumed (%)	
	Larvae	Adults
Adsorption alumina column		
Fraction No:		
17	11	35
18	0	42
19	0	31
20	0	22
21	0	19
22	0	16
23	0	16
24	0	13
25	0	12
26	0	0
Cellulose slurry column		
Fraction No:		
4	0	0
5	0	26
6	0	28
7	20	36
8	32	30
9	100	100
10	92	100

Table 10 (continued)

Fraction	Approximate area of discs consumed (%)	
	Larvae	Adults
Cellulose slurry column		
Fraction No:		
11	63	72
12	46	63
13	49	52
14	40	23
15	0	24
16	0	20
17	0	0
Activated carbon column		
(Average of 5 trials)		
90% ethanol	0	0
60% ethanol	30.6	30.8
30% ethanol	0	0
Distilled water	72.6	34.8
Separatory funnel fractions		
(Average of 5 trials)		
Water (1)	45.4	21.6
Diethyl ether layer (2)	0	6.2
(1) & (2) combined	48.8	73.4

the larvae consumed an average of 45.4% of the treated leaf discs, the adults about 21.%. The larvae did not accept leaf discs treated with the diethyl ether layer, while the adults displayed a slight response, consuming an average of 6.2% of the leaf areas. When the 2 fractions from the separatory funnel were re-combined, no significant change was detected in larval response and they consumed an average of 48.8% of the leaf area. Such re-combination did significantly affect adult response however, for they consumed an average of 73.4% of the treated leaf area.

Tests with sinigrin - *E. americana* did not accept leaf discs treated with sinigrin.

4.D. Preliminary tests to classify plant compounds

Preliminary tests were conducted to classify the unknown compounds in the water and diethyl ether layers from the separatory funnel. The scope of the tests was limited due to the small amount of residue obtained, approximately 0.1 g from the diethyl ether layer and about 0.01 g from the water layer.

Diethyl ether layer - Evaporation of the diethyl ether layer yielded a dark-brown, viscous substance that would not dry completely when exposed to air, and had a distinctive, fruity odour. This substance is insoluble in water at room temperature, and soluble in dilute sodium hydroxide and dilute sodium bicarbonate. According to Shriner, Fuson, and Curtin (1967), low volatility combined with these solubility properties indicates either a high-molecular-weight acid or a substituted phenol. The distinctive odour suggests

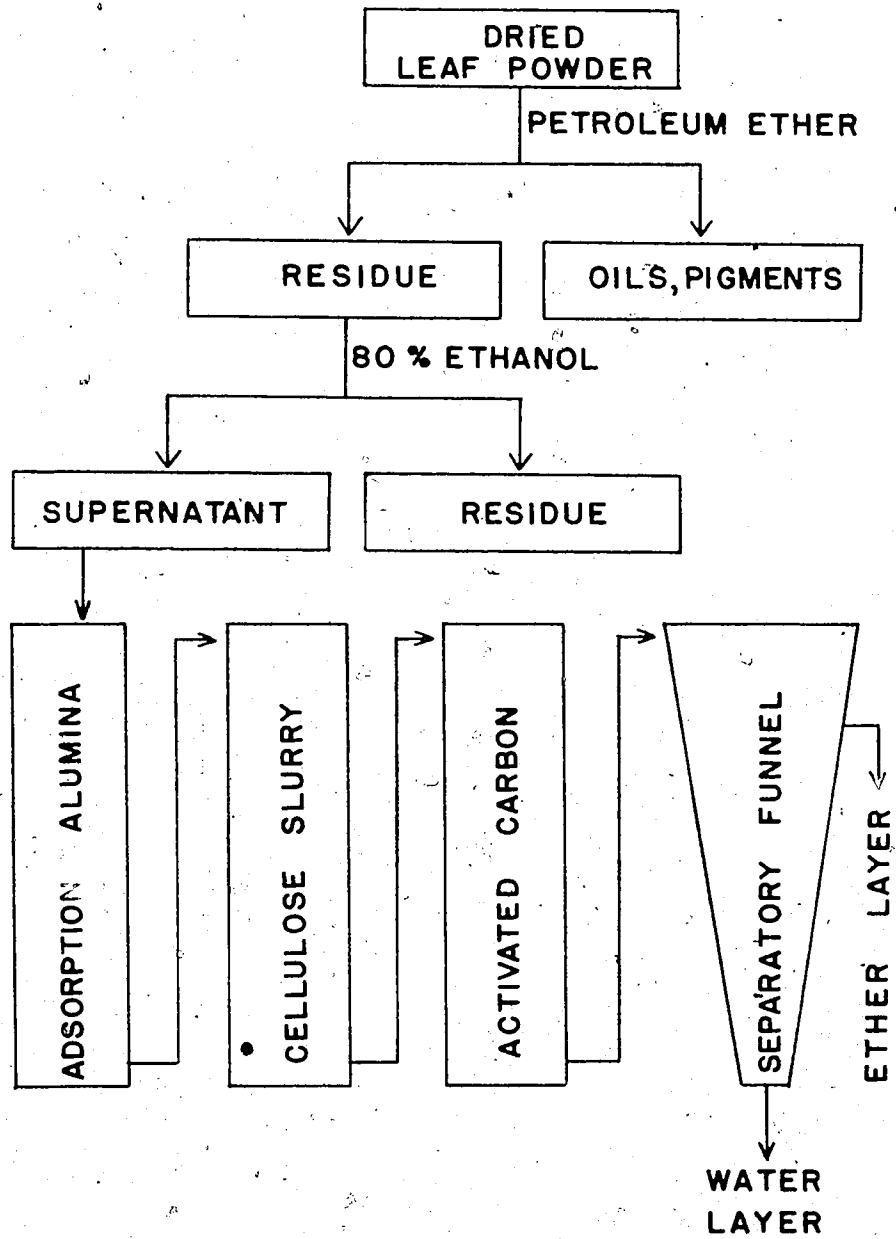


Fig. 5. A flow diagram of the procedure used to refine a chemical feeding stimulant from rape (*Brassica campestris* L.) foliage.

the latter.

Water layer - The water layer fraction has a pH of 6.9, is odourless, and yields a positive reaction with Benedict's solution. According to Shriner, Fuson, and Curtin (1967), a positive reaction to Benedict's solution combined with no solubility in diethyl ether indicates the presence of an aldehyde with a free reducing group. Control tests, using Benedict's solution, were run with glucose and sinigrin, and both yielded a positive reaction.

CONCLUSION AND DISCUSSION

The distribution of *E. americana* in North America and the habits of the stages indicate adaptation to a cool, fairly dry, continental type climate. Winters are spent in the soil as eggs, diapausing in the late embryo stage, while the warmest summer month in Alberta is spent in aestivation.

E. americana is oligophagous and restricted to the Cruciferae. Hatching occurs near cruciferous plants at a time when these plants are in the seedling stage, and the larvae need not search far for food. Phototaxis plays a major role in directing the larvae to the proper environment for feeding and this may be assisted by geotaxis and hygrotaxis. Although no directed movement by larvae toward food plant odours was demonstrated, such odours act as arrestants at very close range, possibly when the larvae are walking on the food plant, while non-food plant odours can act as repellents. That these two effects may combine to direct the larvae to the proper plant for feeding was demonstrated by the tests with growing food and non-food plants (Table 7). Thorsteinson (1960) contended that food plant finding by phytophagous insects is largely by chance, and no response to food plant odours was reported by Pospicil (1972) in larvae of several lepidopteran and coleopteran pests of sugar cane. Although Chin (1950) reported that Colorado potato beetle larvae responded to the odours of potato foliage from a distance of about 5mm, Bongers (1970) concluded that such re-

response is not necessary for survival since the eggs are normally deposited on potato leaves. Similarly, the eggs of *E. americana* are laid on soil beneath food plants and long range response to food plant odours by the larvae is not critical for survival.

Although no response to food plant odours was detected in newly-emerged adults, food plant finding is not critical at this time since the plants that served as larval food still have an ample supply of foliage. During *E. americana*'s July aestivation period, these plants form seed pods and the leaves senesce. Consequently, dispersal and food plant finding is critical after aestivation, and the response to food plant odours coincides with active dispersal in early August.

The striking reversals of phototaxis displayed by the adults coincides with other behavioural changes. Newly-emerged adults are strongly photo-positive (Table 3) and are found on plant stems. The reversals of phototaxis at the beginning and end of July are in synchrony with the aestivation period. The photo-negative response of aestivating adults is coupled with a positive response to moisture and a thigmokinetic response in conjunction with moist substrate. These 3 responses combine to direct *E. americana* to the proper environment for aestivation, since this period is spent under leaf litter and in soil crevices. The second reversal of phototaxis coincides with the termination of the aestivation period.

Copulation was not observed until immediately after dispersal in early August, at which time males responded to female

odours. Copulation after dispersal prevents inbreeding in a local population and increases genetic variation through exchange with other populations.

During the rape foliage fractionation process and later tests to characterize chemical feeding stimulants, it was demonstrated that an aldehyde stimulates larval feeding and synergises with a compound that has phenolic properties to stimulate adult feeding. The fact that larval response is confined to the aldehyde indicates that it is not a nutrient phagostimulant such as a sugar, but more likely an aldehyde peculiar to the Cruciferae, since the larvae are restricted to this plant family. Although the larvae do not respond to sinigrin or to nasturtium foliage which contains sinigrin, a mustard oil glucoside cannot be ruled out as a feeding stimulant since several such glucosides may occur in a single plant (Nayar and Thorsteinson, 1963). Adult feeding response was greatest to the combined effects of the aldehyde and a compound with phenolic properties. Hsiao and Fraenkel (1961) reported that a phenolic compound in potato foliage may be a specific stimulant for the Colorado potato beetle, and as discussed in the literature review, cases of synergism in phytophagous insects has been widely reported.

Since little previous research regarding *E. americana* has been reported, this study can form the basis for further investigations into the biology, food plant relationships, and control of *E. americana*. The description of the stages will aid in field identification, while the information regarding rearing techniques and termination of diapause will be useful in establishing laboratory


colonies. The information regarding the habits of the stages and food plant finding is useful in developing cultural control methods. *E. americana* has recently attracted attention as an economic pest because of increasing rape acreage in Western Canada, and will continue to be a pest as long as volunteer rape is allowed to spread through agricultural lands. Crop rotation, spring tillage, and more efficient methods of rape seed harvesting will help to suppress volunteer rape and can be investigated as methods of cultural control of *E. americana*.

Further investigations can be conducted to identify the plant compounds in rape foliage that initiate feeding by *E. americana*. These chemicals may then be used as bait in insect traps to estimate field population densities. Perhaps varieties of rape lacking these chemical can be developed, much in the same way that rape varieties with low erucic acid content were developed (Williams, 1972).


6. REFERENCES

- Alpin, R. T., M. H. Benn, and M. Rothschild. 1968. Poisonous alkaloids in the body tissue of the cinnebar moth, *Callimorpha jacobaeae* L. *Nature, Lond.*, 219: 747-748.
- Arnason, A. P. 1948. Red turnip beetle. Canada Dept. Agr. Publ. No. 100. 4 p.
- Augustine, M. G., F. W. Fisk, R. H. Davidson, J. B. Lapidus, and R. W. Cleary, 1964. Host plant selection by the Mexican bean beetle, *Epilachna varivestis*. *Ann. ent. Soc. Am.*, 57: 127-134.
- Baker, J. E., and D. M. Morris. 1967. A feeding stimulant for *Scolytus multistriatus* (Coleoptera: Scolytidae), isolated from the bark of *Ulmus americana*. *Ann. ent. Soc. Am.*, 60: 1213-1215.
- Beck, S. D. 1965. Nutrition of the European corn borer, *Pyrausta nubilalis* (Hubn.). IV. Feeding reactions of first instar larvae. *Ann. ent. Soc. Am.*, 49: 399-405.
- Beck, S. D., and W. Hanec. 1958. Effect of amino acids on the feeding behaviour of the European corn borer, *Pyrausta nubilalis* (Hubn.). *J. Insect Physiol.*, 2: 85-86.
- Beller, S., and M. H. Hatch. 1932. Coleoptera of Washington: Chrysomelidae. *Univ. Wash. Publ. in Biology*, 1(2): 103.

- Bierne, B. P. 1971. Pest insects of annual crops in Canada. I. Lepidoptera. II. Diptera. III. Coleoptera. Mem. ent. Soc. Can., 78: 86-87.
- Bongers, W. 1970. Aspects of host plant relationship of the Colorado potato beetle. Agr. Univ., Wageningen, Netherlands. Lab. Ent. Commun. 179. 77 p.
- Breedlove, D. E., and P. R. Ehrlich. 1969. Plant-herbivore co-evolution: lupines and lycaenids. Science, 162: 671-672.
- Brower, L. P. 1958. Bird predation and food plant specificity in closely related procryptic insects. Am. Nat., 92: 183-187.
- Brower, L. P., and J. V. Z. Brower. 1964. Birds, butterflies, and plant poisons: a study in ecological chemistry. Zoologica, N. Y., 49: 137-159.
- Brown, W. J. 1942. The American species of *Entomoscelis* and *Hippuriphila* (Coleoptera: Chrysomelidae). Can. Ent., 74: 172-176..
- Brues, C. T. 1920. The selection of food plants by insects with special reference to lepidopterous larvae. Am. Nat., 54: 313-322.
- . 1924. The specificity of food plants in the evolution of phytophagous insects. Am. Nat., 58: 127-144.
- Burmeister, H. 1836. A manual of entomology. Bradbury and Evans, London. xii + 654 p.
- Chambliss, O. L., and C. M. Jones. 1966. Cucurbitacins: specific insect attractants in Cucurbitaceae. Science, 153: 1392-1393.



Chapman, J. P. and J. C. Sherman. 1967. Oxford regional economic atlas: United States and Canada. Clarendon Press, Oxford. xii + 163 p.



Chin, C. T. 1950. Studies on the physiological relations between the larvae of *Leptinotarsa decemlineata* Say and some solanaceous plants. Tijdschr. PlZiekt., 56: 1-88.

Chittenden, F. H. 1902. Some insects injurious to vegetable crops. U.S.D.A. Div. Ent. Bull. 33: 49-53.

Chun, M. W. 1972. Dynamics of feeding responses in *Pieris brassicae* Linn. as a function of chemosensory input: A behavioural, ultrastructural and electro-physiological study. Agr. Univ., Wageningen, Netherlands. Lab. Ent. Commun. 206. 162 p.

David, W. A. L., and B. O. C. Gardiner. 1966. Mustard oil glucosides as feeding stimulants for *Pieris brassicae* larvae in a semi-synthetic diet. Entomologia exp. appl., 9: 247-255.

Derr, R. F., D. D. Randall, and R. W. Kieckhefer. 1964. Feeding stimulants for western and northern corn rootworm adults. J. econ. Ent., 57: 963-965.

Dethier, V. G. 1937. Gustation and olfaction in lepidopterous larvae. Biol. Bull. mar. biol. Lab., Woods Hole, 72: 7-23.

-----, 1941. Chemical factors determining the choice of food plants by *Papilio* larvae. Am. Nat., 75: 61-73.

- Dethier, V. G. 1953. Host plant perception in phytophagous insects. Int. Congr. Ent. Trans. IX. (Amsterdam, 1951), 2: 81-88.
- . 1954. Evolution of feeding preferences in phytophagous insects. *Evolution*, 8: 33-54.
- . 1966. Feeding behaviour. *In* *Insect behaviour*. P. T. Haskell (ed.). R. ent. Soc. Lond. Symp., 3: 46-58.
- . 1970. Chemical interactions between plants and insects. *In* *Chemical ecology*. E. Sondheimer and J. B. Simeone (eds.). Academic Press, New York. p. 83-102.
- Downey, J. C. 1962. Host-plant relations as data for butterfly classification. *Syst. Zool.*, 11: 150-159.
- Ehrlich, P. R., and P. H. Raven. 1964. Butterflies and plants: a study in co-evolution. *Evolution*, 18: 586-608.
- Essig, E. O. 1926. *Insects of Western North America*. MacMillan Co., New York. xi + 1035 p.
- Ettlinger, M. G. and A. Kjaer. 1968. Sulfur compounds in plants. *Rec. Adv. Phytochem.*, 1: 59-144.
-) Fabre, J. H. 1918. *The wonders of instinct*. T. Fisher Unwin, London. viii + 320 p.
- Feeny, P., K. L. Paauwe, and N. J. Dempog. 1970. Flea beetles and mustard oils: host specificity of *Phyllotreta cruciferae* and *P. striolata* adults (Coleoptera: Chrysomelidae). *Ann. ent. Soc. Am.*, 63: 832-841.
- Feir, D., and S. D. Beck. 1963. Feeding behaviour of the large milkweed bug, *Oncopeltus fasciatus*. *Ann. ent. Soc. Am.*, 56: 224-229.

- Fletcher, J. 1888. Report of the entomologist and botanist. In
Exp. Farms Rpts. 1885-1887. Canada Dept: Agr. p. 152-155.
- . 1905. Insects injurious to grain and fodder crops,
root crops, and vegetables. Canada Exp. Farms Bull. 53:
1-48.
- Fraenkel, G. S. 1953. The nutritional value of green plants for
insects. Int. Congr. Ent. Trans. IX. (Amsterdam, 1951),
9: 90-100.
- . 1959. The raison d'être of secondary plant substances.
Science, 129: 1466-1470.
- . 1969. Evaluation of our thoughts on secondary plant
substances. Entomologia exp. appl., 12: 473-486.
- Hamamura, Y. 1959. Food selection by silkworm larvae. Nature,
Lond., 183: 1746-1747.
- Hamilton, J. 1894. Catalogue of the Coleoptera common to North
America, Northern Asia, and Europe, with distribution and
biology. Trans. Am. ent. Soc., 21: 345-416.
- Heron, R. J. 1965. The role of chemotactic stimuli in the feeding
behaviour of the spruce budworm larvae on white spruce.
Can. J. Zool., 43: 247-269.
- Hocking, B., and I. S. Lindsay. 1958. Reactions of insects to the
olfactory stimuli from the components of an insecticidal
spray. Bull. ent. Res., 49: 675-683.
- Holloway, J. 1964. Host specificity of a phytophagous insect.
Weeds, 12: 25-27.

- accolon, M. 1966. Chemical insect attractants and repellents. *Ann. Rev. Ent.*, 11: 333-422.
- Jenkins, J. N., F. G. Maxwell, J. C. Keller, and W. L. Parrott. 1963. Investigations of the water extracts of *Gossypium*, *Abelmoschus*, *Crotalaria*, and *Phaseolus* for an arrestant and feeding deterrent for *Anthonomus grandis* Boh. *Crop Sci.*, 13: 119.
- Jermy, T. 1958. Untersuchungen über Auffinden und Wahl der Nahrung beim Kartoffelkäfer (*Leptinotarsa decemlineata* Say). *Entomologia exp. appl.*, 1: 197-208.
- , 1966. Feeding inhibitors and food preference in chewing phytophagous insects. *Entomologia exp. appl.*, 9: 1-12.
- Keller, J. C., F. G. Maxwell, J. N. Jenkins, and T. B. Davich. 1963. A boll weevil attractant from cotton. *J. econ. Ent.*, 56: 110-111.
- Kennedy, J. S. 1953. Host plant selection in Aphididae. *Int. Congr. Ent. IX (Amsterdam, 1951)*, 2: 106-113.
- , 1958. Physiological conditions of the host plant and susceptibility to aphid attack. *Entomologia exp. appl.*, 1: 50-65.
- , 1965. Mechanism of host plant selection. *Ann. appl. Biol.*, 56: 317-322.
- King, K. M. 1928. Insects affecting field crops and gardens in Saskatchewan, 1922-1927. *Scient. Agr.*, 9: 373-422.
- LeConte, J. L., and G. H. Horn. 1883. Classification of Coleoptera in North America. Series 507, Smith. Inst., Washington. xxxviii + 567 p.

- Leng, C. W. 1920. A catalogue of Coleoptera in America. North of Mexico. Cosmos Press, Cambridge. xvii + 470 p.
- Linné, C. 1789. Entomologia fauna suecicae descriptionibus aucta. Tome IV: 247.
- Loschiavo, S. R., S. D. Beck, and D. M. Morris, Jr. 1963. Behavioural responses of the smaller European elm bark beetle, *Scolytus multistriatus*, to extracts of elm bark. Ann. ent. Soc. Am., 56: 764-768.
- McIndoo, N. E. 1926. An insect olfactometer. J. econ. Ent., 19: 545-571.
- Mittler, T. E., and R. H. Dadd. 1964. Gustatory discrimination between liquids by the aphid *Myzus persicae* Sulzer. Entomologia exp. appl., 7: 315-328.
- Muller, C. H. 1969. The "co" in co-evolution. Science, 164: 197-198.
- Nayar, K., and G. Fraenkel. 1962. The chemical basis for host selection in the silkworm, *Bombux mori* L. J. Insect Physiol., 8: 505-525.
- . 1963. The chemical basis of host plant selection in the catalpa sphinx, *Ceratonia catalpae*. Ann. ent. Soc. Am., 56: 119-122.
- . 1963a. The chemical basis of host plant selection in the Mexican bean beetle, *Epilachna varivestis*. Ann. ent. Soc. Am., 56: 174-178.

- Nayar, J. K., and A. J. Thorsteinson. 1963. Further investigations into the chemical basis of insect-host relationships in an oligophagous insect, *Plutella maculipennis* (Curtis) (Lepidoptera: Plutellidae). *Can. J. Zool.*, 41: 923-929.
- Neff, D. L., and E. S. Vanderzant. 1963. Methods of evaluating the chemotropic response of boll weevils to extracts of the cotton plant and various other substances. *J. econ. Ent.*, 56: 449-454.
- Pallas, P. S. 1771. *Reise durch verschiedene Provinzen des Russischen Reichs in den Jahren 1768-1774*. Petersburg, Akadam. Buchhand, I (2): 463.
- Person, H. L. 1931. Theory in explanation of the selection of certain trees by western pine beetles. *J. Forest.*, 29: 696-699.
- Pospicil, J. 1972. Olfactory orientation of certain phytophagous insects in Cuba. *Acta ent. bohemoslov.*, 69: 7-17.
- Powell, E. F. 1941. Relationships within the Chrysomelidae. *Am. Midl. Nat.*, 25: 162-181.
- Redtenbacher, L. 1874. *Fauna Austriaca die Käfer*. Druck and Verlag, Wien. Bd. 2, 571 p.
- Richardson, J. W., W. Swainson, and W. Kirby. 1837. *Fauna boreali - Americana*. J. Fletcher (Publ.), Norwich. Part IV: 214.
- Schoonhoven, L. M. 1968. Chemosensory basis of host plant selection. *A. Rev. Ent.*, 13: 115-136.

- Shriner, R. L., R. C. Fuson, and D. Y. Curtin. 1967. The systematic identification of organic compounds. John Wiley & Sons, New York. ix + 458 p.
- Strickland, E. H., and B. Hocking. 1950. Insects of the Alberta farmstead. Univ. of Alta., Faculty of Agr. Bull. No. 55. 114 p.
- Stride, G. O., and R. Straatman. 1962. The host plant relationships of an Australian swallowtail, *Papilio aegus*, and its significance in the evolution of host plant selection. Proc. Linn. Soc. N.S.W., 87: 69-78.
- Thomas, M. K. 1953. Climatological atlas of Canada. Nat. Res. Council Canada No. 3151, Ottawa. 253 p.
- Thorpe, W. H., A. C. Crombie, R. Hill, and J. H. Darrah. 1947. The behaviour of wireworms in response to chemical stimulation. J. exp. Biol., 23: 234-266.
- Thorsteinson, A. J. 1953. The chemotactic responses that determine host specificity in an oligophagous insect, (*Plutella maculipennis* (Curt.), Lepidoptera). Can. J. Zool., 31: 52-73.
- . 1960. Host selection in phytophagous insects. A. Rev. Ent., 5: 193-218.
- Twinn, C. R. 1936. A summary of the insect pest situation in Canada in 1936. Rep. ent. Soc. Ont., 67: 73-87.
- Verschaeffeldt, E. 1910. The cause determining the selection of food in some herbivorous insects. Proc. Acad. Sci. Amsterdam, 13: 536-542.

- Waldbauer, G. P. 1962. The growth and reproduction of malloctomized tobacco hornworms feeding on normally rejected non-solanaceous plants. *Entomologia exp. appl.*, 5: 147-158.
- Watanabe, T. 1958. Substances in mulberry leaves which attract silkworm larvae, *Bombyx mori*. *Nature, Lond.*, 182: 325-326.
- Watson, C. E. 1959. Climates of the States. Alaska. *Climatography of the United States No. 60-49*: U.S. Dept. Commerce, Weather Bureau, Washington.
- Weise, J. 1893. Coleoptera. In *Naturgeschichte der Insecten Deutschlands*. W. F. Erichson (ed.). Nicolaische Verlags-Buchhandlung, Berlin. xiv + 1161 p.
- Whitehouse, F. C. 1919. Entomological Report. In *A. Rept. Alta. Dept. Agr., Edmonton*. p. 152-153.
- de Wilde, J. 1958. Host plant selection in the Colorado potato beetle larva, *Leptinotarsa decemlineata* Say.
- Williams, S. B. 1972. Canadian view of the oilseed industry. *J. Can. Dept. Agr.*, 17 (1): 3-5.
- Yamamoto, R. T., and G. Fraenkel. 1959. Common attractant for the tobacco hornworm, *Protoparce sexta* Johan. and the Colorado potato beetle, *Leptinotarsa decemlineata* Say. *Nature, Lond.*, 184: 206-207.
- Zimsen, E. 1964. The type material of I. C. Fabricius. Munksgaard, Copenhagen. vii + 656 p.

7. APPENDICES

Appendix I. The photo-response of adults of *Entomoscelis americana* Brown in a light-dark choice chamber.

Level of maturation	Run	Light	Dark
Newly-emerged adults	1	19	1
	2	20	0
	3	20	0
	4	18	2
	5	17	3
Beginning of aestivation	1	3	17
	2	2	18
	3	0	20
	4	1	19
	5	4	16
Aestivation 75% complete	1	8	12
	2	13	7
	3	11	9
	4	8	12
	5	9	11

Appendix I (continued)

Level of maturation	Run	Light	Dark
Aestivation complete	1	18	2
	2	19	1
	3	17	3
	4	16	4
	5	19	1

Appendix II. The thigmotaxis response of aestivating adults of *Entomoscelis americana* to openings in a moist substrate in a moist dry choice chamber.

Run	End of chamber with no openings in substrate	End of chamber with openings in substrate:
	In Openings	Not in openings
Chamber with no moist substrate		
1	12	2
2	10	1
3	6	2
4	8	4
5	14	0
Chamber with moist substrate		
1	0	16
2	0	17
3	0	14
4	0	16
5	0	14

Appendix III. The response of males of *Entomoscelis americana* Brown to the odour of gravid females in a moving air olfactometer.

Run	Moist air only (control)		Moist air plus odour of females	
	Neutral	Trap #1	Trap #1*	Trap #2
1a	12	12	4	26
1b	16	10	8	24
2a	32	0	20	12
2b	28	4	16	16
3a	30	2	19	19
3b	27	6	15	17
4a	22	8	15	21
4b	22	10	14	20
5a	24	6	12	24
5b	24	4	12	19

* odour source

Appendix IV. The response of first instar larvae of *Eutomoscelis americana* to the odour of rape foliage in 2-way, screened choice chambers.

Time of check (mins.)	Choice chamber with lettuce		Choice chamber with rape	
	Odour source	No odour source	Odour source	No odour source
15	7	3	7	3
	5	5	5	5
	6	4	4	6
60	7	3	6	4
75	4	6	7	3
90	5	5	2	8
105	4	6	3	7
120	3	7	2	8
135	4	6	6	4
150	5	5	5	5

Appendix V. The response of first instar larvae of *Entomoscelis americana* Brown to the odours of food plants and non-food plants in a moving air olfactometer.

Type of foliage	Moist air only				Moist air plus plant odours			
	Run	Neutral	Trap #1	Trap #2	Run	Neutral	Trap #1*	Trap #2
Rape	1a	12	20	28	1c	14	32	14
	1b	12	22	26	1d	16	18	26
	2a	13	25	22	2c	15	28	17
	2b	13	27	20	2d	15	24	21
	3a	12	23	25	3c	16	24	20
	3b	14	28	18	3d	14	16	30
	4a	12	20	28	4c	20	17	23
	4b	17	17	26	4d	36	12	12
	5a	10	24	26	5c	20	18	22
	5b	10	20	30	5d	24	16	20

*odour source

Appendix V. (continued)

Type of foliage	Moist air only (control)					Moist air plus plant odours						
	Run	Neutral	Trap #1	Trap #2	Run	Neutral	Trap #1*	Trap #2	Run	Neutral	Trap #1*	Trap #2
Lettuce	1a	20	42	38	1b	11	4	85				
	2a	28	40	32	2b	14	7	79				
	3a	16	48	36	3b	17	13	70				
	4a	24	43	33	4b	18	17	65				
	5a	14	47	39	5b	12	7	81				
Dandelion	1a	28	39	33	1b	12	10	78				
	2a	24	44	32	2b	22	14	64				
	3a	30	36	34	3b	26	18	56				
	4a	22	50	28	4b	20	19	61				
	5a	24	41	35	5b	16	11	73				

* odour source

Appendix V. (continued)

Type of foliage	Moist air only (control)			Moist air plus plant odours			
	Run	Neutral	Trap #1	Run	Neutral	Trap #1*	Trap #2
Lamb's quarters	1a	20	38	1b	22	4	74
	2a	32	36	2b	18	16	66
	3a	18	49	3b	17	10	73
	4a	14	40	4b	12	9	79
	5a	26	34	5b	21	2	77
Bean	1a	18	42	1b	20	32	48
	2a	24	40	2b	30	36	34
	3a	16	32	3b	20	41	39
	4a	30	32	4b	22	43	35
	5a	15	43	5b	19	44	37

* odour source

Appendix VI. The response of adults of *Entomoscelis americana* to odours of rape foliage and blossoms in a double air stream olfactometer.

Foliage:	Control (no odour source)					Experimental (odour source)				
	Run	Neutral	Trap #1	Trap #2	Run	Neutral	Trap #1	Trap #2		
Mixed adults	1	6	8	6	1a	2	8*	6		
	2	5	10	5	2a	5	6	9*		
	3	4	9	7	3a	2	12*	6		
	4	4	8	8	4a	2	4	14*		
	5	3	9	8	5a	2	13*	5		
Females	1	12	2	6	1a	6	14*	0		
	2	10	6	4	2a	2	2	16*		
	3	5	8	7	3a	1	18*	1		
	4	5	14	1	4a	2	6	12*		
	5	6	4	10	5a	3	15*	2		

*odour source

Appendix VI. (continued)

		Control (no odour source)			Experimental (odour source)			
	Run	Neutral	Trap #1	Trap #2	Run	Neutral	Trap #1	Trap #2
Foliage:								
Males	1	18	10	12	1a	20	10*	10
	2	16	14	10	2a	10	14	16*
	3	8	12	20	3a	10	15*	15
	4	13	17	10	4a	12	16	12*
	5	11	9	20	5a	12	14*	14
Blossoms:								
Females	1	13	4	3	1a	2	18*	0
	2	13	5	2	2a	0	1	19*
	3	12	2	6	3a	2	17*	1
	4	9	6	5	4a	4	1	15*
	5	16	3	1	5a	1	18*	1
Males	1	8	6	6	1a	2	16*	2
	2	8	4	8	2a	8	0	12*
	3	9	7	4	3a	3	15*	2
	4	5	5	10	4a	4	0	16*
	5	5	9	6	5a	0	18*	2

* odour source

Appendix VII. The response of *Entomoscelis americana* to lettuce leaf discs treated with chemical fractions of rape seed foliage.

	Trial	Approximate area of discs consumed (%)	
		Larvae	Adults
80% ethanol extract:	1	55	49
	2	60	59
	3	44	68
	4	43	22
	5	47	51
Activated carbon column:			
60% ethanol eluate	1	39	23
	2	33	28
	3	32	26
	4	30	32
	5	19	45
Distilled water eluate			
	1	75	43
	2	79	36
	3	63	37
	4	72	28
	5	74	30

Appendix VII. (continued)

	Trial	Approximate area of discs consumed (%)	
		Larvae	Adults
Separatory funnel fractions:			
Water layer (1)	1	47	18
	2	44	22
	3	46	25
	4	53	26
	5	47	17
Ether layer (2)	1	0	5
	2	0	7
	3	0	4
	4	0	6
	5	0	9
(1) & (2) combined	1	65	77
	2	50	79
	3	45	76
	4	38	64
	5	46	71

AUTOBIOGRAPHICAL SKETCH

I was born in Bowsman, Manitoba in 1927 and received my primary education at small, rural schools in central British Columbia. Following completion of Grade IX, I left school in 1942 - not because of a lack of interest, but for economic reasons. I then spent 4 years with various forest product companies in British Columbia and, since these years were spent in forested areas, I developed a keen interest in biological diversity and relationships. I then served over 6 years with the R.C.M. Police, chiefly in rural detachments in the Peace River district of Alberta. I spent the next 14 years in Edmonton where I was employed in the personnel department of Celanese Canada Ltd.

I picked up the threads of my formal education in 1965 by registering for evening high school courses offered by the Edmonton Public School Board and received a Senior Matriculation in 1967. Since I encountered little difficulty with the high school program, I decided to continue my education on a full-time basis and enrolled in Simon Fraser University in January, 1968.

A strong penchant for the life sciences led to my choice of biology at Simon Fraser University, and because of their trimester system, I was able to complete a 4-year program in 3 years. I was awarded a B.Sc. (Hons.) in 1971. While at Simon Fraser University, I became profoundly interested in the unusual world of insects and decided to study entomology at the graduate level.